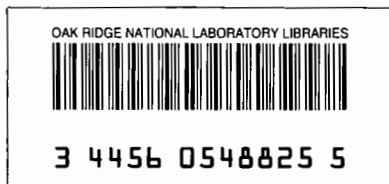


OAK RIDGE NATIONAL LABORATORY
operated by
UNION CARBIDE CORPORATION
for the
U. S. ATOMIC ENERGY COMMISSION

700
175764
Dist 1
Sub. Record

ORNL - TM - 915

18

STUDIES IN HEAT TRANSFER AND FLUID MECHANICS
PROGRESS REPORT FOR PERIOD JANUARY 1 - SEPTEMBER 30, 1963

H. W. Hoffman
J. J. Keyes, Jr.

**CENTRAL RESEARCH LIBRARY
DOCUMENT COLLECTION
LIBRARY LOAN COPY**
DO NOT TRANSFER TO ANOTHER PERSON
If you wish someone else to see this
document, send in name with document
and the library will arrange a loan.

NOTICE

This document contains information of a preliminary nature and was prepared primarily for internal use at the Oak Ridge National Laboratory. It is subject to revision or correction and therefore does not represent a final report. The information is not to be abstracted, reprinted or otherwise given public dissemination without the approval of the ORNL patent branch, Legal and Information Control Department.

LEGAL NOTICE

This report was prepared as an account of Government sponsored work. Neither the United States, nor the Commission, nor any person acting on behalf of the Commission:

- A. Makes any warranty or representation, expressed or implied, with respect to the accuracy, completeness, or usefulness of the information contained in this report, or that the use of any information, apparatus, method, or process disclosed in this report may not infringe privately owned rights; or
- B. Assumes any liabilities with respect to the use of, or for damages resulting from the use of any information, apparatus, method, or process disclosed in this report.

As used in the above, "person acting on behalf of the Commission" includes any employee or contractor of the Commission, or employee of such contractor, to the extent that such employee or contractor of the Commission, or employee of such contractor prepares, disseminates, or provides access to, any information pursuant to his employment or contract with the Commission, or his employment with such contractor.

Contract No. W-7405-eng-26

Reactor Division

STUDIES IN HEAT TRANSFER AND FLUID MECHANICS
PROGRESS REPORT FOR PERIOD JAN. 1 - SEPT. 30, 1963

H. W. Hoffman
J. J. Keyes, Jr.

OCTOBER 1964

OAK RIDGE NATIONAL LABORATORY
Oak Ridge, Tennessee
operated by
UNION CARBIDE CORPORATION
for the
U.S. ATOMIC ENERGY COMMISSION

OAK RIDGE NATIONAL LABORATORY LIBRARIES



3 4456 0548825 5



CONTENTS

	<u>Page</u>
SUMMARY	v
1. INTRODUCTION	1
2. BOILING HEAT TRANSFER AND TWO-PHASE FLOW	5
2.1. Boiling Potassium Heat Transfer	5
2.1.1. Forced-Convection System	5
2.1.2. Superheat Phenomena	21
2.2. Water Boiling in a Multirod Geometry	27
2.3. General Boiling Studies	30
2.3.1. Prediction of Critical Heat Fluxes	30
2.3.2. Randomness in the Critical Heat Flux.	32
2.3.3. Internal Heat Transfer in a Horizontal Tube Immersed in a Water Pool	34
2.4. Swirl-Flow Heat Transfer	35
2.4.1. Heat-Transfer Characteristics of Ethylene Glycol.	35
2.4.2. Swirl-Flow Boiling with Net Vapor Generation	40
3. FLOW DYNAMICS AND TURBULENCE	41
3.1. Vortex Fluid Mechanics	41
3.1.1. Gas Dynamics Studies	42
3.1.2. Magnetohydrodynamic Studies	60
3.2. Turbulence Transport Studies	78
3.3. Boundary-Layer Transient Phenomena	86
4. THERMOPHYSICAL PROPERTIES	97
4.1. Alkali Liquid Metals	97
4.1.1. Thermal Conductivity of Lithium	97
4.1.2. Surface Tension of Potassium	101
4.1.3. Contact Angle Determinations	105
4.2. Miscellaneous Materials	107
4.2.1. Electrical Resistivity of Brass	107
5. BIBLIOGRAPHY.	109



SUMMARY

Boiling Heat Transfer and Two-Phase Flow

Boiling Potassium Heat Transfer. An experimental study of forced-convection saturated boiling with potassium was undertaken to determine critical heat flux limits, heat-transfer coefficients, and two-phase pressure drop characteristics. Data have been obtained for boiling inside of two vertical tubes of different diameters (0.87-in. and 0.325-in.); the heat flux capability of these boilers was 40,000 and 500,000 Btu/hr·ft², respectively.

In the lower-flux (larger diameter) test section, tube-wall temperature oscillations of very high amplitude (± 150 to $\pm 200^\circ\text{F}$) were observed during some periods of operation; these oscillations were regular in frequency and persisted over long times. Stable operation (minimal wall-temperature fluctuation) was found to be possible only when vapor bubbles existed at the boiler inlet.

Critical heat-flux values ranged from $\sim 32,500$ Btu/hr·ft² at an inlet mass flow of 0.15×10^5 lb/hr·ft² to $\sim 345,000$ Btu/hr·ft² at $G = 1.3 \times 10^5$ lb/hr·ft². The results agreed well with the correlation of Lowdermilk, Lanzo, and Siegel based on data for the forced-convection saturated boiling of water. It is not expected that this comparison will be valid for the other alkali liquid metals. When stable high-temperature oscillations occurred, the critical heat flux was reduced by about 40%.

Heat-transfer data for flux levels below the critical show a lesser dependence of (q/A) on ΔT than has been found with water. Further, the data obtained in the low-flux boiler fall significantly below those obtained with the high-flux boiler. The latter results agree reasonably with the preliminary data of Brooks (General Electric Company).

Pressure-loss data (as the ratio of total two-phase to equivalent liquid-only at the same inlet mass flow) have been correlated using the Lockhart-Martinelli parameter. A consistent variation was observed such that the pressure-loss ratio increased with increasing exit quality. Exit qualities ranged between 10 and 86%.

Superheating in alkali liquid metals at their normal boiling temperatures was calculated to vary from 258°F for sodium down to 67°F for cesium in the presence of cavities which would allow only a 30°F superheat in water at atmospheric pressure. It was also shown that the superheating in potassium might be greater than indicated by the calculation, since potassium is generally cleaner, wets the metal better, and more readily fills surface cavities than does water.

Vapor present at the boiler inlet may produce stable operation by eliminating the high superheat necessary for bubble initiation. On the other hand, considerations in terms of an annular flow lead to the observation that evaporation from a thin, superheated liquid film on the wall to the central vapor flow would be sufficient to account for the observed heat transfer.

Water Boiling in a Multirod Geometry. Apparatus has been assembled for an experimental study into the magnitude of the critical heat flux and the two-phase pressure loss for the forced-convection boiling of water at atmospheric pressure flowing along the axis of a heat 7-rod cluster. The effects of rod spacing, inlet subcooling, and outlet quality will be examined. It is hoped to resolve some discrepancies in the literature as to the location of the burnout region, as well as to provide data of value to reactor design.

General Boiling Studies. An additive-type correlation (combining pool-boiling with forced-convection effects) is described for use in predicting the critical heat flux for forced-convection boiling. It was found that 96% of the predicted values agreed with available experimental data to within 40%; this is pointed out as providing a better representation of existing experimental data than given by previously available correlations.

An experimental study into the inherent randomness in the critical heat flux was conducted using an apparatus consisting of a horizontal, electrically heated tube in a pool of saturated water. It was found that there existed an uncertainty in the critical heat flux value which approximated that predicted by Zuber's hydrodynamic instability theory and that

the nature and condition of the boiler surface can constitute an important influence on the critical heat flux.

An experiment with boiling on the inside only of a horizontal tube submerged in a liquid pool was completed. Since the ends of the tube were open, there resulted in most tests a pulsating flow in which liquid flow inward toward the tube center alternated with an outward expulsion of liquid-vapor mixture. This was found to occur primarily with tubes of large L/d ratio; for tubes of small L/d ratio, behavior similar to that observed in other geometric situations in attaining the critical flux was observed.

Swirl-Flow Heat Transfer. Swirl-flow heat transfer with ethylene glycol has been studied as part of a general investigation of the influence of coolant thermophysical properties on heat transfer with this mode of flow. Electrically heated, horizontal tubes containing twisted-tape swirl generators varying in twist (tube diameters per 180-deg turn) from 2.2 to 12.1 were used. Over the experimental ranges of this study, the critical heat fluxes for saturated pool boiling, axial-flow local boiling, and swirl-flow local boiling were found to be $\sim 1/3$, $1/2$, and $3/4$ of those for water at the same conditions of geometry, velocity, pressure, and bulk temperature. The predictions of the additive correlations were in good agreement with these data. A correlation describing nonboiling swirl-flow data for both ethylene glycol and water to within $\pm 12\%$ was developed. Data on nonboiling axial-flow heat-transfer coefficients at high velocities and heat fluxes were higher than predicted by existing standard correlations.

An apparatus is being assembled for two-phase swirl-flow boiling studies.

Flow Dynamics and Turbulence

Vortex Fluid Mechanics. In considering the use of vortex flow for such advanced energy conversion applications as the gaseous core nuclear reactor and the magnetohydrodynamic power generator, knowledge of the interrelationship of the vortex strength and the turbulent energy dissipation is of fundamental importance. Experimental gas dynamics studies

have revealed, for example, that a high level of turbulent shear in the concave wall boundary layer seriously limits the vortex strength attainable with an energy expenditure which is deemed reasonable from the standpoint of the applications. Furthermore, turbulence which may exist in the interior of the flow field is also undesirable from the standpoint of separation efficiency. Specifically, these studies have delineated the effect of tube diameter, mass flow rate, injection velocity and geometry, and pressure on the vortex strength, as well as the effect of turbulence on the separation characteristics of vortex flow. Techniques examined for possible reduction in boundary layer turbulence include uniform wall bleed-off and slit bleed-off. Neither technique, however, produced a significant effect on the vortex strength. The vortex strength was observed to increase significantly with extreme wall cooling. Experiments in which vortices were generated by flow through a porous wall, the pores of which were oriented nearly tangentially, were encouraging, but indicated that an extremely large number of very small, closely spaced pores would likely be necessary to attain the desired limiting condition of a "rotating" wall of gas jets.

An analytical and experimental study concerned with the possible application of a hydromagnetic stabilization technique for vortex flow was initiated. Analysis based on a nondissipative model revealed that magnetic stabilization is possible, using an axial magnetic field, without altering the mean flow. Analysis of a more realistic case, dissipative vortex flow, was initiated. An exploratory experimental investigation into jet-driven, confined vortex-type flow, using an electrolytic solution (concentrated NH_4Cl) as the working fluid and a 62-kilogauss axial magnetic field, demonstrated the significant stabilizing influence of the magnetic interaction. For example, the peripheral tangential Reynolds modulus at transition to instability on the concave wall was increased by the magnetic field, as was the recovery of injection velocity as tangential velocity. An additional magnetic effect of interest is the stabilization of the boundary layer on the circular end wall, and the resulting increase in the ratio of tangential to radial velocity.

Turbulent Transport Studies. An experimental approach to the problem of Reynolds stress determination is proposed based on an improved theory relating the signal of a hot-wire anemometer to the Reynolds stresses. [The Reynolds stresses represent the eddy contribution to the momentum conductivity of the fluid.] A suitable instrument employing an analog computer has been developed and calibrated, and stable hot wire probes have been fabricated. A water-flow loop has been constructed and tested which meets stringent fluid cleanliness, deaeration, and thermal stability requirements. Preliminary results for pipe flow of water at Reynolds modulus of 158,000 have indicated that the level of turbulence in water flows is possibly less than anticipated from existing measurements in air.

Boundary-Layer Transient Phenomena. An investigation into the nature of turbulent instabilities in boundary layers is in progress with the aim of delineating the mechanism of surface thermal transient generation as a potential source of fatigue-type failure and/or accelerated corrosion in reactor heat exchange systems. Exploratory experiments employing an electrically heated 2-in. pipe as the test section with deaerated water in turbulent flow have been carried out for the purpose of instrumentation development and evaluation. These experiments have demonstrated that "gun-barrel" type surface thermocouples will provide quantitative measurements of the surface thermal transients and that the integrated read-out system [employing amplification, recording (magnetic tape and oscillographic), and spectral analysis] is satisfactory. A hot film surface probe for direct determination of instantaneous heat-transfer rates at a fluid-solid interface has been developed. A simple mathematical model which takes into account the breaking up of the viscous sublayer and eddy penetration has been compared with the preliminary experimental results.

Thermophysical Properties

Alkali Liquid Metals. The measurement of the thermal conductivity of molten lithium was completed; final results showed a linear increase with temperature from 25.6 Btu/hr.ft.°F at 600°F to 35.0 Btu/hr.ft.°F at

1500°F. A detailed error analysis indicated an accuracy of $\pm 7\%$ at the lower temperature to $\pm 12\%$ at the upper end of the range. In contrast with sodium and potassium, the thermal conductivity of lithium showed a positive temperature characteristic. A comparison of these results with values derived from recent electrical resistivity and thermal diffusivity measurements indicated a similar trend with temperature, although in magnitude the current data fell 4 to 10% below the data of the other investigators.

Preliminary values were obtained for the surface tension of potassium against helium over the temperature span 70 to 308°C using a maximum bubble pressure technique. The results were significantly higher than data obtained by other investigators using capillary rise techniques.

Experiments were initiated on measuring the contact angle for potassium droplets against various metals in order to determine the extent to which surfaces are wetted by potassium. In preliminary studies on a polished type 316 stainless steel surface, it was observed that the angle of contact varied from 120-deg at 70°C to 0-deg at 500°C some 95 minutes later. A second droplet placed on the surface at 180°C had an initial contact angle of 50-deg.

Miscellaneous Materials. The electrical resistivity of seamless 70-30 brass tubing was experimentally determined and found to vary from 7.4 $\mu\text{ohm-cm}$ at 100°C to 11.8 $\mu\text{ohm-cm}$ at 500°C.

STUDIES IN HEAT TRANSFER AND FLUID MECHANICS
PROGRESS REPORT FOR PERIOD JAN. 1 - SEPT. 30, 1963

H. W. Hoffman

J. J. Keyes, Jr.

1. INTRODUCTION

The design of any specific nuclear reactor rests on such knowledge as is available at the time coupled with test data easily obtainable during the design period. Detailed design commitments cannot be founded on projected test programs of unknown duration and uncertain outcome. However, in accomplishing his function, the design engineer is often placed in the unfair position of having to extrapolate beyond the current state-of-knowledge, hoping that his "guesses" are educated and logical and that his decisions will be justified by successful operation and/or later corroborative developments. It follows then that one way of assisting a rapid rate of advance in successive reactor designs is to anticipate design problems by conducting studies, independent of any specific reactor, on problems common to general reactor types. One such important area of problems is that of Heat Transfer and Fluid Mechanics. This includes extending experimental investigations outside the range of immediate interest so as to generate broader empirical correlations, as well as the development of theoretical and experimental knowledge for new geometries, coolants, and thermal and hydrodynamic conditions.

In addition to this positive effort toward speeding advances in reactor design, the investigator must be alert for and must pursue partially hidden indications of unsuspected hazards and difficulties which might otherwise be overlooked in the stress and rush accompanying the design and development of a reactor system. The identification of the possibility of serious stress cracking and/or enhanced corrosion in heat exchanger tubes operated at unusually high heat flux with turbulent cooling or heating by a fluid of moderate to high thermal conductivity is one example of this type of contribution.

In recognition of these facts, the Engineering Development Branch of the U. S. Atomic Energy Commission has supported for the past several

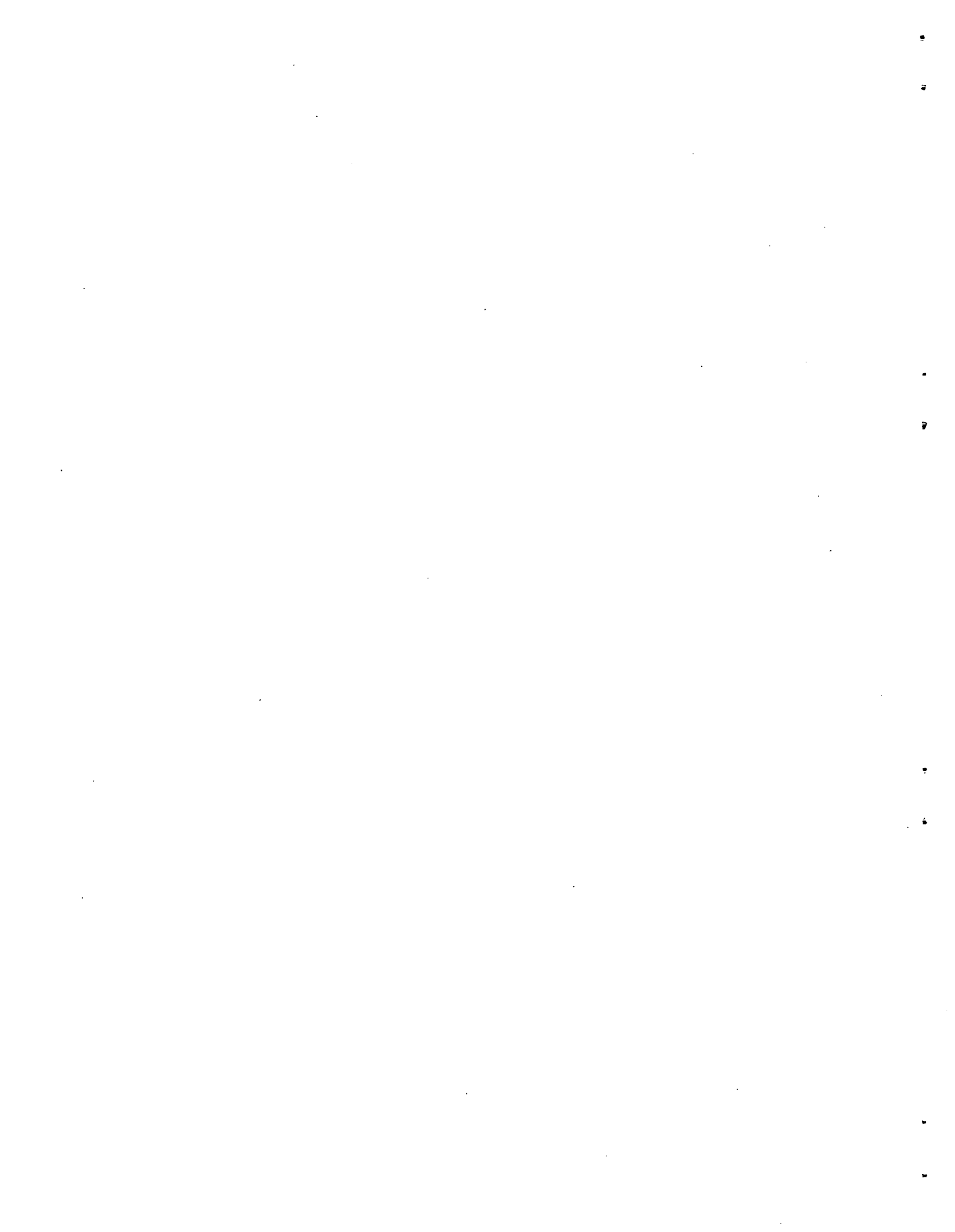
years a program in heat transfer and fluid mechanics at the Oak Ridge National Laboratory aimed at pointing the way toward advances in design of both new and existing reactor concepts. This work is concentrated in the areas of turbulence, two-phase flow, and boiling heat transfer.

Turbulence studies include the measurement of Reynolds stresses and the development of techniques for making such measurements, the effects of hydrodynamic control and magnetic fields in stabilizing a high-strength vortex flow, and the influence of turbulent fluctuations in inducing thermal transients at a heat-transferring surface. While fundamental in form, these investigations are oriented to useful and realistic geometries in practical situations. Thus, as mentioned previously, the last-named area has included the determination of local fatigue cracking and corrosion effects on a metal wall subjected to temperature oscillations and will be extended to relate the influence of upstream flow disturbers (elbows, orifices, etc.) in contributing to these oscillations.

A significant effort is directed to the study of boiling phenomena with water and potassium (primarily) for a variety of flow and geometric conditions. Included are the determination of critical heat flux and heat-transfer coefficients with potassium, the effects of swirl flow on burnout under subcooled and net vapor generation conditions, the influence of rod spacing on the critical heat flux with boiling along a rod bundle, and two-phase pressure loss in channels with forced-convection saturation boiling of potassium. A number of related efforts have developed, principal among these being an investigation of liquid superheat with the alkali liquid metals as a source of instability in the boiling process. Experiments and theoretical studies of the pressure drop and regime transitions in the two-phase flow of liquid metals parallel to rod bundles and of liquid-metal vapor condensation are planned.

In support of all of this work is the experimental determination of the thermophysical properties of coolants and containment materials. At present these studies are restricted to the measurement of the surface tension, density, and thermal conductivity of the alkali liquid metals at temperatures to 2000°F.

This report is the first in a series providing a periodic summation of the results obtained in these studies. The second report will cover the period through June 30, 1964; thereafter, these will be issued semi-annually. A complete listing of reports and open-literature publications issued since the inception of this program is to be found in the bibliography.



2. BOILING HEAT TRANSFER AND TWO-PHASE FLOW

2.1. Boiling Potassium Heat Transfer

2.1.1. Forced Convection System

A. I. Krakoviak

H. W. Hoffman

Introduction

An understanding of the thermal and fluid mechanical characteristics of boiling alkali metals is of great importance in designing light-weight Rankine-cycle nuclear-energy systems to satisfy auxiliary power requirements in satellite or other space vehicles. Knowledge of burnout heat flux limits, heat-transfer coefficients, two-phase pressure losses, and flow stability criteria is of immediate interest; and the experimental program discussed below is intended to provide such information with boiling potassium.

Attempts at prediction of the critical heat flux with the liquid alkali metals in forced-convection boiling at saturation conditions,¹ using correlations developed for water and organic fluids, have yielded widely disparate results. Thus, from the generalized expressions of Griffith,² the estimated peak heat flux (at 50% exit quality) is $\sim 2 \times 10^8$ Btu/hr·ft²; while an additive procedure recently developed by Gambill^{1,3} suggests a value of $\sim 10 \times 10^6$ Btu/hr·ft². Experimentally determined values for the critical heat flux were not available at the inception of this program.

¹W. R. Gambill and H. W. Hoffman, "Boiling Liquid-Metal Heat Transfer," American Rocket Society Paper No. 1737-61, May 1961.

²P. Griffith, "The Correlation of Nucleate Boiling Burnout Data," ASME Preprint No. 57-HT-21; see also MIT Tech. Report No. 9, March 1957.

³W. R. Gambill, "Generalized Prediction of Burnout Heat Flux for Flowing, Subcooled, Wetting Liquids," Chemical Engineering Progress Symposium Series, 59(41): 71-87 (March 1963).

Apparatus

The experimental system assembled for the measurement of the critical heat flux with potassium is depicted schematically in Fig. 2.1. Liquid potassium was pumped from a cooled reservoir through a vertically mounted boiler to a liquid-vapor separator. A restriction at the boiler inlet provided the pressure drop necessary to eliminate hydrodynamic coupling between the boiler and the pumping system. The flow rates of the liquid and the vapor after condensation were determined both volumetrically in calibrated hold tanks and dynamically by electromagnetic flow meters; the boiler exit quality was based on these measurements. A tangential inlet to the separator caused the necessary centrifugal force for separation of the entering vapor-liquid mixtures; at low flows, gravity separation appeared effective. A finned coil cooled by an air blast served as the condenser. Oxygen was kept at a low concentration by the continuous bypass circulation of a small stream of liquid potassium through a heated titanium sponge trap.

Boilers of two designs have been used thus far; these are shown in cut-away schematic in Fig. 2.2. Initial measurements⁴ were made with a test section constructed of a 6-ft long, 1-in.-OD (0.87-in.-ID) type 347 stainless steel tube. The left-hand portion of Fig. 2.2 depicts a typical unit length of this boiler. Heat was supplied by a set of six 3-in.-ID \times 12-in.-long clamshell heaters centered on the boiler tube. Thermocouples (8-mil-diam Pt-Pt 10% Rh) were welded to the outside tube surface at the approximate axial mid-point of each heater; thermowells and pressure taps for establishing the fluid conditions were located at the test section entrance and exit. At the inlet, the boiler tube was welded to a 0.245-in.-ID section; and at the outlet end, to a 0.625-in.-ID line. The maximum heat flux attainable with this configuration was $\sim 40,000$ Btu/hr.ft².

The second boiler is shown as the right-hand portion of Fig. 2.2. This was a 44-in.-long, 0.325-in.-ID (0.028-in.-wall thickness) type 347

⁴H. W. Hoffman and A. I. Krakoviak, Forced-Convection Saturation Boiling of Potassium at Near-Atmospheric Pressure, pp. 182-203, "Proceedings of 1962 High-Temperature Liquid-Metal Heat Transfer Technology Meeting," USAEC Report BNL-756, Brookhaven National Laboratory.

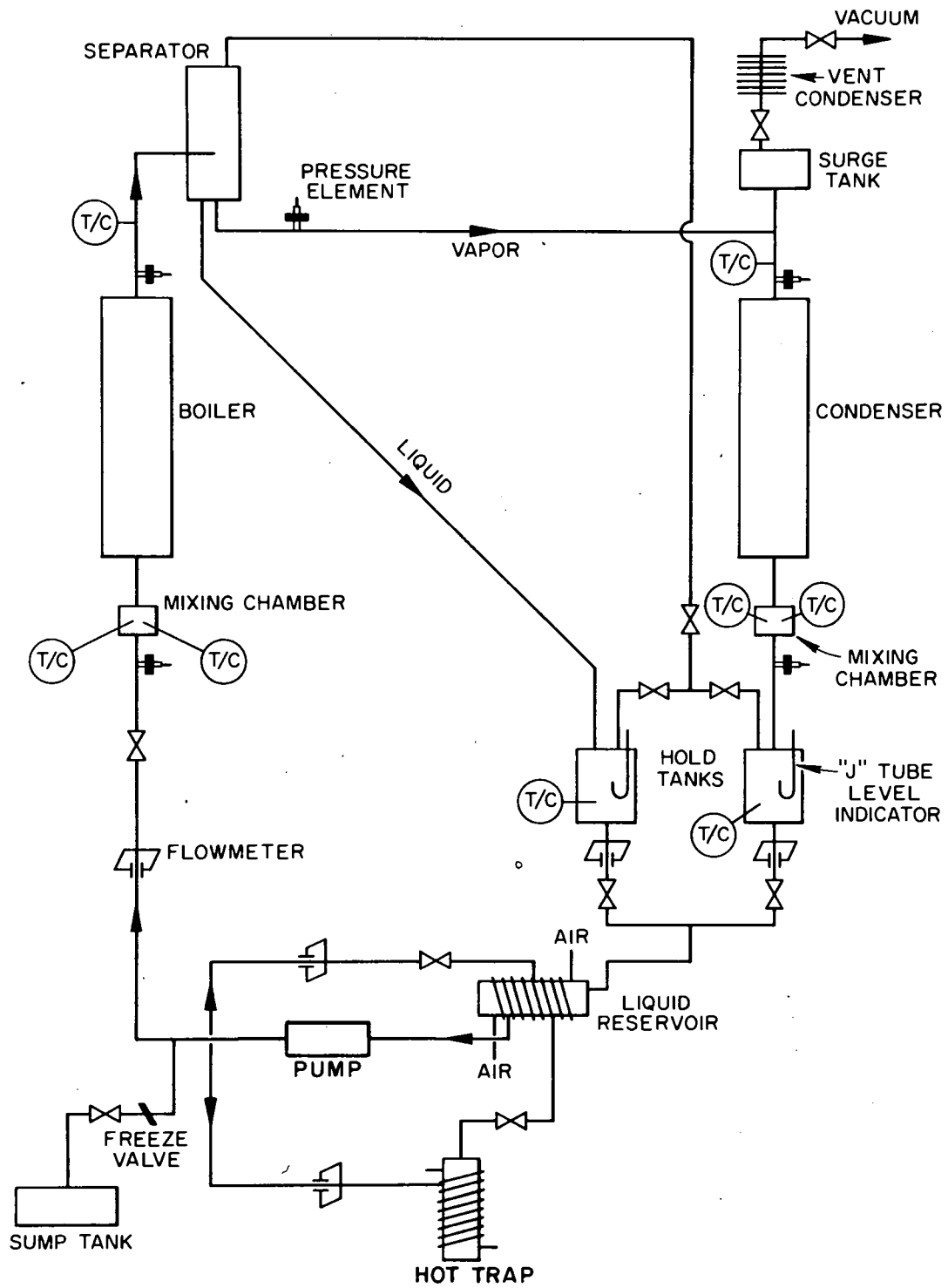
UNCLASSIFIED
ORNL-LR-DWG 46124A

Fig. 2.1. Loop Schematic: Forced-Convection Boiling with Potassium.

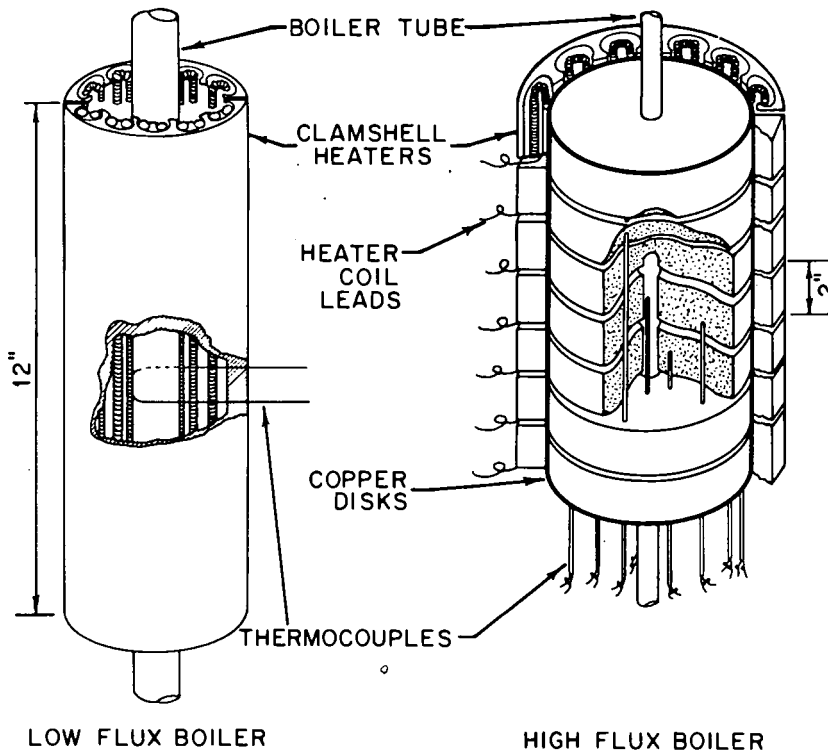
UNCLASSIFIED
ORNL-LR-DWG. 76113R

Fig. 2.2. Test Sections for Boiling Potassium Experiment.

stainless steel tube brazed within a segmented copper sleeve of 5-in. outside diameter. The twenty-one, 2-in.-thick OFHC copper disks comprising this sleeve were separated by 0.119-in. gaps to minimize the axial heat flow. Each disk was heated externally by an individually controlled clamshell heater; the converging geometry of the heat-flow path results in substantially augmented heat fluxes at the fluid-metal interface for reasonable heater temperatures. This boiler design permitted heat fluxes of the order of 500,000 Btu/hr·ft². The radial temperature gradient in each copper block was measured with three logarithmically spaced 0.040-in.-OD sheathed Chromel-Alumel thermocouples. These thermocouple readings were extrapolated to give the temperature at the boiling surface and, in combination with the copper conductivity, the heat fluxes through each copper segment. Finally, the mass of the copper disks provided sufficient thermal capacity to insure against physical burnout of the boiler tube.

Operating Characteristics

Outside tube-wall temperature traces obtained in runs B6.3 through B6.6 during approach to "burnout" are shown in Fig. 2.3; thermocouples 5 and 6 were located near the boiler exit. As indicated in this figure, the critical heat flux was attained by progressively reducing the flow, while maintaining a constant heat flux level in the boiler. The burnout point was indicated by the automatic interruption of boiler power when the wall temperature during any oscillation exceeded a preset value. For the Series B experiments, this temperature limit was 1750°F; in some early runs temperature excursions of as much as 350°F above the mean were noted. In the high-flux boiler (Series A), an increase in wall temperature of 50°F was taken as the power-cutoff criterion.

Under some conditions, tube-wall temperature oscillations of very high amplitude were observed in the low-flux boiler. These fluctuations persisted over long periods and had associated with them extreme variations in both flow and pressure. At the same time, the liquid flow at the pump exit was steady to within the precision of the electromagnetic flowmeter. A typical temperature trace recorded during one such oscillatory situation is shown by the upper curve in Fig. 2.4. The frequency

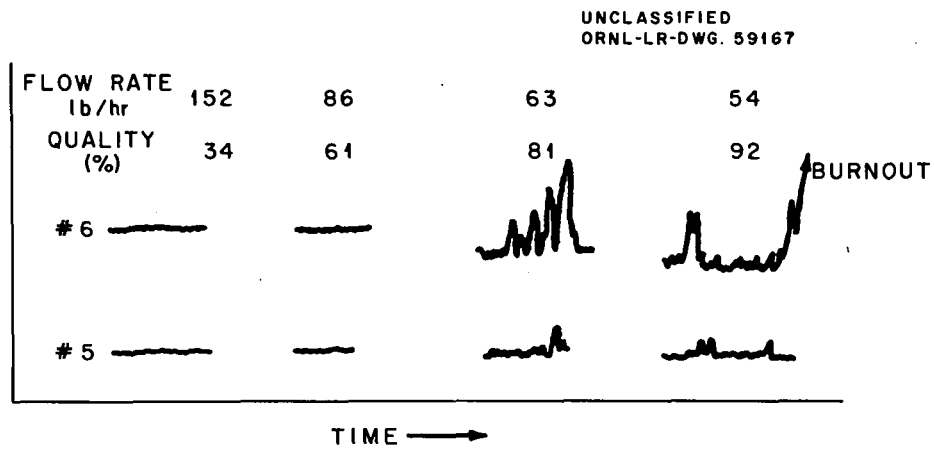


Fig. 2.3. Sequence of Tube-Wall Temperatures During Approach to Burnout.

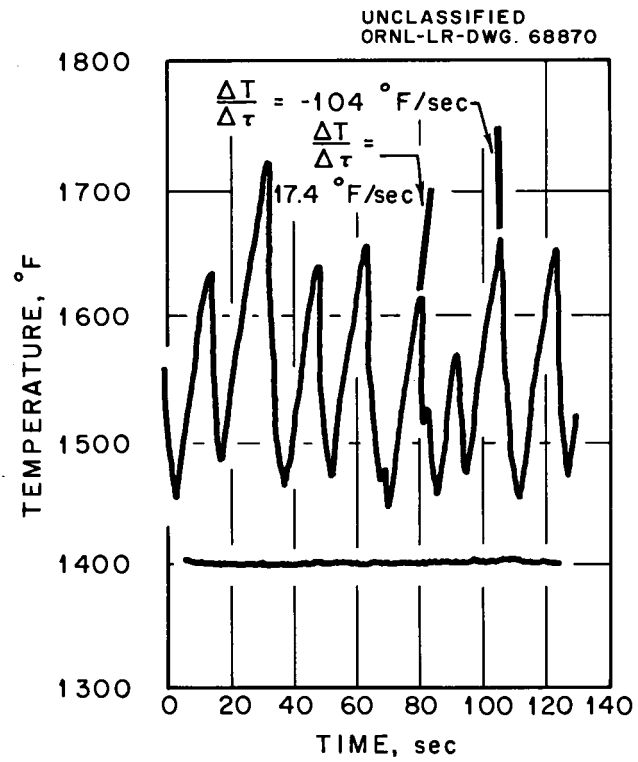


Fig. 2.4. Tube-Wall Temperature Oscillations Observed in Low-Flux Boiler.

of the fluctuation was ~ 0.05 to 0.10 cps with an amplitude of ± 150 to $\pm 200^\circ\text{F}$. In contrast, the lower curve traces a pattern seen under stable conditions at approximately the same inlet mass flow and exit quality (60%). The frequency of the oscillation was significantly higher (of the order of 0.35 cps) with amplitudes of only about $\pm 1^\circ\text{F}$. It was observed that high inlet subcooling (in excess of 40°F) existed for the runs with high-amplitude wall-temperature oscillations. Further, stable operation was possible only when vapor bubbles were present in the liquid at the boiler entrance.

Heat Transfer Results

Data from experiments with both boilers are given in Tables 2.1 and 2.2. As indicated, the Series A data (Table 2.1) correspond to the high-flux, small-diameter boiler. While experiments with the low-flux, large-diameter boiler were completed prior to this reporting period (experiments were terminated by a physical burnout in the pump cell), the pertinent results have been included for completeness; these have been designated Series B and are given in Table 2.2. The mass flow (lb/hr) through the small-diameter tube was essentially as in the low-flux experiments; however, the decreased flow area in the high-flux boiler resulted in appreciably larger mass fluxes (lb/hr·ft²). The heat flux used for correlation was in all cases based on the enthalpy change of the fluid across the boiler. Generally, this value was consistent to within $\pm 20\%$ with the heat flux as calculated from the temperature gradient in the copper disks or the electrical input to the heaters (corrected by precalibration for the external heat loss). Exit qualities in both boilers ranged between 10 and 90%.

The critical heat-flux values obtained in these experiments are shown in Fig. 2.5. In Series A, runs 12-14, 16-22, 30-33, and 36-38 culminated in "burnout"; while in Series B, runs 6.2-6.5 (stable wall temperature) and runs 5.1-5.3 and 8.1-8.3 (oscillating wall temperature) ended with the reaching of the critical heat flux. The $\sim 10\%$ reduction in mass flow arbitrarily selected as an operational procedure was often too large to sharply define the critical heat flux. For example, in Series A, runs 16-22, A21 showed signs of incipient burnout, while A22 had obviously

Table 2.1. Potassium Boiling: Series A Results.*

Run No.	$10^{-5} \times$ Inlet Mass Flow (lb/hr·ft ²)	Inlet Fluid Temperature (°F)	Exit Fluid Temperature (°F)	Exit Quality (wt % vapor)	Boiler ΔP (psi)	Heat Flux Q/A (fluid) (Btu/hr·ft ²)	Heat Balance		$\frac{\Delta T_{sat}}{(T_{w,1} - T_{sat})}$
							$\frac{Q_{electric}}{Q_{fluid}}$	$\frac{Q_{thru\ copper}}{Q_{fluid}}$	
1	1.58	1422.0	1392.8	10.9	2.7	60,200	0.96	0.72	7.5
2	1.49	1428.8	1389.7	17.9	3.4	94,000	0.97	0.79	11.0
3	1.21	1423.6	1388.0	21.4	2.8	92,300	0.98	0.80	11.1
4	1.51	1448.7	1402.1	21.1	4.4	112,000	1.18	0.90	19.0
5	1.33	1427.7	1394.2	23.1	3.3	107,600	1.01	0.93	16.3
6	1.09	1425.3	1395.6	27.9	2.8	99,900	1.08	1.01	15.3
7	1.23	1434.7	1404.6	27.1	3.4	109,400	1.09	0.94	15.1
8	0.99	1439.4	1409.2	33.4	2.8	108,600	1.02	0.95	12.2
9	1.41	1443.9	1373.9	34.3	6.8	155,600	0.99	0.94	27.6
10	1.13	1438.5	1373.3	43.2	6.1	158,000	0.98	0.93	24.1
11	0.99	1436.3	1374.7	48.4	5.3	157,200	0.99	0.98	20.1
12	1.40	1508.2	1428.4	50.4	7.1	245,800	1.09	1.01	28.6
13	1.21	1494.6	1413.7	58.3	6.4	247,500	1.10	0.99	33.0
14	1.08		1410*	67.1	6.4	253,000	1.07		
15	1.35		1385*	60.7	9.8	266,800	1.22		
16	1.44	1469.7	1370.5	47.8	8.9	220,300	1.14	1.16	44.6
17	1.25	1463.0	1370.8	54.0	7.9	218,200	1.15	1.18	42.0
18	1.17	1458.2	1366.6	58.2	7.7	221,100	1.14	1.16	40.1
19	1.04	1451.9	1366.6	64.8	6.9	220,400	1.14	1.12	39.2
20	0.90	1453.2	1360.6	75.6	6.3	222,700	1.12	1.18	40.2
21	0.87		1362*	77.7	6.1	220,500*			
22	0.77		1360*	86.2	5.7	220,500*			

Table 2.1. Potassium Boiling: Series A Results[†] (continued)

Run No.	10 ⁻⁵ × Inlet Mass Flow (lb/hr·ft ²)	Inlet Fluid Temperature (°F)	Exit Fluid Temperature (°F)	Exit Quality (wt % vapor)	Boiler ΔP (psi)	Heat Flux Q/A (fluid) (Btu/hr·ft ²)	Heat Balance		ΔT _{sat} (T _{w,i} - T _{sat})
							$\frac{Q_{\text{electric}}}{Q_{\text{fluid}}}$	$\frac{Q_{\text{thru copper}}}{Q_{\text{fluid}}}$	
23	1.421	1424.4	1394.5	19.4	3.9	106,920	1.120	0.8588	14.34
24	1.126	1418.9	1392.8	24.3	3.6	107,740	1.028	0.7853	12.50
25	1.143	1448.6	1403.0	31.7	5.4	145,690	1.080	0.9790	19.57
26	1.226	1442.6	1401.6	37.2	4.8	146,200	1.086	1.0691	16.35
27	1.782	1461.1	1382.3	35.4	8.6	197,220	1.117	1.0638	39.68
28	1.578	1460.7	1386.5	40.5	7.8	201,600	1.092	1.0821	35.75
29	1.844	1466.4	1386.7	36.8	8.9	292,590	1.085	0.9834	40.72
30	2.115	1479.0	1397.3	32.2	9.6	290,020	1.097	1.0044	41.12
31	1.467	1472.1	1402.0	46.5	7.7	297,350	1.095	1.0201	36.43
32	1.147	1465.9	1402.6	58.7	6.7	296,430	1.0953	1.0177	34.77
33	0.9367	1460.0*	1402.0*	73.4	6.5	304,960	1.0647		
35	2.06	1447.4	1415.7	17.1	3.7	174,000	1.000	0.92	
36	2.05	1481.9	1401.9	34.2	8.3	343,200	1.06	0.98	45.2
37	1.54	1463.7	1393.5	45.5	6.9	349,500	1.04	0.98	39.8
38	1.27	1450.6	1388.0	53.8	6.1	345,100	1.05	0.98	47.1
39	1.20	1462.4	1395.8	57.5	4.9	347,100	1.05	0.98	55.5
40	2.08	1484.1	1405.3	34.2	8.7	346,900	1.06	0.99	43.4
41	1.81	1472.8	1394.4	39.9	7.7	357,000	1.03	0.95	41.1

[†]High-flux boiler (0.325-in.-ID).

*Estimated.

Table 2.2. Potassium Boiling: Series B Results.[‡]

Run No.	$10^{-5} \times$ Inlet Mass Flow (lb/hr·ft ²)	Inlet Fluid Temperature (°F)	Exit Fluid Temperature (°F)	Exit Quality (wt % vapor)	Boiler ΔP (psi)	Heat Flux Q/A (fluid) (Btu/hr·ft ²)	Heat Balance		ΔT_{sat} ($T_{w,i} - T_{sat}$)
							$\frac{Q_{electric}}{Q_{fluid}}$	$\frac{Q_{thru\ copper}}{Q_{fluid}}$	
5.1*	0.28	1321.3	1391.9	42.4		32,080			
5.2*	0.25	1335.7	1396.0	45.1		32,360			
5.3*	0.22	1328.4	1386.0	50.0		30,750			
6.2	0.37	1401.5	1404.7	32.5	1.9	31,890	1.22		11.9
6.3	0.37	1404.3	1390.9	34.3	2.0	32,970	1.18		13.3
6.4	0.21	1378.1	1354.6	60.8	1.8	33,060	1.18		15.7
6.5	0.15	1361.2	1363.6	81.3	1.6	32,370	1.21		13.8
7.1	0.29	1373.0	1369.5	48.9	2.2	37,630	1.18		22.7
7.2	0.29	1365.5	1348.7	49.5	2.5	37,630	1.19		26.0
7.3	0.28	1395.1	1365.3	51.2	2.3	37,970	1.18		22.1
8.1*	0.23	1200.9	1307.2	33.0		21,900			
8.2*	0.15	1215.0	1312.2	50.9		21,000			
8.3*	0.13	1207.0	1300.9	61.0		21,100			

*Low-flux boiler (0.87-in.-ID).

*Runs with high-amplitude tube-wall temperature oscillations.

exceeded the limit; both points are plotted in Fig. 2.5. Comparison is made for the data of each boiler to an extrapolation of the results of Lowdermilk, Lanzo, and Siegel⁵ for the forced-convection saturation boiling of water,

$$(q/A)_{bo} = 270 (l/d)^{0.2} (d/L)^{0.85} G^{0.85} , \quad (2.1)$$

as adjusted to the specific geometries of the boilers. In Eq. 2.1, $(q/A)_{bo}$ is the critical heat flux (Btu/hr·ft²); d , the boiler diameter (ft); L , the boiler heated length (ft); and G , the mass flux (lb_m/hr·ft²). For runs through A29 the length of the high flux region (expressed in L/d) was 71; for runs A30 through A41, the heated length was 45. The total boiler length was 135 L/d . The agreement between the potassium experimental values and those predicted from water experience is seen to be quite good. Since the thermal properties of water and potassium are not too dissimilar, this result is not unexpected. Where stable wall-temperature fluctuations of high amplitude existed, the critical heat flux was reduced by about 40%; this is indicated by the dashed line in Fig. 2.5. The exit quality with this condition (~30%) is to be contrasted with the values of 85 to 95% observed when stable operation existed.

Data for heat fluxes below the critical are shown in Fig. 2.6 as a function of a mean superheat based on a linear fluid-temperature variation.⁴ For the low-flux boiler, the small pressure loss across the test section makes this a reasonable assumption. For the high-flux boiler, the choice of a straight-line fluid-temperature path is somewhat more questionable. However, in view of uncertainties in the calculated inside wall temperature, no allowance was made for possible curvature; it was estimated that this could introduce an error of as much as 5% in ΔT_{sat} . The dispersion in ΔT_{sat} on any flux level, which originally appeared to relate systematically to the exit quality, now seems to be more random. Some separation existed in the copper-stainless bond for runs following A22; this, coupled with the loss of a significant number of thermocouples,

⁵W. H. Lowdermilk, C. D. Lanzo, and B. L. Siegel, "Investigation of Boiling Burnout and Flow Stability for Water Flowing in Tubes," NACA-TN-4382, September 1958.

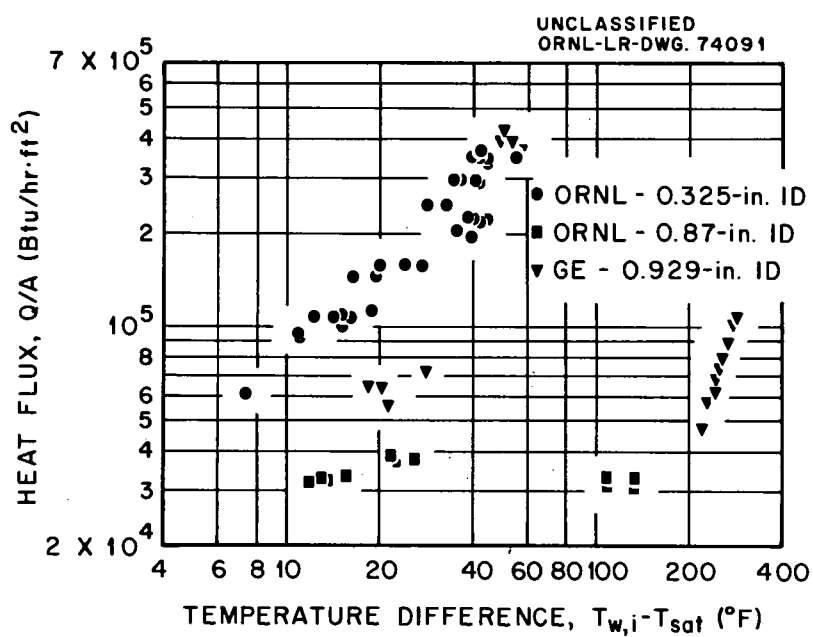


Fig. 2.6. Boiling Potassium Heat Transfer.

may account for the lack of consistency. Results obtained by Brooks⁶ using a concentric double-tube boiler with heat transfer from sodium to potassium have been included for comparison.

Pressure-Drop Data

The pressure loss across the boiler is shown in Fig. 2.7 as the variation of the pressure-loss ratio (total two-phase to equivalent liquid-only at the same inlet mass flow) with the exit quality expressed as the Lockhart-Martinelli⁷ parameter; a consistent pattern, with the total two-phase pressure drop increasing as the exit quality increased, was observed. In viewing this result, it should be kept in mind that the pressure taps were located approximately 2 ft upstream of the boiler entrance and about 1 ft beyond the exit; and thus, the data include the (unknown) losses associated with flow through an inlet mixing chamber, around exit-end thermowells, and through an expansion at the exit. Data obtained for the forced-convection boiling of water, when presented in similar form but with the exclusion of losses incurred outside the confines of the boiler, fall about a factor of three higher. A better comparison between potassium and water would be in terms of the frictional portion only of the pressure drop; however, information on the slip ratio in a mixed potassium liquid-vapor flow needed to account for the acceleration contribution to the total momentum change is not now available.

Future Experiments

A new boiler, similar in essential detail to the high-flux section shown in Fig. 2.2 is being constructed. This unit will contain Pt-Pt 10% Rh thermocouples for improved reliability and will include three positions along the tube at which wall temperatures will be measured directly. Pressure taps will be located at the inlet and exit and at the midlength of the boiler.

⁶R. D. Brooks, "Alkali Metals Boiling and Condensing Investigations," Quar. Prog. Rep. Jan. 1 - Mar. 31, 1962, General Electric Co., Flight Propulsion Laboratory, Cincinnati, Ohio.

⁷R. W. Lockhart and R. C. Martinelli, "Proposed Correlation of Data for Isothermal Two-Phase, Two-Component Flow in Pipes," Chem. Eng. Prog., 45: 39-48 (1949).

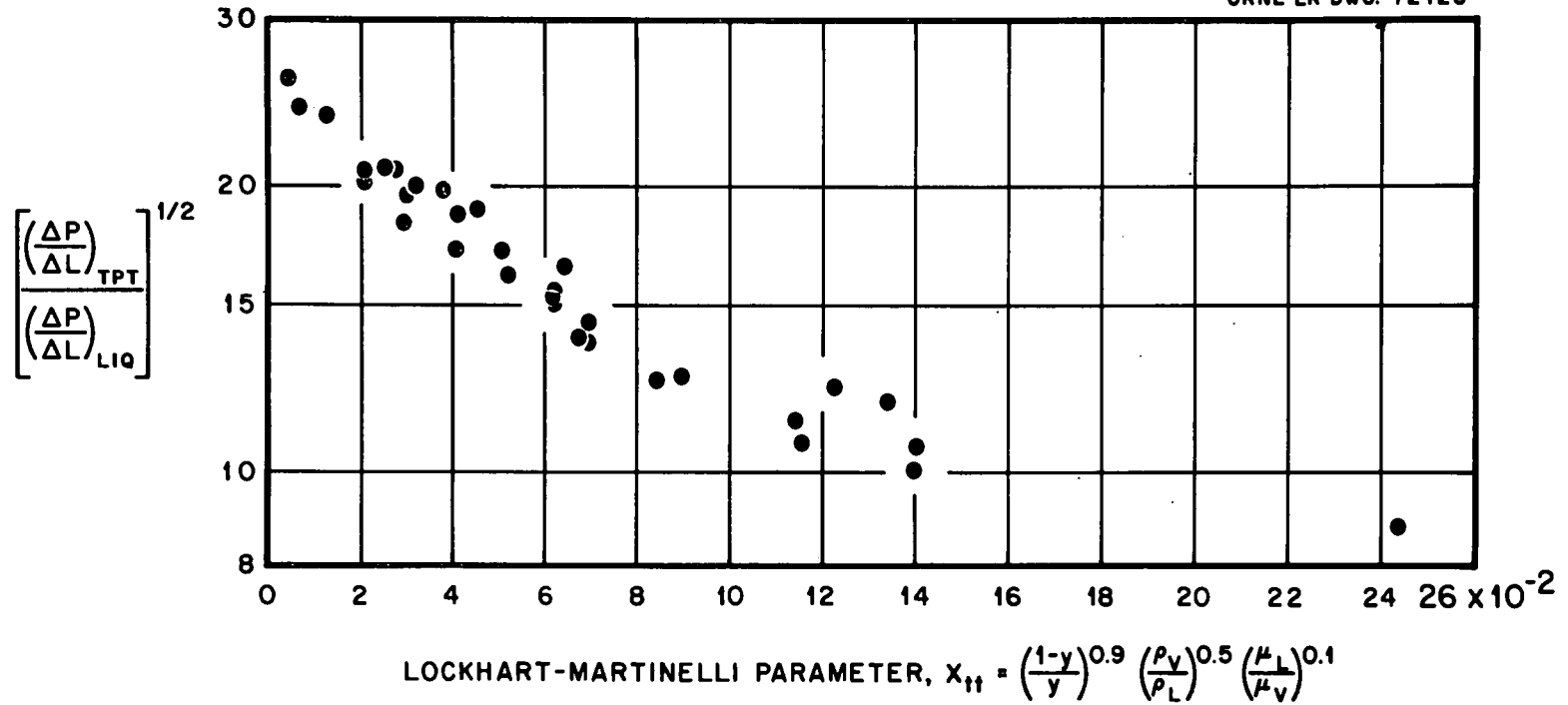


Fig. 2.7. Pressure Drop with Flow of Boiling Potassium Through a 0.325-in.-diam Tube.

Following completion of a series of recalibration experiments, the current boiler will be removed; and the loop prepared for the installation of the new test section.

2.1.2. Superheat Phenomena

A. I. Krakoviak

Analysis

A continued examination of the data obtained in the forced-convection loop as discussed above, along with that reported on the performance of a number of other natural circulation and forced-convection systems used in materials compatibility studies at ORNL, has led to a detailed consideration of the role of liquid superheat in the boiling process with alkali liquid metals.⁸ For example, in one small natural-convection apparatus with potassium, a boiling instability of a cyclic nature was noted.⁹ Temperature records show that the temperature of the liquid in the boiler increased from ~1600°F to ~1690°F over a period of 40 to 60 seconds; during this time the vapor temperature decreased. The fluid then erupted or exploded, and both liquid and vapor temperatures abruptly approached the value (1600°F) corresponding to the normal boiling temperature for the conditions of this loop; this process would then repeat in a cyclic fashion. It would appear then that substantial liquid superheat is required to initiate bubble formation and to sustain boiling. This can be demonstrated analytically as follows:

Consider first the condition for equilibrium of a spherical vapor bubble in a liquid pool; this can be expressed as,

$$P_v - P_\ell = \frac{2\sigma}{r} \quad , \quad (2.2)$$

⁸A. I. Krakoviak, "Notes on the Liquid Metal Boiling Process," USAEC Report ORNL-TM-618, Oak Ridge National Laboratory, 1963.

⁹E. E. Hoffman (in discussion of paper by A. I. Krakoviak), "Proceedings of 1963 High-Temperature Liquid-Metal Heat Transfer Technology Conference," USAEC Report ORNL-3605, Oak Ridge National Laboratory, (in preparation).

where P_v is the pressure of the vapor within the bubble; P_ℓ , the pressure in the liquid external to the bubble; r , the bubble radius, and σ , the surface tension of the liquid at the vapor-liquid interface. For bubble growth, P_v must be greater than P_ℓ . When evaporation into the bubble also exists, the temperature of the liquid exceeds that corresponding to the saturation temperature of the liquid at pressure, P_v . This excess temperature, over the saturation value at P_ℓ , is termed the liquid superheat.

If Eq. 2.2 is combined with the Clausis-Clapyron relation, as done by Ellion,¹⁰ there results the expression:

$$T_{w,i} - T_{sat} \cong \frac{2 R T_{sat}^2 \sigma}{h_{fg} P_\ell r}, \quad (2.3)$$

wherein it has been assumed that the specific volume of the liquid can be neglected in comparison with that of the vapor and that the gas law relation, $PV = RT$, describes the specific volume of the vapor. In Eq. 2.3, $T_{w,i}$ is the temperature of the surface on which the bubble forms; T_{sat} , the absolute temperature of the saturated liquid at P_ℓ ; R , the gas constant; and h_{fg} , the latent heat of vaporization of the liquid. This equation then predicts the approximate liquid superheat required for equilibrium for a bubble of radius, r .

Equation 2.3 has been tested and found adequate by a number of experimenters. Griffith and Wallis¹¹ studied nucleation of water, ethanol, and methanol from a copper surface containing conical cavities of 0.0018-in. diameter at the base. With this value for r , the calculated liquid superheat agreed well with the experimental results for the superheat required to maintain ebullition. Berenson¹² obtained similar results in

¹⁰M. Ellion, "Study of Mechanism of Boiling Heat Transfer," Jet Propulsion Laboratory Memorandum 20-88, March 1954.

¹¹P. Griffith and J. D. Wallis, "The Role of Surface Conditions in Nucleate Boiling," Chemical Engineering Symposium Series, 56: 49-63 (1960).

¹²P. Berenson, "Transition Boiling Heat Transfer from a Horizontal Surface," MIT Technical Report No. 17, Heat Transfer Laboratory, Massachusetts Institute of Technology, March 1960.

his investigation of the effects of surface roughness on the superheat involved in the boiling of liquid pentane.

Since Eq. 2.3 appears to represent the results for water and several organic fluids, it is presumed that the equation may also be applicable with liquid metals. For ease in calculation, the evaluation of the liquid superheats required for boiling with the several liquid metals has been made in comparison with water. Thus, using Eq. 2.3,

$$\frac{(T_{w,i} - T_{sat})_w}{(T_{w,i} - T_{sat})_x} = \frac{(\sigma T_{sat} V_{fg})_w}{(\sigma T_{sat} V_{fg})_x} \times \frac{(h_{fg} r)_x}{(h_{fg} r)_w}, \quad (2.4)$$

where the subscripts, w and x, denote respectively water and liquid metal, and V_{fg} is the specific volume change between liquid and vapor ($\cong V_v$, the vapor volume). Taking 30°F as the superheat required to sustain bubble formation from a particular surface with cavities of radius, r, immersed in water at atmospheric pressure, the superheats with the liquid metals were determined to have the values given in Table 2.3.

Table 2.3. Estimated Liquid Superheats Required to Sustain Boiling with the Alkali Liquid Metals

Fluid	Superheat, °F
Na	258
K	125
Rb	101
Cs	67

One further factor may be considered in relation to the superheat problem. The boiling sites (cavities) available on a natural surface (such as a pipe wall) will show a normal distribution of sizes. From Eq. 2.3, it is seen that as the temperature of the surface rises, bubble formation will begin first in the cavities of largest radius. As these sites are used up, the wall temperature will continue to rise and smaller and smaller cavities will be brought into action. Presumably these

cavities are not wet by the fluid; i.e., the fluid does not displace trapped or adsorbed gases. On the other hand, liquid metals wet most metals easily. It is to be expected then that the boiling site distributions will be drastically skewed, predominating in very small cavities. The superheats required to initiate bubble formation with the liquid metal will thus significantly exceed that required with water. In addition, since the liquid metals used are generally of very high purity and are in contact with clean surfaces in the absence of inert gases, the comparison of Eq. 2.4 should be made with water under similar conditions. It has been observed that for distilled, deaerated water in contact with a very clean surface the liquid superheat may be as high as 90°F. Thus, the values given in Table 2.3 may be as much as a factor of three greater.

The thermal diffusivities and the thermal conductivities of the liquid alkali metals grossly exceed those for water; e.g., the thermal conductivity of potassium is nearly 50 times that for water, and the thermal diffusivity ratio, K to H_2O is of the order of 335. Thus considering conduction only, the radial temperature distributions in a static column of water and potassium will be significantly different; a comparison is made in Fig. 2.8 for the condition of a uniform heat input of 30,000 Btu/hr.ft² through the wall of a circular tube of 1-in. diameter. With water, a bubble nucleating at the wall grows rapidly in the thin film of superheated liquid near the surface (~0.005 in. as indicated in Fig. 2.8b) and either collapses after leaving the wall, if the bulk fluid is subcooled, or remains as a stable or a slowly growing entity, if the bulk fluid is saturated. In contrast, with potassium, the bubble (once formed) remains in a highly superheated environment even at a distance far from the wall and can be expected to grow rapidly (even explosively) until the total energy available from the superheat is consumed. The energy available per unit volume in such a situation (assuming again a tube of 1-in. diameter for which the centerline temperature is ~340°F above saturation) is sufficient to vaporize the potassium to a quality of about 7.5%. This quality corresponds to a void fraction of 0.99 (assuming zero slip). The mechanism pictured

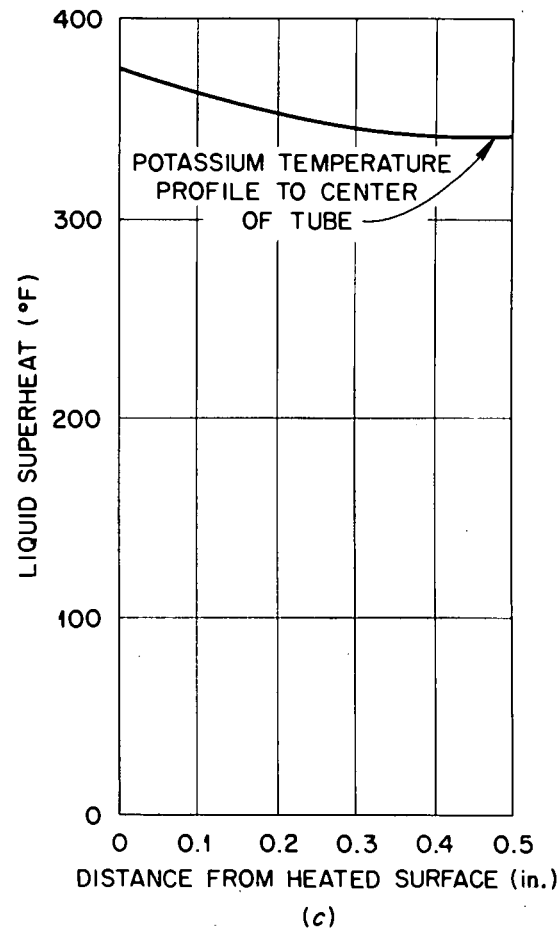
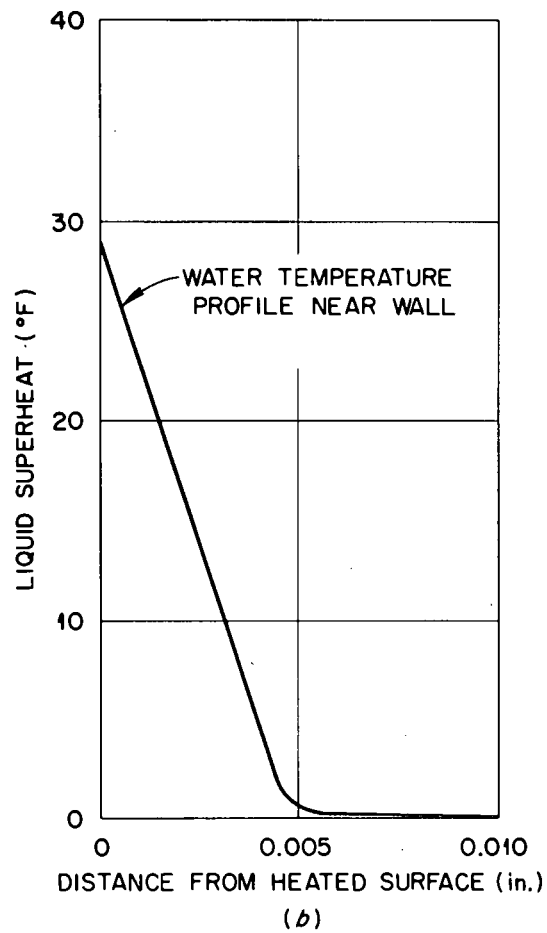
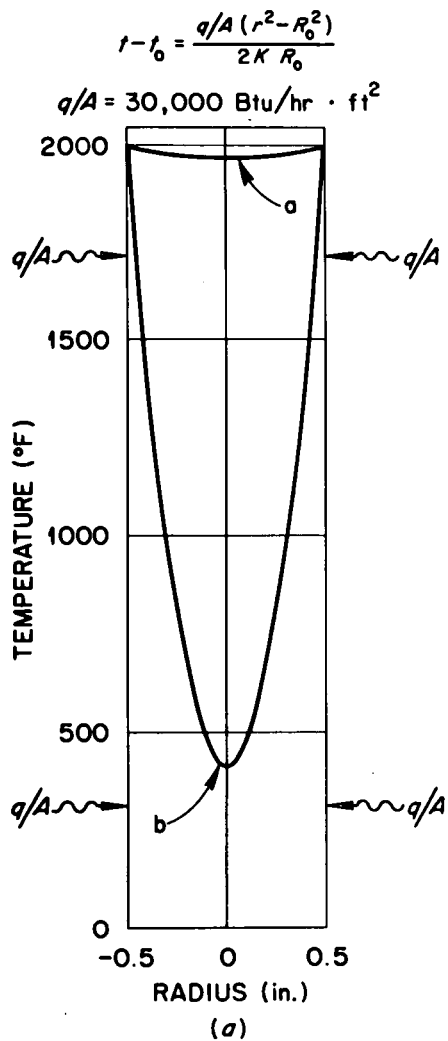


Fig. 2.8. Comparison of Radial Temperature Distributions in Water and Potassium Due to Conduction.
 $q/A = 30,000 \text{ Btu/hr} \cdot \text{ft}^2$; $D = 1 \text{ in.}$

is consistent with the pattern of temperature oscillations observed in the low-flux boiler during the previously described periods of high-amplitude tube-wall temperature fluctuations.^{4,13}

As noted earlier, stable performance (i.e., essentially steady tube-wall temperatures) has been observed only when vapor existed at the boiler inlet. This vapor was generated either by flashing across the inlet flow restriction or by allowing some boiling in the inlet mixing chamber; the inlet quality has been estimated at ~ 0.5 wt %. It is possible then that stability resulted from the presence of the bubbles in the liquid, thus circumventing the high superheat necessary for bubble nucleation. At the same time, the data of Radovcich and Moissis¹⁴ for the flow of air-water mixtures in a vertical tube suggest that an annular flow will exist for the conditions of this experiment (potassium flowing at $G = 0.6 \times 10^5$ lb/hr.ft² in 0.325-in. diameter tube with 0.5% inlet quality). The thickness of the liquid film on the wall has been calculated to be ~ 0.040 -in., assuming zero slip. Thus, allowing even the conservative superheat value given in Table 2.3 for potassium, conduction alone will sustain a thermal flux through a potassium film of 0.040-in. thickness of nearly 0.67×10^6 Btu/hr.ft² without nucleation. Hence, in all experiments to date, the heat transferred during stable operation can be accounted for by conduction through a thin liquid film on the tube wall followed by evaporation at the interface between the liquid film and the central gaseous core.

Experiment

Experiments to quantitatively define the above phenomena and hopefully to verify the predicted superheats have been initiated. A small natural circulation loop will be used. Since the design of this apparatus is still in a preliminary stage, further description will be postponed to a later report.

¹³Previous Section 2.1.1, Operating Characteristics.

¹⁴N. A. Radovcich and R. Moissis, "The Transition from Two Phase Bubble Flow to Snug Flow," MIT Report No. 7-7673-22, Department of Mechanical Engineering, Massachusetts Institute of Technology, June 1962.

2.2. Water Boiling in a Multirod Geometry

J. L. Wantland

The design optimization of a multirod fuel element cooled by a boiling liquid flowing axially along the rod cluster requires a knowledge of the maximum allowable (burnout) heat flux and of the two-phase pressure drop as these factors are influenced by the element geometry. The problem of burnout, in particular, for such complex geometries has received considerable attention during the past few years. It has been generally concluded¹⁵⁻¹⁹ from studies with internally heated annuli and with 3-, 7-, and 19-rod clusters that the burnout heat flux is lower than for single round ducts at the same conditions of quality, mass velocity, and pressure. Becker,¹⁶ for example, indicates that at the same heat flux and static pressure, the burnout steam quality was of the order of 75% in a round tube of 10 mm diameter and only 20% in a 3-rod cluster at 6 mm separation. While the causes of this difference have not been completely established, data on the film thickness with the flow of air-water mixtures in an annulus²⁰ indicate a thinner film on the central rod than on the tube wall. Becker concludes

¹⁵S. Levy, E. E. Polomik, C. L. Swan, and A. W. McKinney, "Eccentric Rod Burnout at 1000 lbf/in.² with Net Steam Generation," Int. J. Heat Mass Transfer, 5: 595-614 (July 1962).

¹⁶K. M. Becker, "Burnout Conditions for Flow of Boiling Water in Vertical Rod Clusters," A.I.Ch.E. Journal, 9: 216-222 (March 1963).

¹⁷"Basic Experimental Studies on Boiling Fluid Flow and Heat Transfer at Elevated Pressures," Task XIII Progress Reports MRP-X-3-61 through MPR-X-2-62, Columbia University (1961-1962).

¹⁸G. M. Hesson et al., "Preliminary Boiling Burnout Experiments with a 19-Rod Bundle Geometry in Axial Flow," USAEC Report HW-73395, Hanford Laboratories, 1962.

¹⁹J. G. Collier, "Heat Transfer and Fluid Dynamic Research as Applies to Fog Cooled Power Reactors," Atomic Energy of Canada Limited Report CRARE-1108, June 1962.

²⁰G. F. Hewitt and A. T. G. Stevens, "Two-Phase Annular Flow of Air/Water Mixtures in an Annulus. Part I: Film Thickness and Pressure Drop Measurements over a Range of Phase Flow Rates," British Atomic Energy Authority Report AERE-R-3957.

from his study that the ratio (η) of the heated perimeter to the total wetted perimeter is a significant variable and that as the number of heated elements in the cluster increases (i.e., as $\eta \rightarrow 1.0$) the burnout quality should approach that for flow inside tubes.

There exists, however, significant disagreement between various investigators as to the physical location of the burnout region. Thus, Levy et al.,¹⁵ studying an eccentric annulus, report burnout on the heated central rod in the region of closest approach to the outer wall of the annulus. It was also observed that, at the smallest gap, the burnout heat flux was reduced 15 to 30% below the concentric annulus value. In contrast, Becker¹⁶ with a 3-rod cluster found that burnout conditions existed on the portion of the rods facing the least restricted flow areas and that there was no significant effect of rod spacing. [Becker's data show the absolute difference in quality at burnout between a 6 mm and a 2 mm spacing to be 7% (the percentage change is about 25%). It is not at all clear that this should be considered insignificant.] The investigations of Becker and Levy differ primarily in (1) the pressure level and (2) the shape, area, and boundary conditions for the flow channel surrounding a unit rod. Both of these factors could be of importance in explaining the discrepancies between the two experiments.

With the goal of resolving some of these uncertainties, an experimental investigation of the phenomena associated with boiling in multirod geometries has been initiated. The effects of rod spacing, inlet subcooling, and outlet quality on the burnout heat flux will be considered over a range of near atmospheric pressure using deaerated, demineralized water as the test fluid. In a later aspect of this study, an apparatus will be constructed to examine boiling with potassium in a 7-rod geometry.

A photograph of the experimental system assembled for these studies is given in Fig. 2.9. The outer shells of all major loop components have been fabricated from flanged sections of glass piping to allow visual observation of phenomena occurring during boiling runs; at the same time, easy removal and exchange of individual units will be possible. The boiler will contain a cluster of seven 1/2-in. diameter Firerods of 10-in. heated length arranged in a triangular array with six rods surrounding

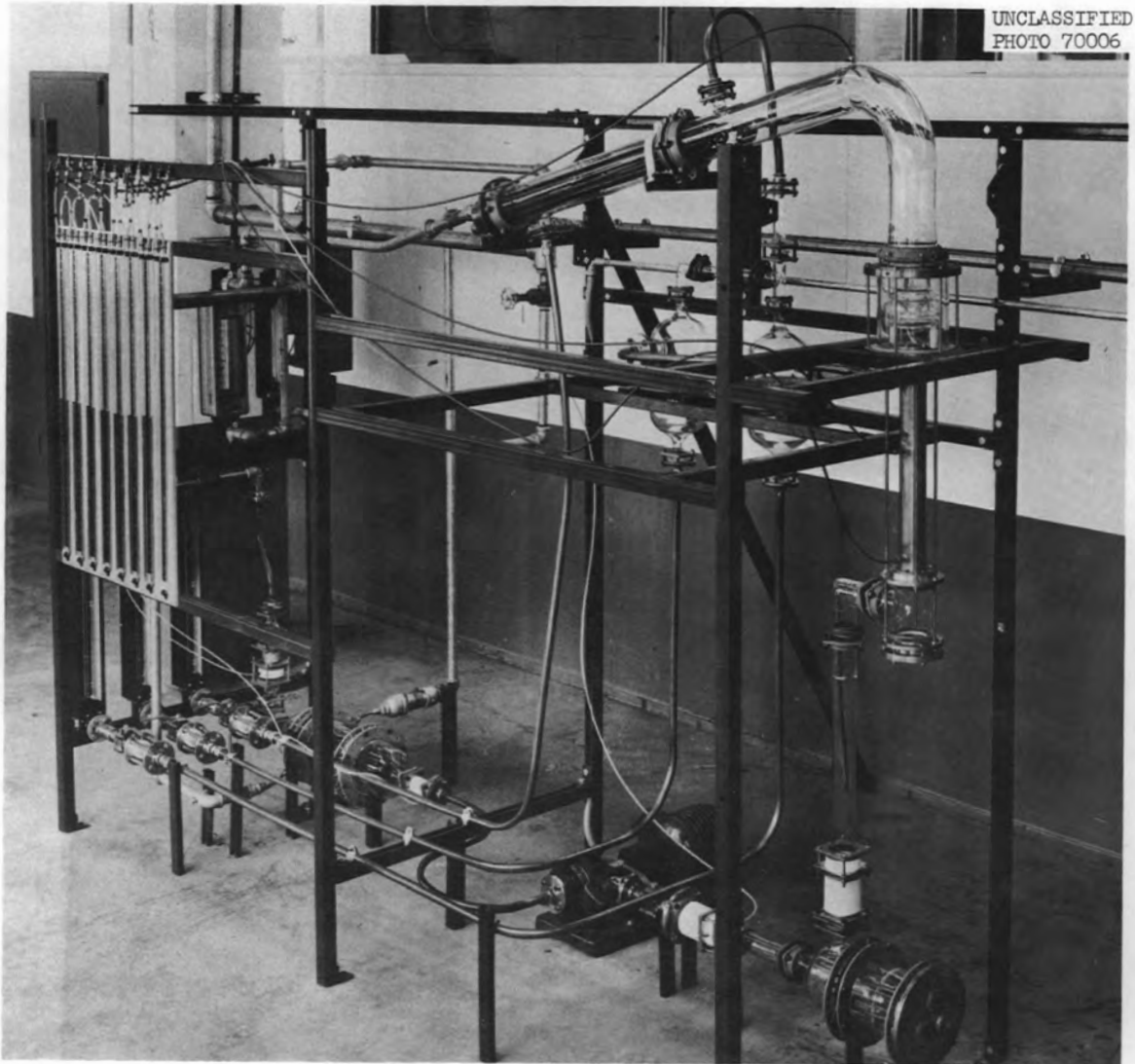


Fig. 2.9. View of Apparatus for Study of Critical Heat Flux with Water Boiling in a Multirod Channel.

the central seventh rod. Surface heat fluxes to 1.6×10^5 Btu/hr.ft² will be possible. Thermocouples embedded in the rods near the surface will provide both information on surface temperatures and the input signal to a device for protection against actual physical burnout. Boiler clusters with rods at spacings of 1/16, 1/8, and 3/16 in. in channels of 1 3/4-, 2-, and 2 1/4-in. diameter, respectively, are being fabricated for the initial studies; the corresponding ratios of heated-to-total perimeter are 0.67, 0.64, and 0.61. Dummy rod sections may be inserted in the channel to simulate hydrodynamic conditions of an infinite array of rods. The effects of roughness elements attached to the channel wall on the burnout flux will also be considered. Operation under both natural- and forced-circulation conditions will be possible.

2.3. General Boiling Studies

W. R. Gambill

2.3.1. Prediction of Critical Heat Fluxes

The fact that a boiling system is characterized by a peak of critical heat flux for which transition occurs from efficient nucleate boiling to high-thermal-resistance film boiling has prompted the proposal of many equations for predicting the peak flux. For a constant heat-input device such as a nuclear reactor, such a prediction is of prime importance; since the rapid rise of surface temperature which follows attainment of the critical heat flux usually results in melting or burnout of the heater surface; the term "burnout heat flux" is often used, as here, to denote the heat flux at the critical boiling transition.

Although previous correlations have been useful for specific limited conditions, they are generally characterized by one or more shortcomings which considerably restrict their generality:

1. The form of the equation may be such as to predict a critical flux of zero when the subcooling is zero, which is contrary to experience.
2. The equation may be applicable to only a single fluid, usually water.

3. The equation may have been statistically derived in a fashion far removed from physical considerations, an arbitrary attempt being made to relate the critical flux to the numerous experimentally controlled variables.

4. A given correlation, when compared with data other than those from which it was derived, is often found simply to give poor agreement with the other data.

A new additive correlation, generally applicable to flowing, sub-cooled, wetting liquids, has been developed²¹ in which a term representing the boiling contribution to the critical heat flux in the absence of forced convection is added to a term representing the equivalent forced-convection contribution in the absence of boiling. The predictions based on this superposition method have been compared with all available pertinent experimental data (1389 tests). These data are for seven fluids in tubular, annular, rectangular, and rod geometries over very broad ranges of flow conditions: velocity, V , 0.005-174 ft/sec; pressure, P , 4.2-3000 psia; subcooling, Δt_{sub} , 0-506°F; acceleration, a , 1-57,000 gee; and burn-out heat flux, ϕ_{bo} , $0.01 \times 10^6 - 37.4 \times 10^6$ Btu/hr.ft². When those data are excluded which can be shown to be unrepresentative of burnout under the experimental conditions, a selected data field of 941 tests remains, for which 96% of the predictions agree with the experimental values within a maximum deviation of 40%. If deviations which include 90% of the data are compared for all available data for burnout with water coolant only (943 tests), it is found that the additive correlation gives a deviation ~37% less than Bernath's extended correlation.²²

The correlation may be summarized as follows:

$$\phi_{\text{bo}} = (\phi_{\text{bo}})_{\text{boil}} + (\phi_{\text{bo}})_{\text{nb}} \quad , \quad (2.5)$$

²¹W. R. Gambill, "Generalized Prediction of Burnout Heat Flux for Flowing, Subcooled, Wetting Liquids," Chemical Engineering Progress Symposium Series, 59(41): 71-87 (March 1963).

²²L. Bernath, "A Theory of Local Boiling Burnout and Its Application to Existing Data," Chemical Engineering Progress Symposium Series, 56(30): 95-116 (1960).

where

$$(\phi_{bo})_{boil} = K L_v \rho_v \left[\frac{\sigma g_c a (\rho_l - \rho_v)}{\rho_v^2} \right]^{1/4} \times F_{sub} \quad (2.6)$$

and

$$F_{sub} = 1 + \left(\frac{\rho_l}{\rho_v} \right)^{0.923} \left(\frac{c_p \Delta t_{sub}}{25 L_v} \right) \quad (2.7)$$

In addition:

$$(\phi_{bo})_{nb} = h_{nb} (t_w - t_b)_{bo} \quad (2.8)$$

In these equations, ϕ_{bo} is the burnout heat flux; K , a constant (0.12 to 0.17); L_v , the latent heat of vaporization of the coolant; ρ_l and ρ_v , the liquid and vapor densities, respectively; σ , the surface tension; g_c , the force-to-mass conversion constant, a , the total acceleration acting on the cooled surface; subscripts 'boil' and 'nb' denote boiling and nonboiling, respectively; c_p , the constant-pressure specific heat; Δt_{sub} , the subcooling; h , the surface heat-transfer coefficient, and t_w and t_b , the wall and bulk coolant temperatures, respectively. Equation 2.7 is Kutateladze's empirical dimensionless subcooling factor for pool-boiling burnout as described by Bonilla.²³ The wall temperature at burnout, $(t_w)_{bo}$, is evaluated with Bernath's generalized plot²² of the liquid-film superheat at burnout as a function of the reduced saturation temperature.

2.3.2. Randomness in the Critical Heat Flux²⁴

In an effort to ascertain experimentally the inherent uncertainty of the critical heat flux in saturated pool boiling (a matter which has

²³C. F. Bonilla, pp. 399-431 of Chapter 9 ("Heat Removal") in Nuclear Engineering, McGraw-Hill Co., Inc., New York, 1957.

²⁴W. R. Gambill, "An Experimental Investigation of the Inherent Uncertainty in Pool-Boiling Critical Heat Fluxes to Saturated Water," to be presented at A.I.Ch.E. National Meeting, San Juan, Puerto Rico, September 1963.

been inconclusively debated for some time), a series of 234 tests was conducted with distilled, deionized water outside horizontal, a-c heated, A-nickel tubes in a pool 6 × 6 × 9-in. deep. The maximum relative uncertainty in the derived critical heat flux values was ±3%.

Six tests were conducted with tubes which were taken to physical burnout, and ~50 additional tests were made with each of four tubes protected by a burnout detector circuit which terminated the applied current before the wall temperature exceeded ~450°F. The results may be summarized as follows (for saturated water at an average pressure of 14.4 psia):

Table 2.4. Summary of Results in Study of Randomness in Critical Heat Flux

Tube No.	No. Tests	$10^{-6} \phi_{crit}$, Btu/hr·ft ²	
		Range	Average
1-6	6	0.368-0.546	0.464
7	49	0.334-0.548	0.472
8	50	0.483-0.596	0.537
9	52	0.413-0.498	0.457
10	54	0.299-0.450	0.353
10a	23	0.201-0.369	0.280

The range of heat fluxes given in Table 2.4 correspond to values of 'K' in the Kutateladze-Zuber burnout equation (Eq. 2.6 when $F_{sub} = 1$) of 0.076 to 0.224. The average temperature of the cooled surface at the critical flux for all the tests was 252°F, which corresponds to an average critical superheat of 41°F.

Large critical fluxes were observed when a very thin dark deposit or coating became visible on the tube surface, and its absence generally corresponded to smaller critical fluxes. The coating, when it formed, did not affect the measured surface roughnesses, which were ~14 μin. rms (±3 maximum).

Tests made with tube No. 9 were conducted under conditions of minimum surface variability, and for this test section, the maximum scatter in

the critical fluxes ($\pm 9.3\%$) was approximately triple the maximum relative experimental uncertainty. If the maximum relative experimental uncertainty is taken as equivalent to ± 3 standard deviations when considering tube No. 9 only, it may be shown that the probability of the existence of an inherent uncertainty in the critical-flux phenomenon is $>99.5\%$, when the evaluation is made at the 99.95% confidence level.

It is concluded that (a) there is an inherent uncertainty or intrinsic randomness in the critical flux determined under saturated pool boiling conditions which approximates that predicted by Zuber's hydrodynamic instability theory,²⁵ and (b) that the nature and condition of the cooled surface can constitute an important influence on the critical heat flux.

2.3.3. Internal Heat Transfer in a Horizontal Tube Immersed in a Water Pool

Pool heat-transfer studies have previously been conducted with externally and internally cooled vertical tubes and with externally cooled horizontal tubes, but no study of internally cooled horizontal tubes has appeared. An exploratory investigation of this case was accordingly conducted using ac-heated nickel tubes which were externally vacuum jacketed. Since the ends of the tubes were open and most of the heat was directed radially inward, a pulsating flow condition was obtained in a majority of the tests, during which liquid flow inward toward the tube center alternated with two-phase pulses of water and steam toward the ends. This pulsating flow was characteristic of tubes of large L/D ratio; and with such tubes, the wall temperatures increased gradually without sudden excursions as the heat flux was increased. With tubes of small L/D ratio, however, behavior characteristic of critical-flux attainment was observed, at which flux the wall temperature rose rapidly.

A total of 171 tests was conducted with water at atmospheric pressure using tube of 1/8-, 1/4-, and 3/8-in. outside diameter, nominal heated lengths of 4, 8, and 12 in., and three degrees of pool subcooling. An

²⁵N. Zuber and M. Tribus, "Further Remarks on the Stability of Boiling Heat Transfer," University of California Engineering Department Report 58-5, January 1958.

additional series of 31 tests was conducted in an air environment. The data are being reduced to show the dependence of average and maximum wall temperature and two-phase pulse rate on average heat flux for various diameters, lengths, and subcoolings.

2.4. Swirl-Flow Heat Transfer

W. R. Gambill

2.4.1. Heat-Transfer Characteristics of Ethylene Glycol²⁶

In order to gain a more complete understanding of the influence of physical properties on swirl-flow heat transfer, a swirl-flow study of ethylene glycol was initiated for comparison with the results obtained previously using water. The program was broadened to finally encompass the pool boiling, forced-convection nonboiling and local boiling, and burnout characteristics of ethylene glycol in both axial and swirl flow. A few tests were made under cooling conditions.

Apparatus

The system used was basically the same as that used for the water studies²⁷ (Fig. 2.10). Moyno and turbine pumps were used singly or together to pump the glycol through horizontal copper or 347 stainless steel test sections, resistance heated by 60 cycles/sec ac current. The glycol was contained in a mixed overhead holdup drum which could be steam heated or water cooled with internal coils. A cooler tube, which followed the heater tube in some tests, was externally jacketed to form an annular flow passage for longitudinal flow of cooling water; 40-gauge (3-mil-diam) chromel/alumel thermocouples were embedded in the cooler tube wall. An upstream calming section longer than 40 diameters was used in all axial-flow tests. Swirl flow was generated with thin

²⁶W. R. Gambill and R. D. Bundy, "High-Flux Heat-Transfer Characteristics of Pure Ethylene Glycol in Axial and Swirl Flow," A.I.Ch.E. Journal, 9(1): 55-59 (1963).

²⁷W. R. Gambill, R. D. Bundy, and R. W. Wansbrough, "Heat, Burnout, and Pressure Drop for Water in Swirl Flow Through Tubes with Internal Twisted Tapes," USAEC Report ORNL-2911, Oak Ridge National Laboratory, 1960; see also, Chem. Eng. Prog. Symposium Series, 57(32): 127-137, (1961).

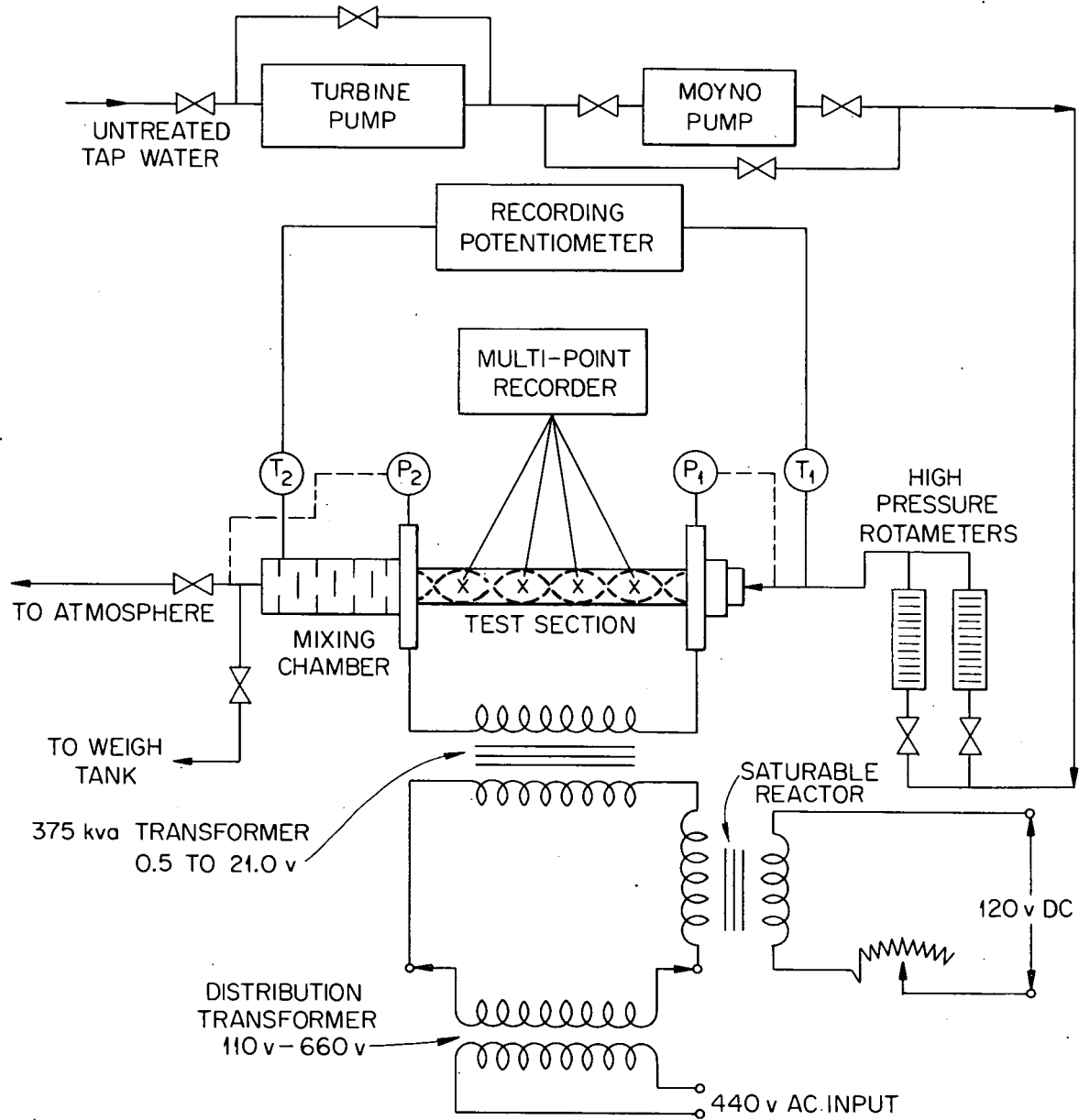
UNCLASSIFIED
ORNL-LR-DWG 29245A

Fig. 2.10. Experimental Apparatus for Vortex-Flow Heat-Transfer Studies.

(15-mil-thick) twisted tapes, onto which the tubes were drawn; a description of these tubes is to be found in Ref. 27.

Burnout tests were concluded by physical destruction of the test section (usually near the flow exit). Burnout was attained by slowly increasing the heat flux at essentially constant velocity, pressure, and inlet glycol temperature.

The pool boiler measured nominally $6 \times 6 \times 9$ in. deep. The horizontal heater tube was silver soldered across two insulated copper end plates which served as electrodes; the bottom and sides were made of welded stainless steel plate. Thermocouples (chromel/alumel in all tests) were placed inside the heater tube and longitudinal traverses made under heating conditions to determine the location of the isothermal zone. External silver voltage leads and the four internal thermocouples were then located within this zone.

Three analyses of the glycol in the loop were made during the tests; the composition ranged from 99.6 to 99.8 wt % glycol (balance water). No glycol decomposition or wall deposition was noted.

Nonboiling Heat Transfer - Axial Flow

The axial-flow data were correlated to within average and maximum deviations of 7.3% and 17.8% respectively, by:

$$(N_{Nu})_{bm} = 0.00465 (N_{Re})_b^{0.98} (N_{Pr})_b^{0.6} \quad (2.9)$$

where, N_{Nu} , N_{Re} , N_{Pr} represent the Nusselt, Reynolds, and Prandtl moduli, respectively. The subscript b indicates that bulk properties are used in evaluating the modulus; and the subscript m, that this is a mean value.

Note that at the high Reynolds moduli and heat fluxes of this experiment, the Nusselt modulus dependence on the Reynolds modulus is very close to the first power rather than the more commonly observed 0.8 power.

Nonboiling Heat Transfer - Swirl Flow

Both the glycol and the earlier water²⁷ swirl-flow heating data have been correlated to within an average deviation of $\pm 12.0\%$ by the relation:

$$\left[\frac{(N_{Nu})_{sm}}{(N_{Re})_a^{0.89} (N_{Pr})^{0.6}} \right] = 0.00675 \left[\frac{(\rho \beta \Delta t)_f u_a^2}{y^2 D_i} \right]^{0.0344} \quad (2.10)$$

in which the dimensional group on the right side of the equation (proportional to the buoyant force per unit fluid volume in the boundary layer) should be evaluated in units of lb/ft³, ft/sec, ft, and °F. In Eq. 2.10, ρ is the fluid density; β , the volumetric coefficient of thermal expansion of the coolant; Δt , the film temperature difference; u_a , the axial coolant velocity; y , the tape-twist ratio expressed as inside tube diameters per 180-deg twist; and D_i , the internal tube diameter. The subscript s indicates swirl flow; m, the mean value; and a, that the Reynolds modulus is based on the axial flow velocity and the tube inside diameter.

Burnout Heat Flux

The atmospheric pressure, saturated, pool-boiling critical flux for ethylene glycol was found to be ~168,000 Btu/hr·ft².

The forced-convection axial- and swirl-flow burnout data obtained are given in Table 2.5. The predictions of the additive burnout correlation²¹ are in good general agreement with these data.

Conclusions

It was concluded that:

1. The friction-factor equation as given in Ref. 27 is adequate for predicting isothermal friction factors for a variety of fluids in swirl flow.
2. Organic fluids, and perhaps water, give larger nonboiling axial-flow heat transfer coefficients at high velocities and heat fluxes than predicted by standard correlations. For such conditions the Reynolds number exponent appears to be nearer 1.0 than 0.8.
3. Use of the buoyant force per unit coolant volume gives a better overall correlation of heating and cooling swirl-flow heat transfer coefficient data than does $(N_{Gr}/N_{Re}^2)_a$. Equation 2.10 adequately correlates all available ORNL swirl-flow heating data.

Table 2.5. Forced-Convection Burnout Tests with Ethylene Glycol

Test No.	Test Section					t_{b1} , °F	P_{bo} , psia ^c	$(V_a)_{bo}$, fps	$(t_{sat})_{bo}$, °F	$(t_b)_{bo}$, °F	$(\Delta t_{sub})_{bo}$, °F	a/g, gees ^d	$\frac{x_{bo}}{L_h}$	$(\phi_{bo})^e$, 10^{-6} Btu/hr·ft ²
	D_i , in.	L_h , in.	Material	y^a	$\bar{\epsilon}$, μ in. rms ^b									
1	0.249	11.91	Copper	4.73	17.7	138	41.0	25.4	427	337	90	212	0.96	3.68
2	0.249	11.88	Copper	2.26	24.3	72	279.0	72.0	536	117	419	7510	0.26	9.00
3	0.136	13.81	Copper	2.43	63.3	148	140.0	63.2	493	416	77	9190	0.96	5.32
4	0.249	11.98	Copper	7.73	43.3	73	170.0	38.0	506	80	426	178	0.04	4.38
5	0.249	11.98	Copper	11.81	27.9	127	43.9	62.3	431	264	167	204	0.96	5.99
6	0.249	11.98	Copper	12.10	20.4	98	20.4	35.0	398	259	139	62	0.96	3.97
7	0.249	11.98	Copper	12.05	27.5	115	33.3	97.5	418	234	184	484	0.96	8.11
8	0.249	11.98	Copper	7.74	21.5	73	19.9	28.2	397	252	96	98	0.96	3.42
9	0.249	11.98	Copper	2.18	22.7	145	27.1	66.8	408	311	97	6940	0.96	8.03
10	0.249	11.98	Copper	No tape	32.9	124	19.5	17.3	396	240	156	1	0.96	2.06
11	0.249	12.94	Copper	No tape	29.6	127	31.7	88.4	415	234	181	1	0.89	6.25
12	0.249	12.10	Copper	No tape	37.8	149	31.4	60.2	415	260	155	1	0.96	4.89
13	0.249	7.25	347 ss	2.45	27.3	111	36.9	21.4	439	115	324	564	0.07	2.33
14	0.249	7.19	347 ss	2.38	28.2	103	64.2	30.6	450	108	342	1221	0.07	3.40
15	0.249	11.98	Copper	No tape	25.8	124	87.7	67.3	467	203	264	1	0.66	6.23
16	0.249	11.90	Copper	No tape	f	122	29.1	40.6	412	227	185	1	0.94	3.42

^aChecked by x-ray measurements.^bAverage value determined after test at 3 and 8 axial positions.^cAll pressures are subcritical.^dCalculated from equation based on rotating slug-flow model (ref. 1).^eThe local ϕ_{bo} at the burnout site, which is the value listed, differed from the tube-average ϕ_{bo} by <5% in all cases.^fNot measured.

4. With saturated pool boiling, axial forced-convection local boiling, and swirl forced-convection local boiling, respectively, ethylene glycol is characterized, for the variable ranges of this study, by burnout heat fluxes $\sim 1/3$, $1/2$, and $3/4$ those for water at the same conditions of geometry, velocity, pressure, and bulk temperature.

2.4.2. Swirl-Flow Boiling with Net Vapor Generation

Test sections were designed and fabricated for use in the two-phase swirl-flow boiling studies. These test sections are 1/4- and 1/2-in.-ID A-nickel tubes 22 in. long fitted with internal twisted tapes of 0.015-in.-thick Inconel. The initial objective of the study is the determination of critical heat fluxes over the following variable ranges: exit pressure = 15 to 30 psia, inlet water velocity = 1 to 3 fps, tape twist ratio = 2.5 to 8.0 inside diameters per 180-deg twist, inlet subcooling = 0 to 30°F, exit quality = 30 to 80 wt %, all with a vertical orientation of the test section. Three heat exchangers - a preheater, a condenser, and a liquid return cooler - have also been designed and ordered.

3. FLOW DYNAMICS AND TURBULENCE

3.1. Vortex Fluid Mechanics

J. J. Keyes, Jr.

Consideration of the unique fluid mechanical properties of vortex-type flows has stimulated interest in the application of these flows to certain advanced energy conversion concepts. The magnetohydrodynamic vortex power generator, for example, utilizes a plasma in vortex flow interacting with a magnetic field to generate an electric field.²⁸ The cavity gaseous fission reactor concept described by Kerrebrock and Meghreblian²⁹ depends on a vortex velocity field for containment of the fissionable material. These applications require operation with a high ratio of tangential to radial through-flow velocity; hence, energy losses due to viscous dissipation through turbulence must be minimized so that the energy required to sustain the vortex will be small compared with the energy output of the device.

Vortex-type flows are also of general concern in connection with separation processes in the nuclear field; e.g., gas-phase separation of isotopic species, liquid-vapor separation in chemical processing and in Rankine cycle space power systems, and liquid-solid separation in chemical processing. There is also much interest in flows having a strong tangential component (e.g., swirl flow) for heat-transfer applications, as discussed in Section 2.4 of this report. Internal swirl and vortex flows are closely related, particularly with regard to boundary-layer phenomena. In considering the use of vortex flow for gas separation or for heat transfer, a knowledge of the interrelationship of the vortex strength and the turbulent energy dissipation is of fundamental importance.

²⁸W. S. Lewellen and W. R. Grabowsky, "Nuclear Space Power Systems Using Magnetohydrodynamic Vortices," Am. Rocket Soc., 693-700 (May 1962).

²⁹J. L. Kerrebrock and R. V. Meghreblian, "An Analysis of Vortex Tubes for Combined Gas-Phase Fission-Heating and Separation of the Fissionable Material," USAEC Report ORNL-CF-57-11-3, Oak Ridge National Laboratory, April 11, 1958.

3.1.1. Gas Dynamics Studies

The vortex gas dynamics work at ORNL has aimed at providing the following basic fluid mechanical information needed in evaluating the various applications of jet-driven vortex flow:

1. Vortex strength (peripheral, tangential velocity, or Mach number) as a function of such key variables as tube diameter, mass flow rate, injection velocity and geometry, and pressure, with the aim of obtaining the maximum vortex strength per unit of input power.
2. Turbulence levels as functions of appropriately defined Reynolds moduli.
3. The separation characteristics of vortex flow for a mixture of light and heavy gases, including effects of turbulence.

The experimental work conducted thus far, much of which is reported in Refs. 30 through 34, has provided a fair elucidation of item 1; and it now appears possible to generate vortexes in small diameter tubes (1.0 in. or less) of sufficient strength to be of preliminary interest for gaseous reactor and other applications. Due to the high level of

³⁰J. L. Kerrebrock and J. J. Keyes, Jr., "A Preliminary Experimental Study of Vortex Tubes for Gas-Phase Fission Heating," USAEC Report ORNL-2660, Oak Ridge National Laboratory, February 6, 1959.

³¹J. J. Keyes, Jr. and R. E. Dial, "An Experimental Study of Vortex Flow for Application to Gas-Phase Fission Heating," USAEC Report ORNL-2837, Oak Ridge National Laboratory, April 16, 1960.

³²J. J. Keyes, Jr., "An Experimental Study of Gas Dynamics in High Velocity Vortex Flows," Proceedings of the 1960 Heat Transfer and Fluid Mechanics Institute, pp. 31-46, Stanford University Press, Stanford, California, 1960.

³³J. J. Keyes, Jr., "An Experimental Study of Flow and Separation in Vortex Tubes with Application to Gaseous Fission Heating," Am. Rocket Soc., 1204-1210 (September 1961).

³⁴H. W. Hoffman et al., "Fundamental Studies in Heat Transfer and Fluid Mechanics, Status Report July 1, 1959 - February 29, 1960," USAEC Report ORNL-CF-60-10-6, Oak Ridge National Laboratory, October 1960.

turbulent shear near the periphery, however, the efficiency of vortex formation has been low in the experiments carried out thus far.[§] Interpreted in terms of a practical device, this means that bleed-off (radially outward or axially) of a significant fraction of the inlet mass flow would be required to sustain the vortex without exceeding the allowable exit mass flow rate as determined by diffusional velocities.

Preliminary separation experiments have been performed³¹⁻³³ which suggest that turbulence may be effectively suppressed by the strong density gradient in the central region of the vortex field. The effect of turbulence in the outer region of the vortex on separation has been quantitatively ascertained, but intuitively it is believed that only low-turbulence levels can be tolerated in this region.

Specific vortex tube geometries studied in the initial phase of the investigation²⁸⁻³⁴ are described in Table 3.1. Figure 3.1 is a photograph depicting four typical vortex tube geometries studied. For all geometries, the radial static pressure distribution, from which tangential velocities were determined by the method described in Ref. 31, was measured by means of pressure taps drilled in the closed end of the tube.

The nomenclature employed in correlating the data is as follows:

M_p tangential Mach number at the tube periphery

M_j injection Mach number

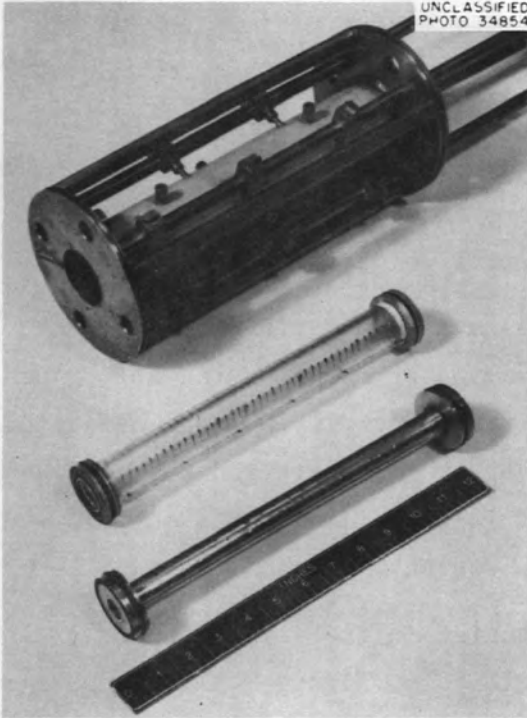
$m \equiv 2 \pi r Q_r \rho$ mass flow rate, lb/sec·ft

$N_{Re_r} \equiv \frac{m}{2 \pi \mu}$ radial Reynolds modulus

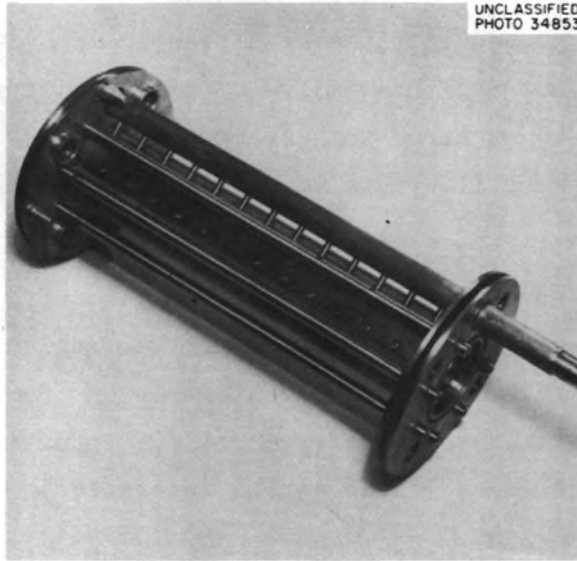
$N_{Re_{t,p}} \equiv \frac{2 r_p Q_p \rho_p}{\mu_p}$ tangential peripheral Reynolds modulus

$\alpha = \frac{M(r' = 0.8)}{M_j}$ jet velocity recovery ratio

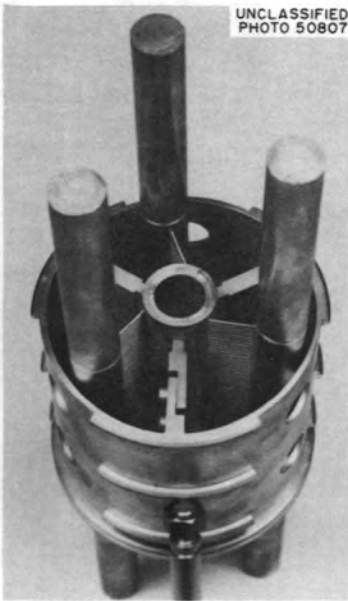
[§] Efficiency of vortex formation is directly proportional to vortex strength and inversely proportional to the net power input required to sustain the vortex.



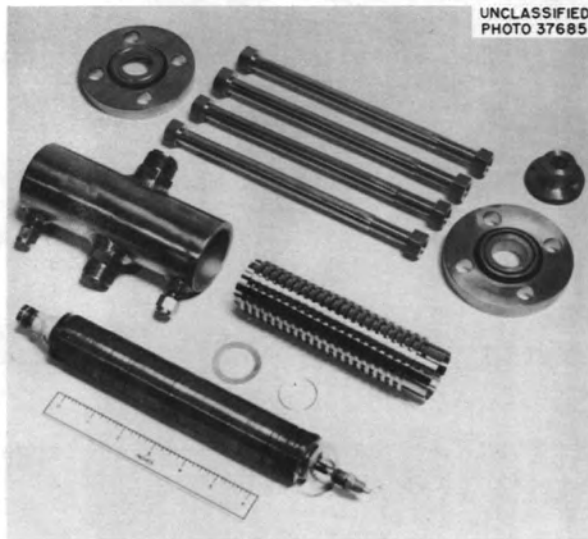
2-in.-DIAM POROUS TUBE WITH 1-in.- AND 0.6-in.-DIAM INSERTS



2-in.-DIAM SLIT-FED TUBE



1-in.-DIAM TUBE SLOTTED FOR BOUNDARY-LAYER BLEED OFF



ASSEMBLY OF 1-in.-DIAM LAMINATED TUBE; WIDE WASHERS CORRUGATED TO GIVE A TOTAL OF 360,000 INJECTION JETS

Fig. 3.1. Typical Vortex Tubes.

Note that the only dimensional quantity is m , the mass flow rate; Q_r and Q_p are the radial and tangential peripheral velocity, respectively; ρ and μ are fluid density and absolute viscosity, respectively.

Table 3.1. Description of Experimental Vortex Tubes

Tube No.	Tube ID, 2 r_d , in.	Tube Length, in.	Injection Geometry			Exit Radius	
			Description	Diam or Width, in.	Radial Position r'_a	Tube Radius r'_e	
1	2.00	12.0	12 nozzles	0.0135	0.92	0.140	
2	2.00	12.0	12 nozzles	0.0100	0.84	0.140	
3	2.00	12.0	12 nozzles	0.0135, 0.0330	0.92	0.0625-0.250	
3A	1.00	12.0	12-164 nozzles	0.020	0.90	0.280-0.500	
3B	0.63	3.25, 6.0, 12.0	11-54 nozzles	0.020	0.90, 0.95	0.380-0.525	
4A	2.00	12.0	12-in.-long slit	0.002	1.00	0.140	
4B	2.00	12.0	12-in.-long slit	0.002	0.92	0.140	
5	0.64	3.5	12 nozzles	0.028	0.88	0.308-0.362	
6	0.315	1.75	60 nozzles	0.0135	0.90	0.3-0.5	

The values of peripheral tangential Mach number, M_p , which were observed in 0.64- and 2.0-in.-diameter tubes with N_2 gas injected at room temperature and at sonic velocity, $M_j = 1$, are indicated in Fig. 3.2 as a function of the mass flow rate. The data include measurements with tube wall pressures of 83 and 108 psia. It must be pointed out that, based on the original laminar flow analysis,²⁹ a peripheral Mach number approaching unity should be achievable at the allowable mass flow rates of 0.01 to 0.02 lb/sec·ft. Note, however, that in this range of mass flows

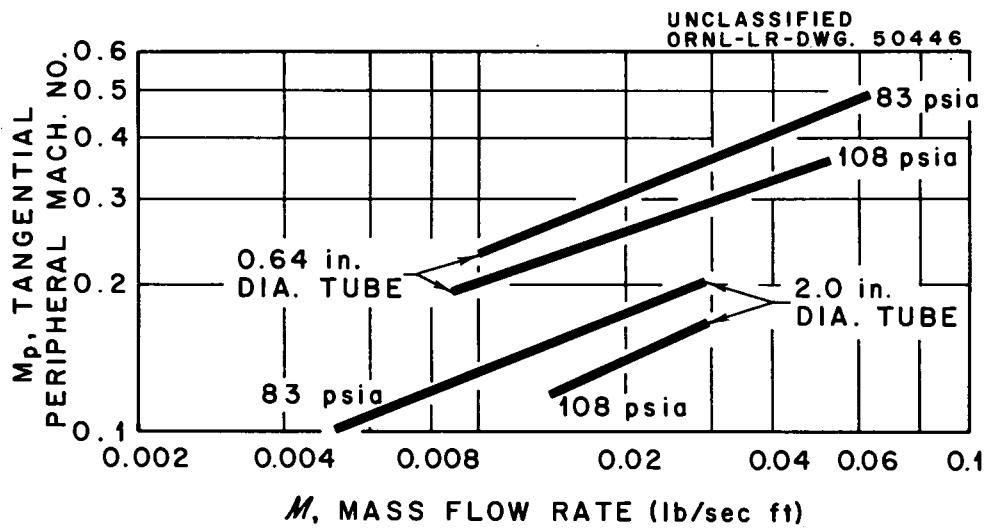


Fig. 3.2. Tangential Peripheral Mach Number vs Mass Flow Rate.
 $M_j = 1.0$; based on experimental results for N_2 gas, $75^\circ F$.

the values of M_p actually observed varied from approximately 0.10 to 0.18 for the 2-in. tube, and from approximately 0.2 to 0.3 for the 0.64-in. tube. The highest peripheral Mach number of 0.49 was observed in a 0.64-in.-diameter tube, and required a mass flow rate of 0.06 lb/sec-ft. Since the observed velocities were significantly lower than would be expected for laminar flow, it is probable that boundary layer turbulence existed with correspondingly high wall shear.

Figure 3.3 illustrates the effect of decreasing tube diameter on the tangential Mach number to injection Mach number ratio plotted as a function of radial position. The humps in the curves for the 0.64- and 0.20-in. tubes may be associated with secondary flow and/or injection effects. Note that, as the tube diameter decreases with corresponding decrease in $N_{Re_{t,p}}$, the velocity ratio generally increases. The concave downward shape of the profile for the 0.32-in.-diameter tube suggests that the turbulent boundary layer may, in this case, represent a significant fraction of the tube radius. Three-dimensional flow effects also play an important role.

Preliminary estimates of the degree of turbulence in vortex flow were made by comparison of observed velocity profiles with published solutions of the Navier-Stokes equations in terms of virtual viscosity (molecular viscosity plus eddy viscosity). Figure 3.4 shows the observed ratio μ^*/μ of virtual to molecular viscosity near the periphery as a function of tangential peripheral Reynolds modulus, $N_{Re_{t,p}}$, for three tubes sizes, N_2 and He gas. At the lowest Reynolds modulus, 4×10^4 , $\mu^*/\mu \cong 30$; and at the highest Reynolds modulus, 1.6×10^6 , the ratio is nearly 700. The ratio would, of course, be unity for laminar flow. Since the operating Reynolds modulus may be in the range from 1×10^5 to 1×10^6 , it is suggested that turbulence will probably exist near the periphery.

It must be pointed out that the estimates of virtual viscosity are based on a two-dimensional flow analysis in which the radial mass flow is assumed uniform and equal to that which exhausts at the center of the

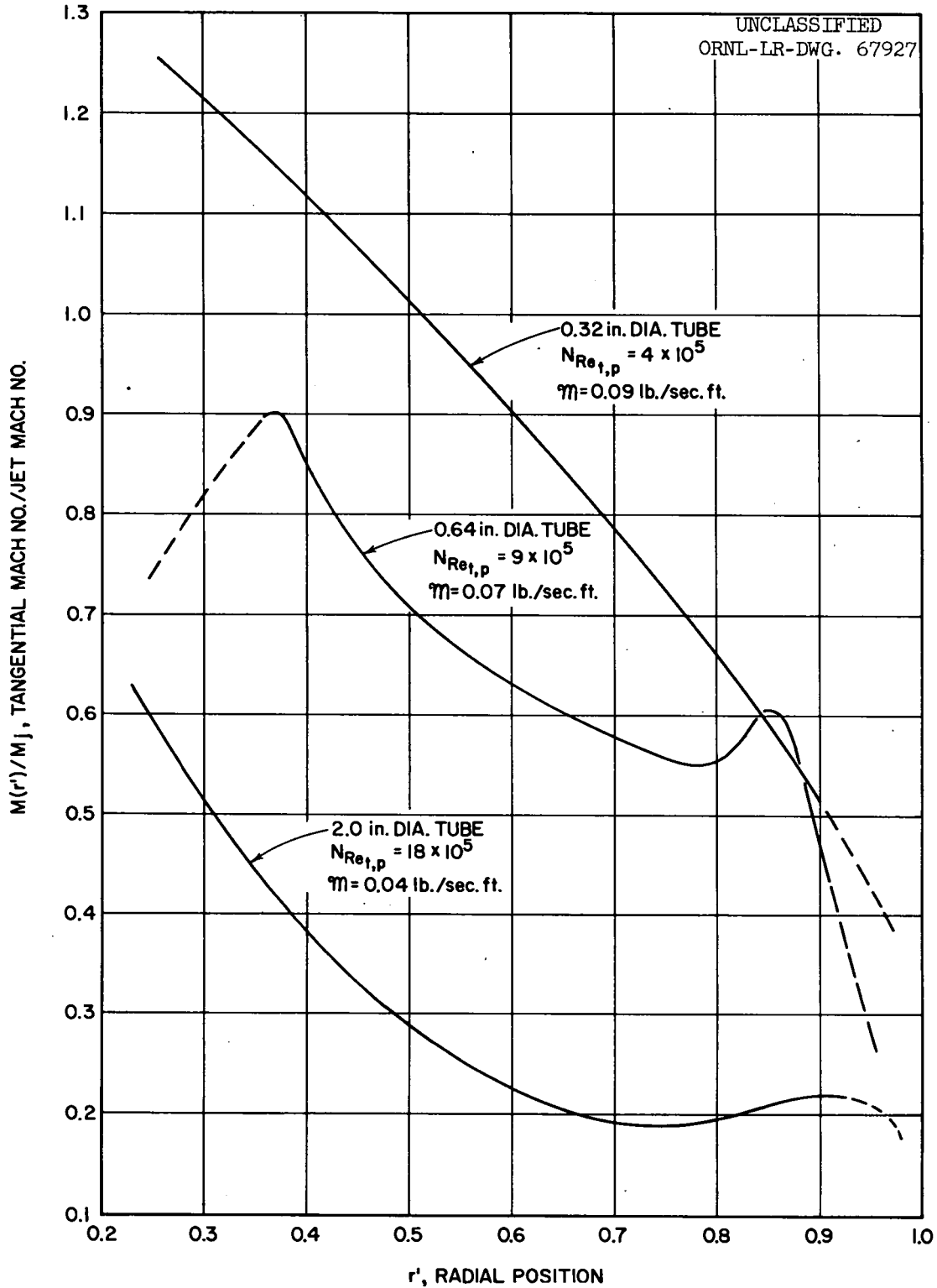


Fig. 3.3. Comparison of Tangential Mach Number Profiles for Jet-Driven Vortex Tubes of 0.32-, 0.64-, and 2.0-in. Diameter.

UNCLASSIFIED
ORNL-LR-DWG 41033R

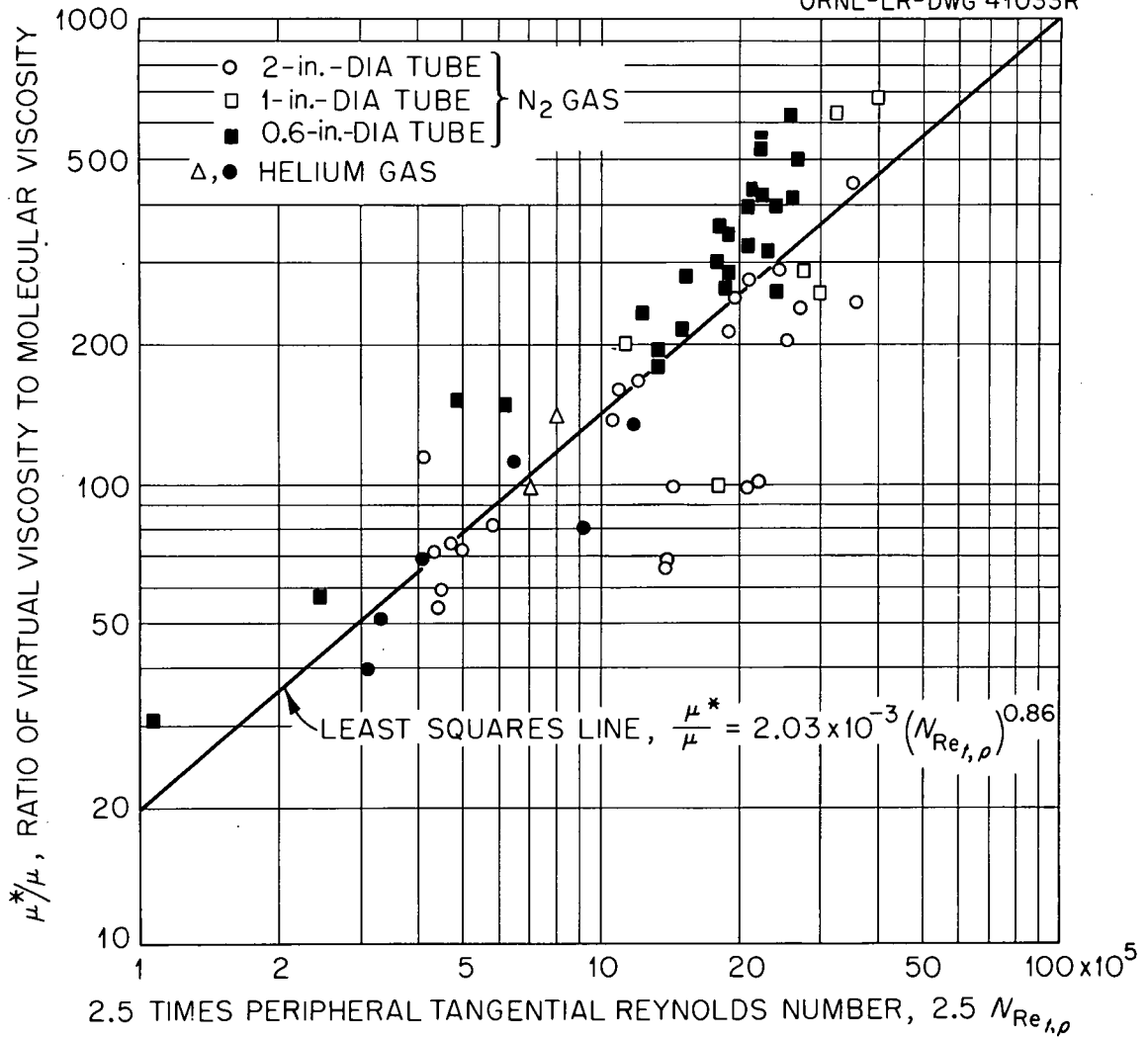


Fig. 3.4. Variation of Ratio of Virtual Viscosity to Molecular Viscosity with Peripheral Reynolds Modulus. 0.6-, 1.0-, and 2.0-in.-diam tubes; N_2 and He gas.

tube. Measurements by Kendall³⁵ at the Jet Propulsion Laboratory indicate that this is not really true and that some of the flow is carried in the boundary layers on the wall and end plates. Neglect of this component of the flow means that the viscosities estimated in this work are upper limits.

The intensity of turbulent wall shear is of obvious interest in relation to fluid friction characteristics of vortex tubes. Estimates of maximum coefficients of skin friction, C_f , have been made from tangential velocity and virtual viscosity data, making use of a torque balance in which the driving torque due to the decrease in momentum of the feed jets is equated to the sum of the torque due to wall shear and the internal fluid torque.³² Figure 3.5 is a graph of C_f obtained in this manner versus the peripheral tangential Reynolds modulus, including data for 5/8-, 1-, and 2-in.-diameter vortex tubes. The data scatter about the least-squares line represented by the equation:

$$C_f = 0.35 (N_{Re_{t,p}})^{-0.27} \quad (3.1)$$

The lower (dashed) curve is a plot of the Schoenherr average law for turbulent C_f on a flat plate with zero pressure gradient. Since the Schoenherr equation is based on a length Reynolds modulus, which is not directly comparable with the Reynolds modulus as defined for vortex flow, the lower curve should be considered for reference purposes only.

Separation experiments were carried out utilizing helium and a heavy fluorocarbon vapor C_8F_{16} (molecular weight 400). The heavy gas was introduced as a dilute mixture with helium through the porous wall of the 2-in.-diameter vortex tube described in Fig. 3.1. An 0.008-in.-OD probe introduced radially at the midaxial position was used to withdraw gas for analysis by measurement of thermal conductivity.

A relationship between the tangential Mach number at the radius of maximum mole fraction of heavy component and the exit mass flow rate is

³⁵James M. Kendall, Jr., "Experimental Study of a Compressible Viscous Vortex," California Institute of Technology Technical Report No. 32-290, Jet Propulsion Laboratory, June 5, 1962.

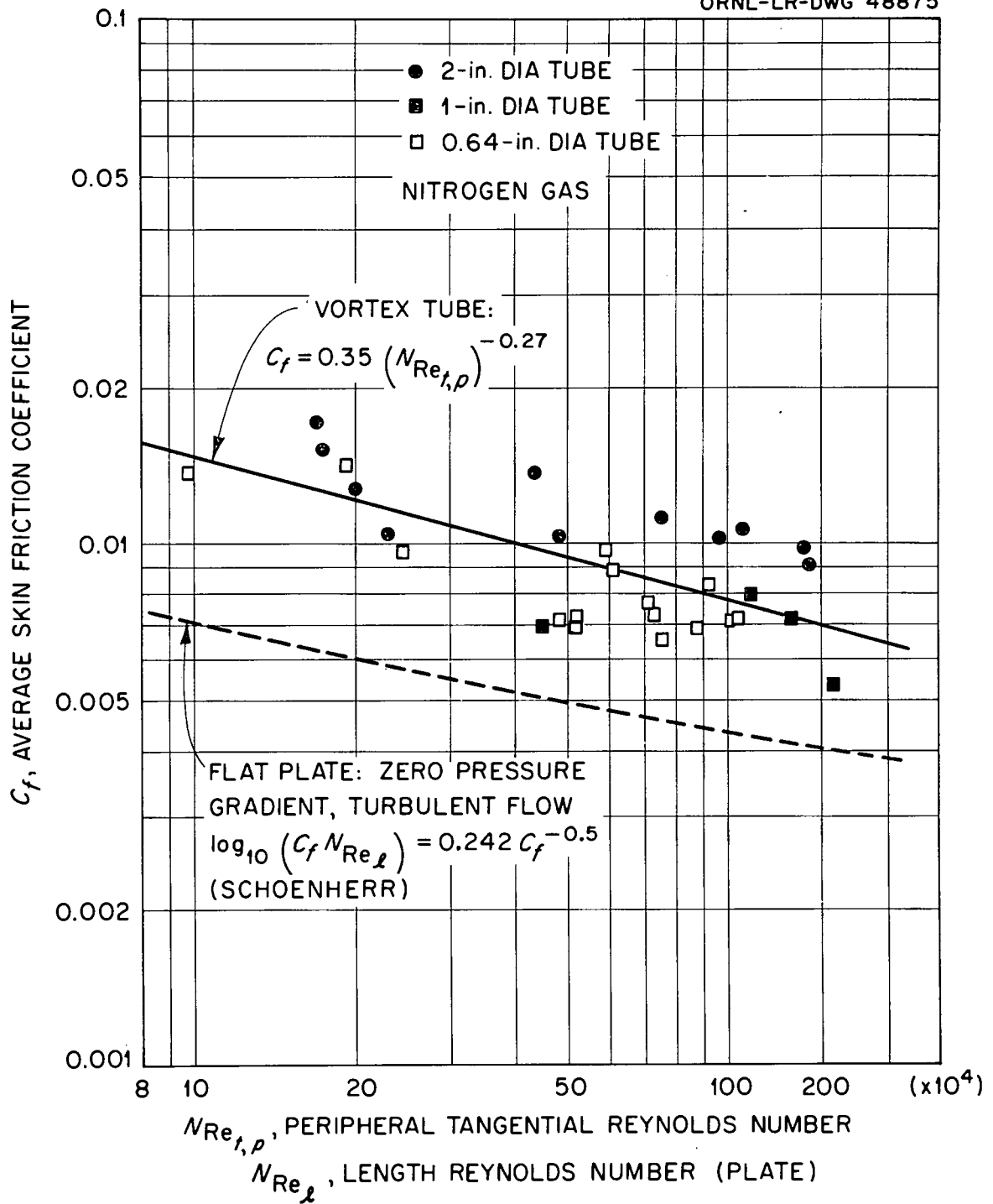


Fig. 3.5. Comparison of Skin Friction Coefficients for Vortex Tube and Flat Plate.

derived in Ref. 29 for laminar flow. For the special case of a very dilute mixture, as employed in the experiments, the relationship is

$$M_m^2 = \frac{m_e (1 - x_e/x_m)}{2 \pi (\rho D_{12})_m (m_2/m_1 - 1) \gamma}, \quad (3.2)$$

where M_m is the tangential Mach number at the radius of maximum mole fraction; m_e , the exit mass flow rate per unit tube length; x_e/x_m , the ratio of mole fractions of heavy component in the exit gas stream and at the peak; $(\rho D_{12})_m$, the density-molecular diffusivity product at the peak; m_2/m_1 , the mass ratio; and $\gamma = c_p/c_v$. From an examination of this equation, it is seen that M_m varies directly as the square root of the exit mass flow rate and inversely as the square root of the diffusivity. In view of the small magnitude of diffusivity for C_2F_6 in helium near room temperature, the equation can be satisfied for values of M_m which are experimentally attainable only if the exit mass flow rate is low. Thus, it was necessary in the experiment to introduce excess mass flow in order to generate the required vortex strength and to bleed off all but the allowable exit flow.

Operating conditions and results for three typical separation runs are summarized in Table 3.2. The peaks in mole fraction of heavy component were observed to occur at positions varying from 11 to 21% of the radius. The tangential Mach numbers observed at the radius of peak mole fraction were determined with the sample probe inserted and, thus, reflect the effect of the probe on the vortex strength. These Mach numbers were 0.70, 0.70, and 0.55, respectively.

Mole fraction ratios x_e/x_m of 0.5 and 0.67 were measured for runs 1 and 2. The calculated Mach numbers at the peak position for runs 1 and 2 were obtained from the preceding equation, using an experimental value of molecular diffusivity for C_2F_6 -He, corrected for temperature. Note that the observed and calculated values of M_m agree to within 20%.

From these initial exploratory experiments, it was concluded that high wall friction due to turbulence in the boundary layer on the inside surface of the vortex tube is an important factor limiting the attainment

of high vortex strength at low mass throughput. An investigation of techniques for possible reduction in boundary layer turbulence was therefore initiated. For example, experiments were carried out with uniform wall bleed-off, utilizing 2-in.-diameter nozzle and slit-fed tubes 3 and 4 with porous walls, for the purpose of determining whether reduction in wall shear by boundary-layer stabilization could be observed. In no case, however, was a significant increase in vortex strength measured for bleed flows up to three times the exit flow. The vortex strength was observed to increase with extreme wall cooling, however, suggesting that strong density and viscosity gradients in the boundary layer may reduce turbulent shear. Additional study of the influence of temperature gradients is planned.

Table 3.2. Summary of Operating Conditions and Results for He-C₂F₆ Separation Experiments in a 2-in.-diameter Vortex Tube

Parameter	Run		
	1	2	3
Inlet helium mass flow rate, m_i (lb/sec.ft)	0.023	0.030	0.030
Bleed ratio, R_B	15.6	9.4	17.5
Wall pressure, p_p (psia)	56.3	40.8	53.0
Exit diameter, $2r_e$ (in.)	0.221	0.250	0.250
Bleed off position, r'	0.25, 0.40	1.00 (wall slit)	0.40 (axial)
Observed mole fraction peak position, r'_m	0.15	0.11	0.21
Observed Mach number at r'_m , M_m	0.70	0.70	0.55
Observed ratio of exit mole fraction to that at r'_m , x_e/x_m	0.50	0.67	-
Calculated M_m	0.58	0.81	-
Ratio of observed M_m to calculated M_m	1.2	0.87	-

Measurements were also made of velocity distributions in a 1-in.-diameter by 6-in.-long tube, in which the boundary layer could be bled off through carefully shaped and oriented wall slits (Fig. 3.1, lower left). The gas was injected through 60 small nozzles (three rows of

20 each), and bled-off through 0.005-in. wall slits spaced about 0.1 in. apart circumferentially. It was originally thought that a reduction in boundary-layer turbulence might be achieved in much the same fashion as as for the case of a slotted aircraft wing with suction. No significant effect on wall friction was observed, but the model did afford a means of investigating a technique for uniform removal of the excess mass flow required for generation of strong vortexes.

Figure 3.6 is a typical tangential Mach number profile obtained with slit bleed-off. Note that 94% of the inlet mass flow was removed through the slitted wall, with 6% (or 0.024 lb/sec.ft) exhausted through the exit orifice located at one end of the tube. With an injection Mach number of about 1.3 and 50 psia tube pressure, a peripheral Mach number of 0.64 was generated with a maximum in the velocity of $M = 1.05$.

Finally, some experiments have been carried out in which vortexes were generated by flow through a uniformly porous wall, the pores of which were oriented nearly tangentially (Fig. 3.1, lower right). By greatly increasing the number of jets (in this case pores) and thus decreasing the spacing between adjacent jets, it was reasoned that, in the limit, a situation within the boundary layer would be approached in which adjacent jets would ride on each other, thus forming a rotating gaseous "wall" with minimum interaction at the solid surface. Furthermore, because of the very small equivalent diameter of each individual pore, the jet flow would likely be laminar; and, hopefully, there would result less turbulence in the boundary layer. It is apparent that to attain this result would indeed require an enormous number of microscopic pores, since the allowable void fraction of the wall is low.

An initial effort to develop a material with tangentially oriented pores was made. The first tube utilizing this method of vortex generation consisted of a stack of 2-mil brass washers, alternate washers having been corrugated by means of a die-stamp operation described in Ref. 36. Washers (0.2-in. wide) stamped with the equivalent of 120 corrugations (corresponding to 240 pores per washer) were stacked alternately with 0.05-in.

³⁶C. J. King and E. G. Farrier, "Construction of Oriented Flow Devices," USAEC Report K-1549, Oak Ridge Gaseous Diffusion Plant, December 7, 1962.

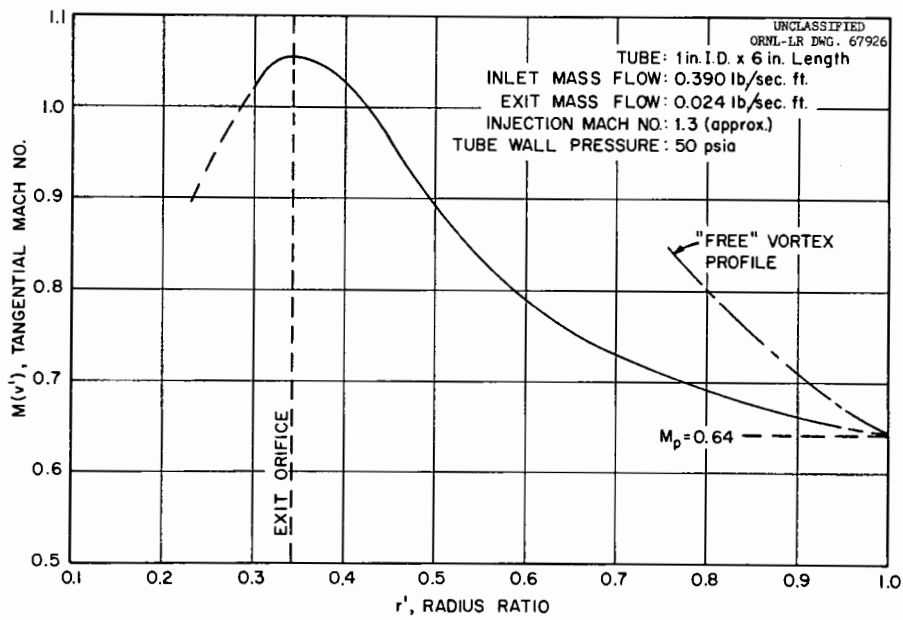


Fig. 3.6. Typical Tangential Mach Number Profile for a Slitted Vortex Tube with Wall Bleed-Off.

plane spacer washers to give slit-like pores about $14 \text{ mils} \times 0.1 \text{ mil}$ in cross section and 65 mils in length. Injection Reynolds moduli for pores of this size are in the range from 10 to 100. Figure 3.7 illustrates the final washer assembly, which was 1-in. ID \times 6 in. in length; there were 3000 washers with 360,000 pores in this device. Four adjustable tie bolts were employed to vary the pressure on the stack, and thus to permit wide variations in porosity. Gas entered from the annular jacket and was removed through a 0.5-in. orifice at one end. Taps for measuring the radial pressure gradient were provided at both ends of the tube.

Figure 3.8 compares values of the jet velocity recovery ratio, $\alpha = M_{O.S.}/M_j$, observed with the multipored laminated tube (solid circles) with values observed using conventional jet-driven tubes of 0.32-, 0.64-, and 1.0-in. diameter. For laminar vortexes, α should vary with radial Reynolds modulus and should be at least 0.9 for $N_{Re,r} \geq 100$.³⁷ It is seen from this figure that, when compared on the basis of $N_{Re,r}$, the values of α for the laminated tube fall generally above those for conventional jet-driven tubes; and, indeed, in some runs at high $N_{Re,r}$ (>800), values approaching unity were observed for α . The fact that α may be less than that predicted by laminar theory at $N_{Re,r} < 800$ (as evidenced by the point at $N_{Re,r} = 500$) suggest that, as with the conventional jet-driven tubes, the flow field near the wall is probably turbulent. Additional data at low $N_{Re,r}$ is obviously needed to support this observation.

The comparison in terms of radial Reynolds modulus fails to take into account the fact that injection velocities for the laminated tube were from 2 to 10 times lower than for the "conventional" vortex tubes, α was found in previous studies to depend on the injection velocity.³¹ An attempt to take this into account is shown in Fig. 3.9, in which α is plotted against the ratio $N_{Re,r}/M_j$. While this plot appears to correlate the data for the laminated tube (solid circles) with data for the other tubes, better than does the plot of α versus $N_{Re,r}$, this apparent improvement might be due to the fact that M_j appears in the denominator in both ordinate and abscissa, thereby producing perhaps a better correlation

³⁷M. L. Rosenzweig, "Summary of Research in the Field of Advanced Nuclear Propulsion - January-June 1961," Report TDR-594(1203-01)STR, Space Technology Laboratory.

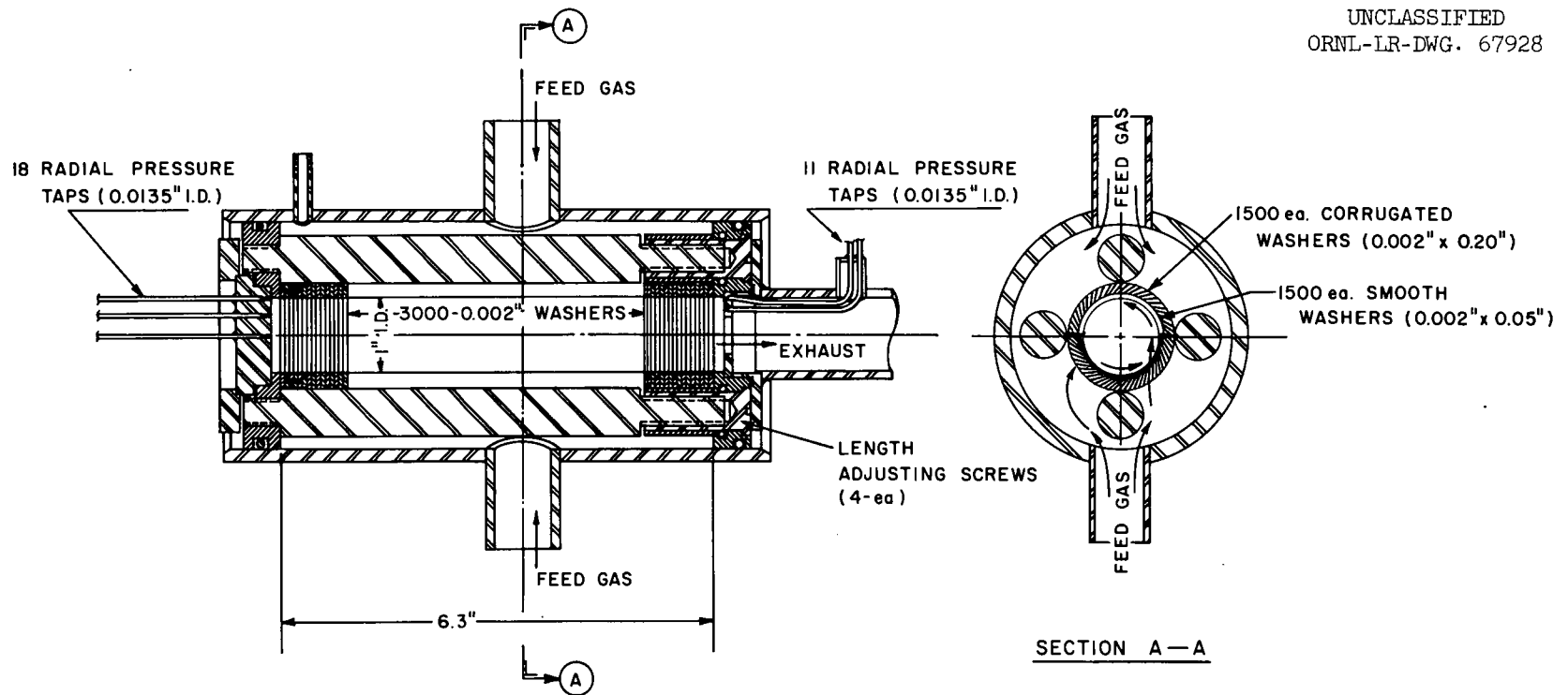


Fig. 3.7. Multipored Laminated Vortex Tube Assembly.

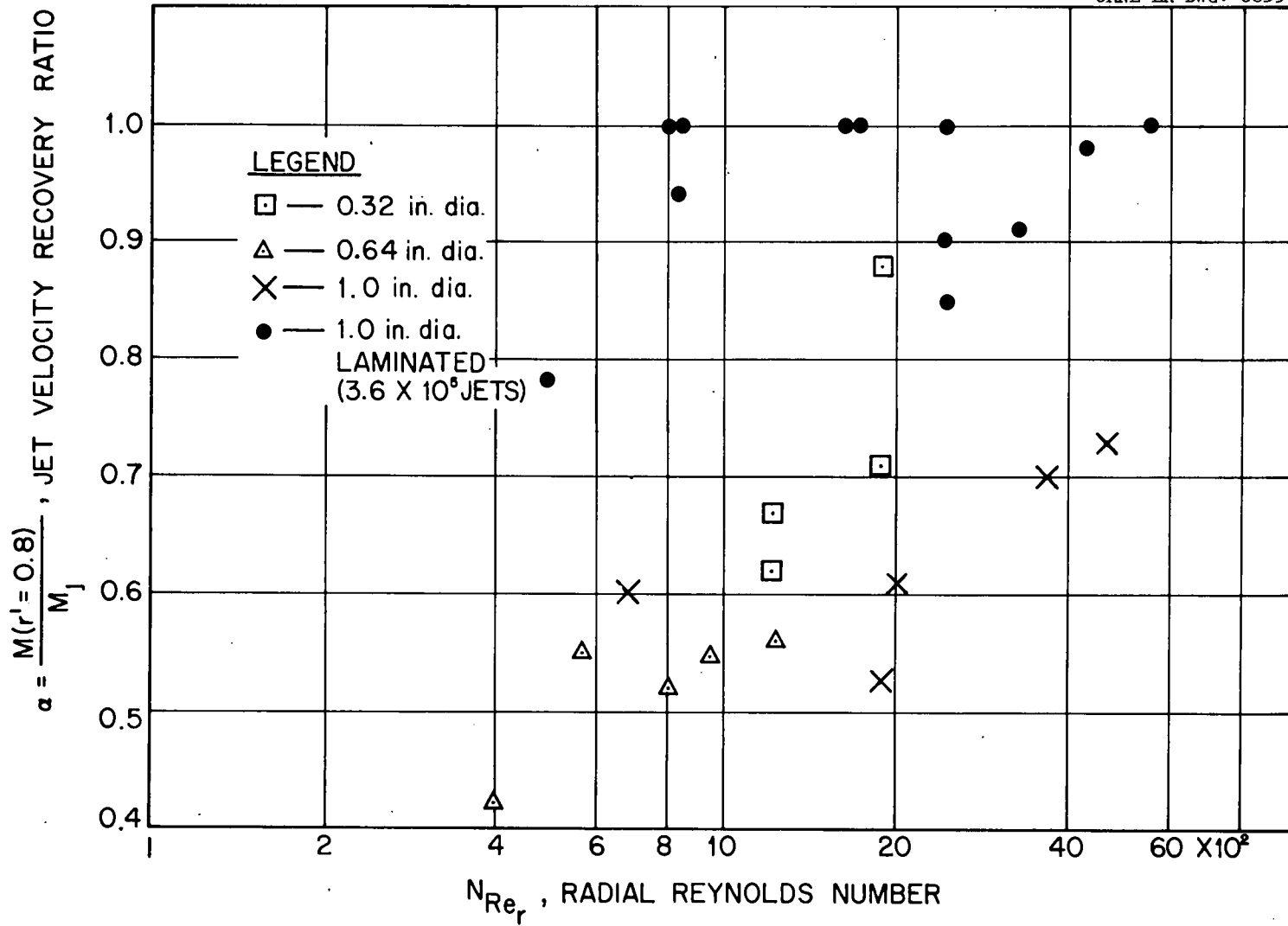


Fig. 3.8. Variation in Jet Velocity Recovery Ratio with Radial Reynolds Modulus for Conventional and Multipored Laminated Vortex Tubes.

UNCLASSIFIED
 ORNL-LR-DWG. 68358

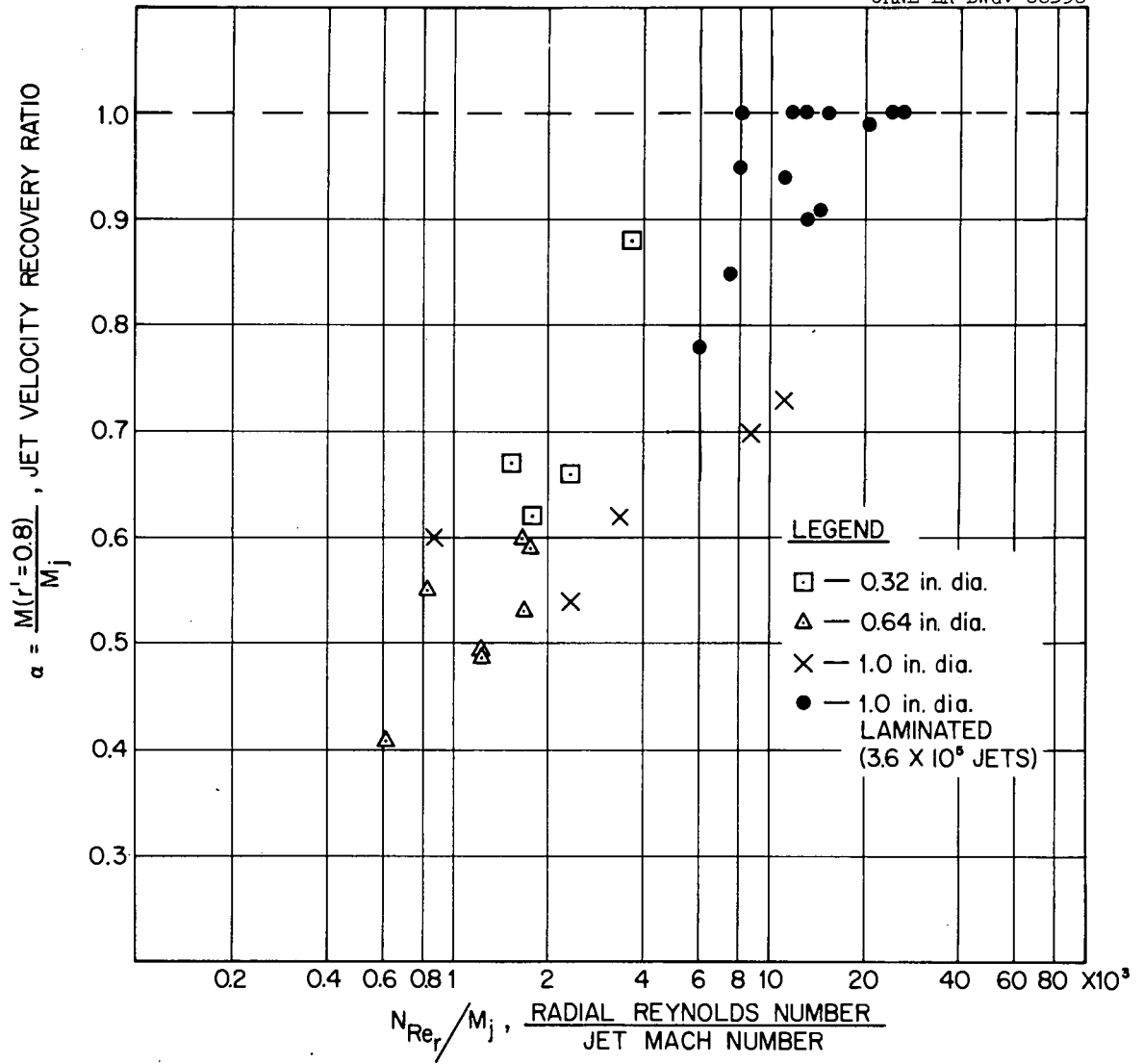


Fig. 3.9. Variation in Jet Velocity Recovery Ratio with Radial Reynolds Modulus Divided by Jet Mach Number for Conventional and Multi-pored Laminated Vortex Tubes.

than the data warrant. If this plot does correlate significantly the effect of both $N_{Re,r}$ and M_j , then it would appear that recovery ratios for the multipored, laminated vortex tube are somewhat higher than those for "conventional" 1-in.-diameter jet-driven vortex tubes (crosses), but not significantly higher than the ratios observed in 0.32-in.-diameter tubes (open squares); this indicates that many times the number of pores used in this model, and hence much smaller pores, may be necessary to attain the limiting condition of a "rotating wall" of high velocity gaseous jets. Techniques for increasing the number of pores without increasing the free area or pore length-to-diameter ratio are under study.³⁶

3.1.2. Magnetohydrodynamic Studies

J. J. Keyes, Jr. W. K. Sartory
T. S. Chang

As has been indicated, attempts to reduce turbulence levels in vortex flows by purely hydrodynamic means have met with limited success. An alternative method which can, in principle, produce a significant stabilizing influence over the entire flow field involves the interaction between the velocity field in an electrically conducting medium and a suitably oriented magnetic field, making use of the Lorentz force which might be considered as a restoring body force exerted on a fluid volume element when it is displaced from its position of equilibrium. Since in the cases of power conversion and gaseous reactor applications operation will be at sufficiently high temperature to sustain ionization in the gas (either thermally or by alkali-metal ion seeding), the possibility of magnetohydrodynamic (MHD) stabilization should not be overlooked. For example, Chang³⁸ has shown that a uniform axial magnetic field is in principle capable of completely stabilizing an inviscid, perfectly conducting, pure vortex flow ($1/r$ velocity profile) against small perturbations without altering the mean flow. In the case of jet-driven

³⁸T. S. Chang, "Magnetohydrodynamic Stability of Vortex Flow - A Nondissipative, Incompressible Analysis," USAEC Report ORNL-TM-402, Oak Ridge National Laboratory, October 1962.

vortexes, however, the jets themselves can introduce forced boundary oscillation which may prevent complete stabilization, although partial stabilization may be effected.

A general analysis of MHD effects in vortex flows³⁹ has indicated that there exist several promising applications. One potential advantage of MHD is the possibility of utilizing magnetic interaction effects on the end walls which introduce forces acting to retard the short-circuiting inward radial boundary-layer flow discussed in Refs. 35 and 40. This application is considered in Ref. 41.

Analysis of magnetic stabilization of vortex motion based on a dissipative assumption (viscous fluid with finite electrical conductivity) has also been considered, and a class of exact stationary solutions of incompressible, magnetohydrodynamic flow with cylindrical symmetry under the action of an externally applied magnetic field in the direction of the axis of symmetry have been obtained. These solutions do not depend on the finite conductivity of the fluid medium or on the externally applied, uniform magnetic field.

Dimensionless forms of the pertinent equations characterizing the stabilization of pure, dissipative vortex flow have also been obtained. Similarity parameters include:

the peripheral tangential Reynolds modulus, $\S N_{Re\theta} = \frac{r_o Q_o \rho}{\mu}$, (3.3)

the peripheral magnetic Reynolds modulus, $R_M = \mu_o \sigma Q_o r_o$, (3.4)

³⁹J. J. Keyes, Jr., "Some Applications of Magnetohydrodynamics in Confined Vortex Flows," USAEC Report ORNL-TM-479, Oak Ridge National Laboratory, February 28, 1963.

⁴⁰F. N. Peebles and H. J. Garber, "Studies of the Swirling Motion of Water Within a Spherical Vessel," USAEC Report ORNL-CF-56-1-161, Oak Ridge National Laboratory, January 1956.

⁴¹W. S. Lewellen and W. S. King, "The Boundary Layer of a Conducting Vortex Flow over a Disk with an Axial Magnetic Field," Report No. ATN-63(9227)-1, Aerospace Corporation, December 7, 1962.

\S Note that the tangential peripheral Reynolds modulus has been redefined in terms of radius, so that $N_{Re\theta} = 1/2 N_{Re_{t,p}}$ with $Q_o = Q_p$; μ is the molecular viscosity.

the peripheral Alfvén modulus, $A = \sqrt{\mu_0 \rho} Q_0 / B_0$, (3.5)

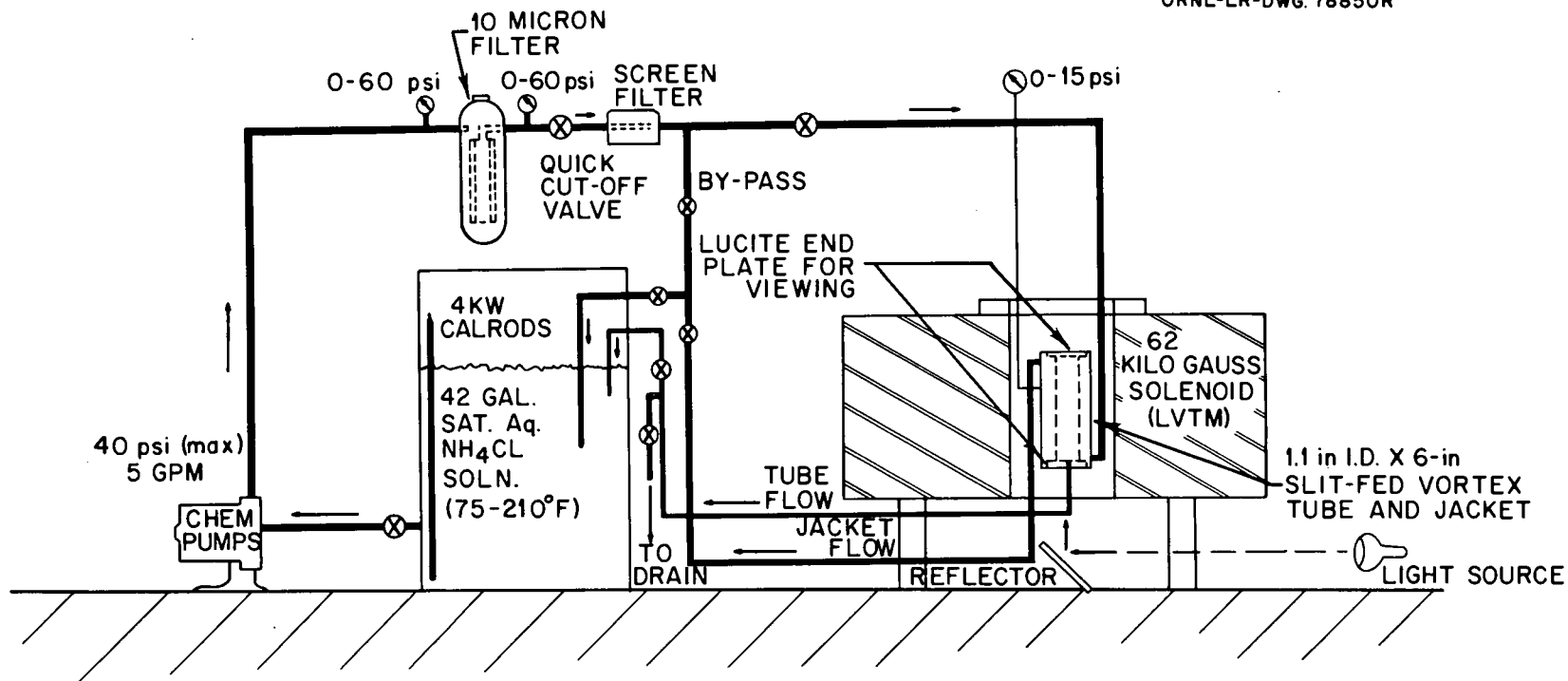
the magnetic interaction parameter, $S = \sigma B_0^2 r_0 / \rho Q_0$, (3.6)

and the peripheral Hartmann modulus, $H = \sqrt{\sigma / \mu} B_0 r_0$. (3.7)

In these expressions, μ_0 is the magnetic permeability; σ , the electrical conductivity; and B_0 , the applied magnetic field strength.

The general formulation for the magnetic stabilization of dissipative vortex flow was simplified for the case of marginal stability with very large Reynolds modulus flow. It was found that when the assumptions $N_{Re_\theta} \gg 1$, $S \gtrsim 1$ are satisfied, the criterion for marginal stabilization becomes equivalent to that for nondissipative vortex flow.³⁸ A more general characteristic solution for the magnetic stabilization of dissipative vortex flow is being considered, and an attempt will be made to include the boundary-layer region in the solution.

An exploratory experimental study was initiated, which is intended to establish whether an MHD stabilization effect does indeed exist for jet-driven vortex flow of a conducting fluid and to determine the nature and magnitude of this effect in stabilizing the flow against turbulent breakdown and in influencing the secondary flow structure. The apparatus is diagrammed in Fig. 3.10. The magnet is a 6.4-in.-ID air core solenoid (water-cooled copper) located in the ORNL Thermonuclear Division Magnet Laboratory. This magnet provides a maximum field of 62.3 kilogauss, with 0.2% variation radially and 10% variation axially for the 1.1-in. ID by 6-in. long vortex tube model used in the experiments. A concentrated aqueous solution of NH_4Cl (350 g/liter) is employed as the conducting fluid. The conductivity of this electrolyte is 0.88 mho/cm at the maximum operating temperature of 210°F, which is about that of a low-temperature alkali metal "seeded" plasma. Aqueous NH_4Cl is a relatively easy fluid to handle; its physical properties are close to those of water at corresponding temperatures, and it permits the use of flow visualization techniques. Figure 3.11 is an overall view of the apparatus, showing the 62 kilogauss solenoid at the left. Figure 3.12 depicts the vortex tube installed in the solenoid.



63

Fig. 3.10. Schematic Flow Diagram for MHD Experiment No. 1.

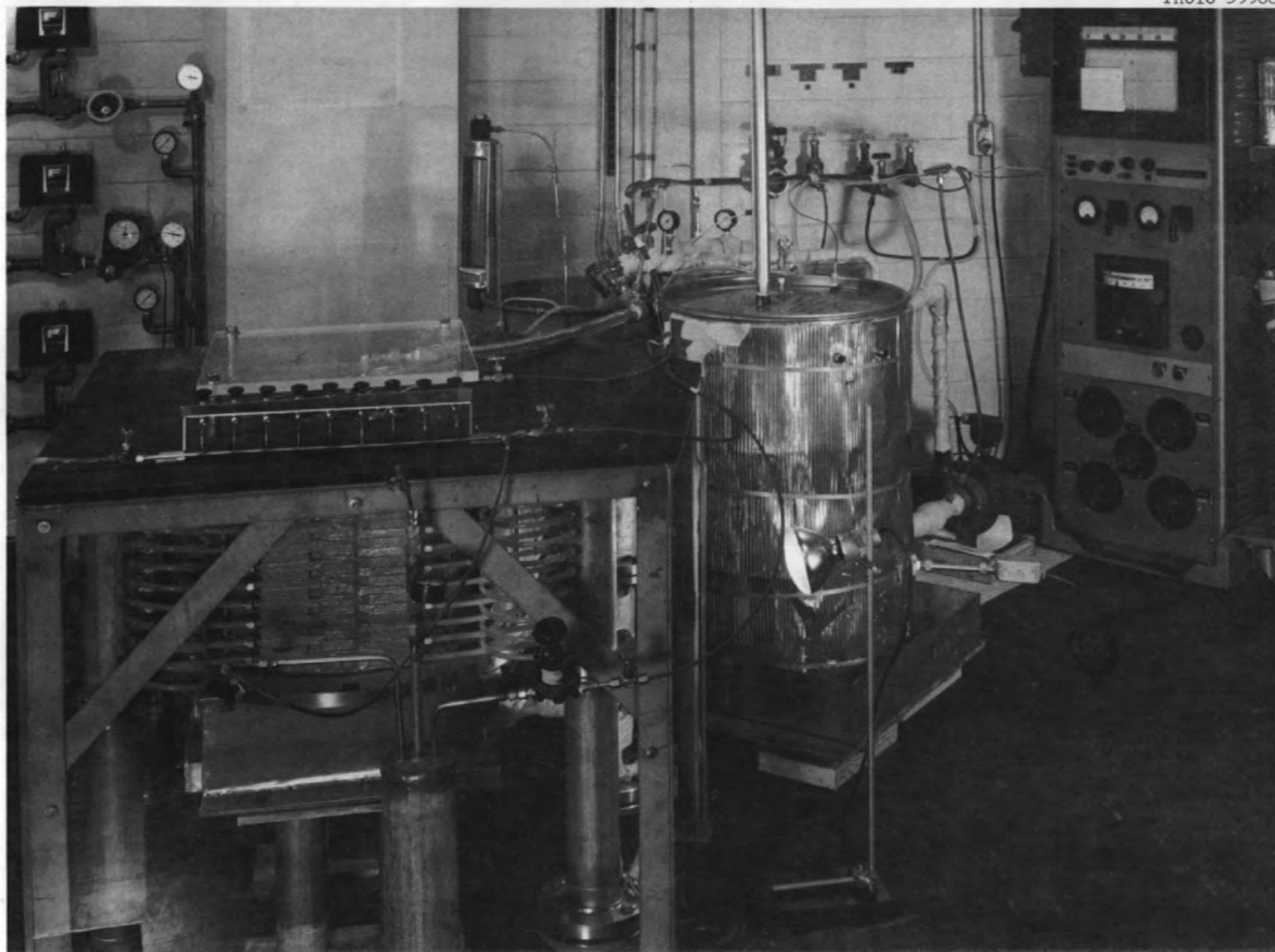


Fig. 3.11. MHD Vortex Experiment Using 62-Kilogauss Solenoid (Left) in ORNL Magnet Laboratory.

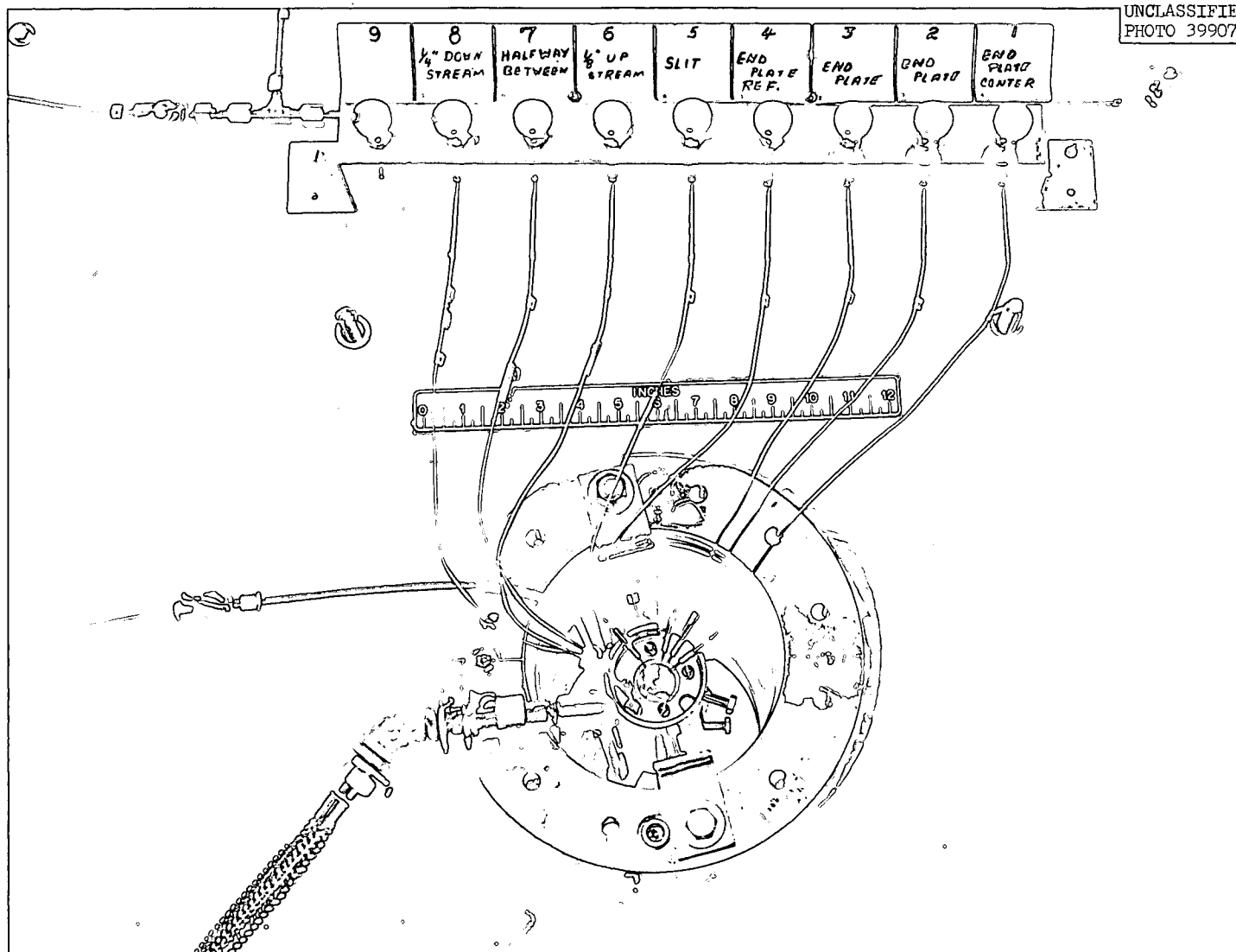


Fig. 3.12. Vortex Tube Installed in 62-Kilogauss Solenoid in ORNL Magnet Laboratory.

The vortex flow field is generated by tangential injection through two 0.012-in. slits extending the length of the tube and fed from an annulus as indicated in Fig. 3.13. The solution exits through a 1/8-in. hole at the center of one end of the tube. The assembly is fabricated of type 316 stainless steel (nonmagnetic), with Plexiglas end walls for viewing in the axial direction. Also indicated are taps for injection of dye into the cylindrical wall boundary layer. Observation of the dye filaments at various positions (emerging from, directly downstream, half way between, and directly upstream of a slit) is the primary technique for determining effects of the magnetic field on flow stability. Dye injection is also used for approximate determination of tangential velocity, when this velocity is sufficiently low (< 10 cm/sec) for observation of the time required for a puff of dye to complete a prescribed number of revolutions at a known radius. Effects in the end wall boundary layer are made evident by observation of dye introduced through the end wall opposite the outlet, as indicated at the right of Fig. 3.13. The dye employed is a very dilute solution of red coal-tar color in saturated aqueous NH_4Cl to provide a fluid having properties essentially identical with those of the working fluid.

The initial experiments have included:

1. Visual observation and photograph of dye patterns in the boundary layers and in the interior of the flow field, as influenced by the appropriate Reynolds moduli and by the magnetic parameters (Eqs. 3.4-3.7); emphasis has been on determination of the effect of the magnetic field on laminar flow stability.

2. Determination of the influence of the magnetic interaction on the tangential velocity near the vortex tube periphery. Variation in operating temperature (from 77°F to 210°F , producing significant variations in electrical conductivity, σ , and molecular viscosity, μ), mass flow rate, m , and applied magnetic field strength, B_0 , enabled operation in the range $4 < N_{\text{Re}_r} < 50$, $200 < N_{\text{Re}_\theta} < 6000$, $0 < S < 4$, and $0 < H < 41$.

The most striking observation of the effect of the magnetic field is the suppression of boundary-layer instabilities which are initiated at very low N_{Re_θ} . For example, with no magnetic field, the boundary layer

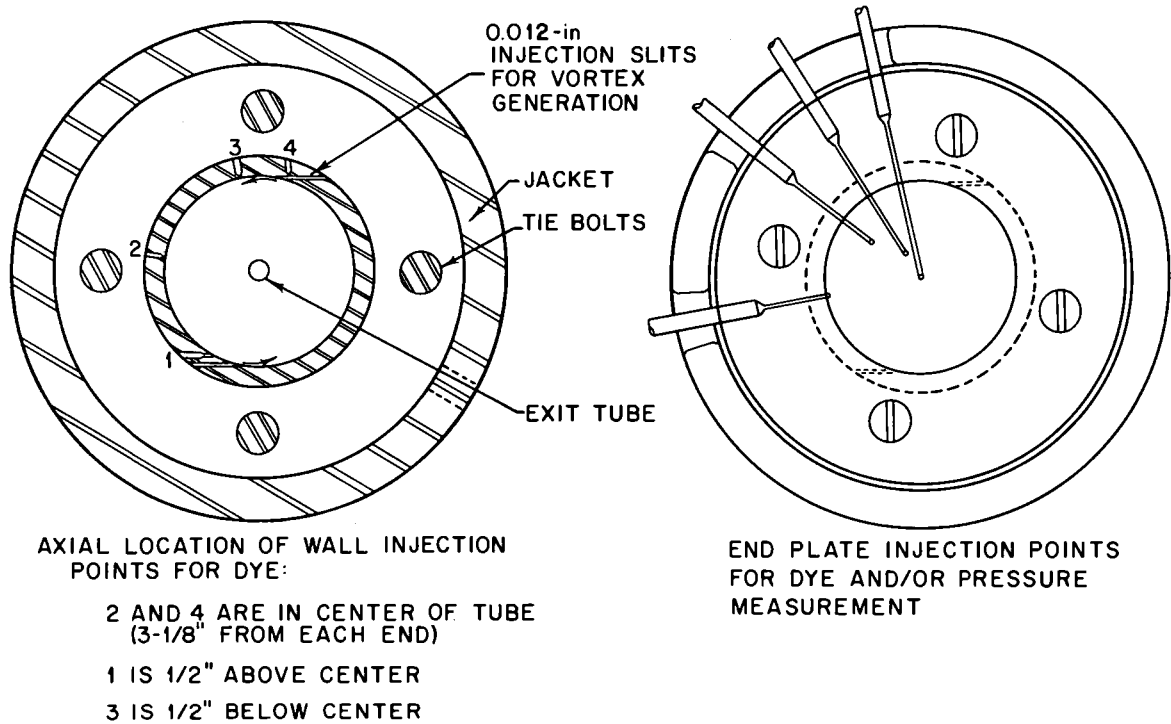
UNCLASSIFIED
ORNL-LR-DWG. 78852R

Fig. 3.13. 1.1-in.-Diam Tangential Slit-Fed Vortex Tube for MHD Studies.

on the concave cylindrical wall exhibits an oscillatory-type instability at $260 < N_{Re_\theta} < 410$. This instability may arise as a result of the rapid deceleration of the impinging jet by the action of wall shear; the decelerated fluid "separates" momentarily from the wall and is convected radially by the action of the radial pressure gradient induced by the mean tangential motion. The phenomenon thus has characteristics similar to those of the Taylor-Goertler instability for flow over concave walls. The jet interaction complicates the mechanism, however. The large-scale perturbations in flow near the wall appear to trigger a general disordering of the motion in the interior of the fluid, resulting in gross mixing and disappearance of any well-defined laminar patterns. Figure 3.14 includes photographs of dye traces injected at the tube wall $1/4$ in. downstream from a slit (mid-axial position 3, Fig. 3.13, left).[§] Rotation is clockwise in the figure. For the photograph at the left, there is no applied magnetic field, $N_{Re_\theta} = 700$ ($H = S = 0$), and the boundary-layer instability just discussed occurs. The dye filament becomes unstable in about $1/4$ revolution and gross radial mixing is evident, particularly near the periphery. As depicted in the photo at the right of Fig. 3.14, application of a 62 kilogauss axial magnetic field with $N_{Re_\theta} = (H = 39, S = 1.8)$ completely suppresses the boundary-layer instability and the entire flow field exhibits a generally well-defined laminar characteristic. Although the dye filament remains intact, small perturbations which are believed to be induced by vortex shedding from the lips of the injection slits persist for several revolutions. Since the magnetic interaction effect depends on the characteristic length or scale of the disturbance, it is not surprising that the field fails to suppress these very small eddies. The field does function, however, to prevent growth of the small eddies into full-scale disturbances.

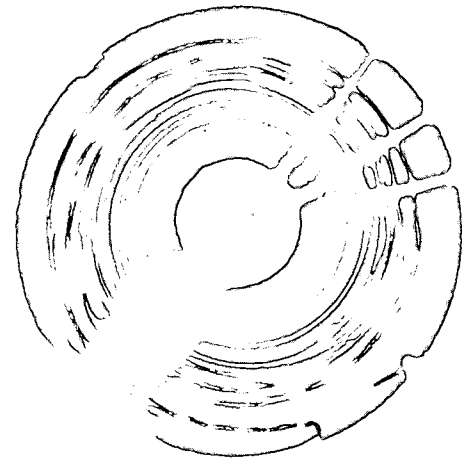
The 62-kilogauss field was observed to completely stabilize the boundary flow up to N_{Re_θ} of about 1600 at 210°F ($H = 41, S = 1.08$). Above this value of tangential Reynolds modulus, instabilities occur near the periphery but the amplitude of the associated eddies and the

[§]The dye traces were photographed using 35 mm Eastman Kodak Company Ektachrome film with an exposure time of $1/1700$ sec.

UNCLASSIFIED
PHOTO 39938



$N_{Re_\theta} = 700$
 $H = S = 0$



$N_{Re_\theta} = 850$
 $H = 39 \quad S = 1.8$

Fig. 3.14. Effect of a 62-Kilogauss Axial Magnetic Field on Vortex Flow of a Conducting Liquid.
 $N_{Re_r} = 10.6.$

amount of radial mixing is reduced as compared to the case of no magnetic field. Figure 3.15 illustrates the effect of the field when N_{Re_θ} is above the transition value of 1200 for this particular run at 200°F, $H = 39$. In the upper pair of photographs, the dye is injected through one of the slits (position 4, Fig. 3.13, left), whereas in the lower pair the dye is injected downstream from a slit (position 3). The field is seen to have a significant stabilizing influence. In fact, some stabilization, especially in the interior of the flow field, was observed for $N_{Re_r} = 53$, $N_{Re_\theta} = 5800$ ($H = 39$, $S = 0.27$).

It should be noted that the use here of two tangential slits to drive the vortex is especially conducive to generation of instabilities in the boundary layer because of the large asymmetric velocity perturbations associated with the jet flow. The fact that, even in this unfavorable case, the magnetic interaction is able to stabilize the flow to a significant extent is encouraging. Vortexes generated by multipored injection as previously discussed (page 54) should be more easily stabilized.

Figure 3.16 includes photographs depicting flow in the end wall boundary layer for a main flow tangential Reynolds modulus (i.e., outside the end wall boundary layer) of 425, which is slightly above the maximum observed transition point without an applied field. Here the dye is injected into the boundary layer near the periphery (as indicated in Fig. 3.14, right). Note the instability in the dye trace for $\underline{H} = \underline{S} = 0$ (Fig. 3.16, left). When the axial magnetic field is applied, giving $H = 31$, $S = 2.2$ (Fig. 3.16, right), stabilization of the boundary-layer flow is evident. Note particularly the suppression of the dye trace fluctuations and the increase in the tangential velocity relative to the radial velocity. Analysis of these photographs indicates, for example, that the ratio of tangential to radial velocity is increased from approximately 1 to approximately 12 by application of the field. The average velocity ratio for the main flow (based on total volumetric flow rate and jet area and assuming two dimensionality) is about 35. Stabilization of the end wall boundary layer should effectively reduce the short-circuiting radial mass flow as discussed in Refs. 37 and 40.

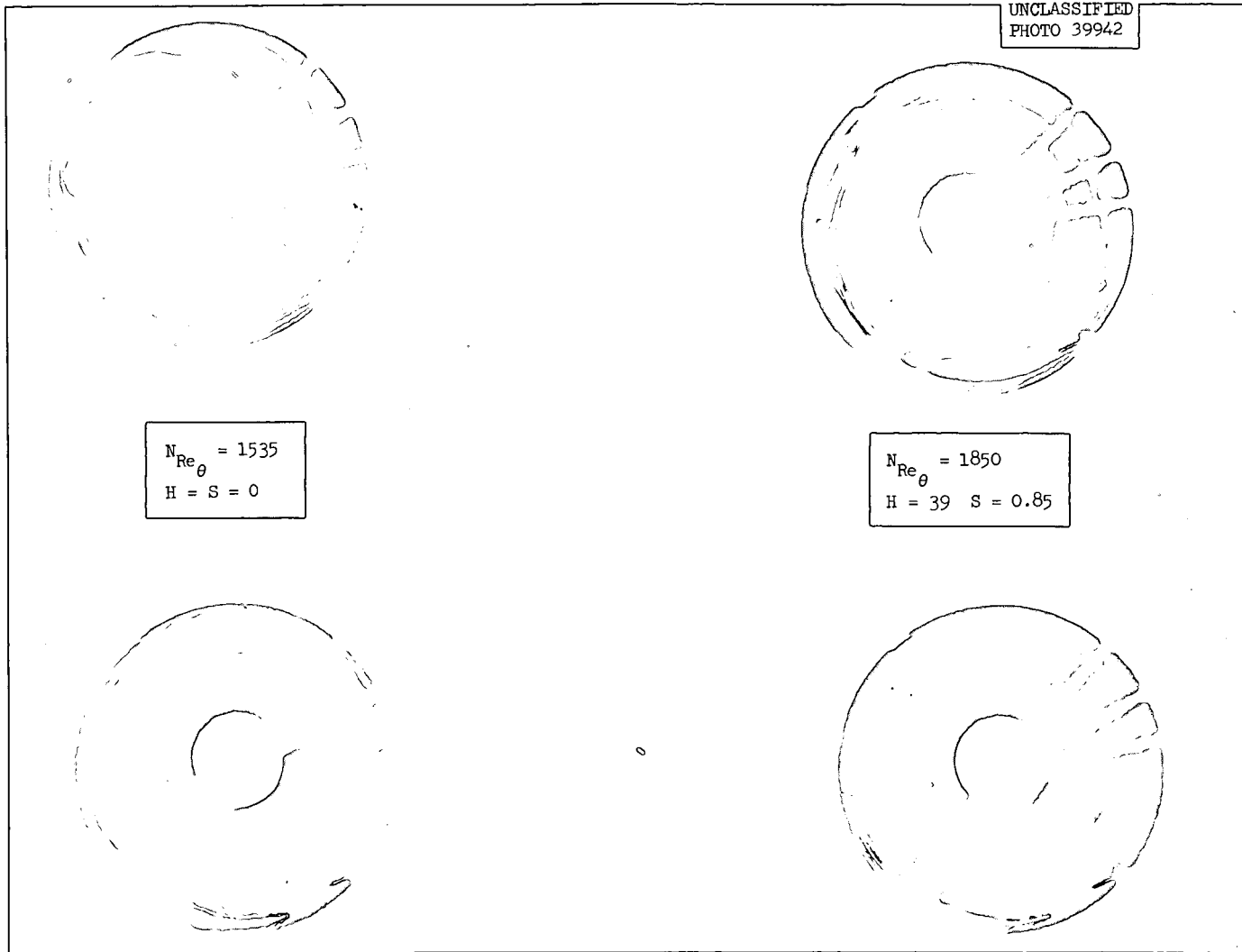


Fig. 3.15. Effect of a 62-Kilogauss Axial Magnetic Field on Vortex Flow of a Conducting Liquid.
 $N_{Re_r} = 18.0.$

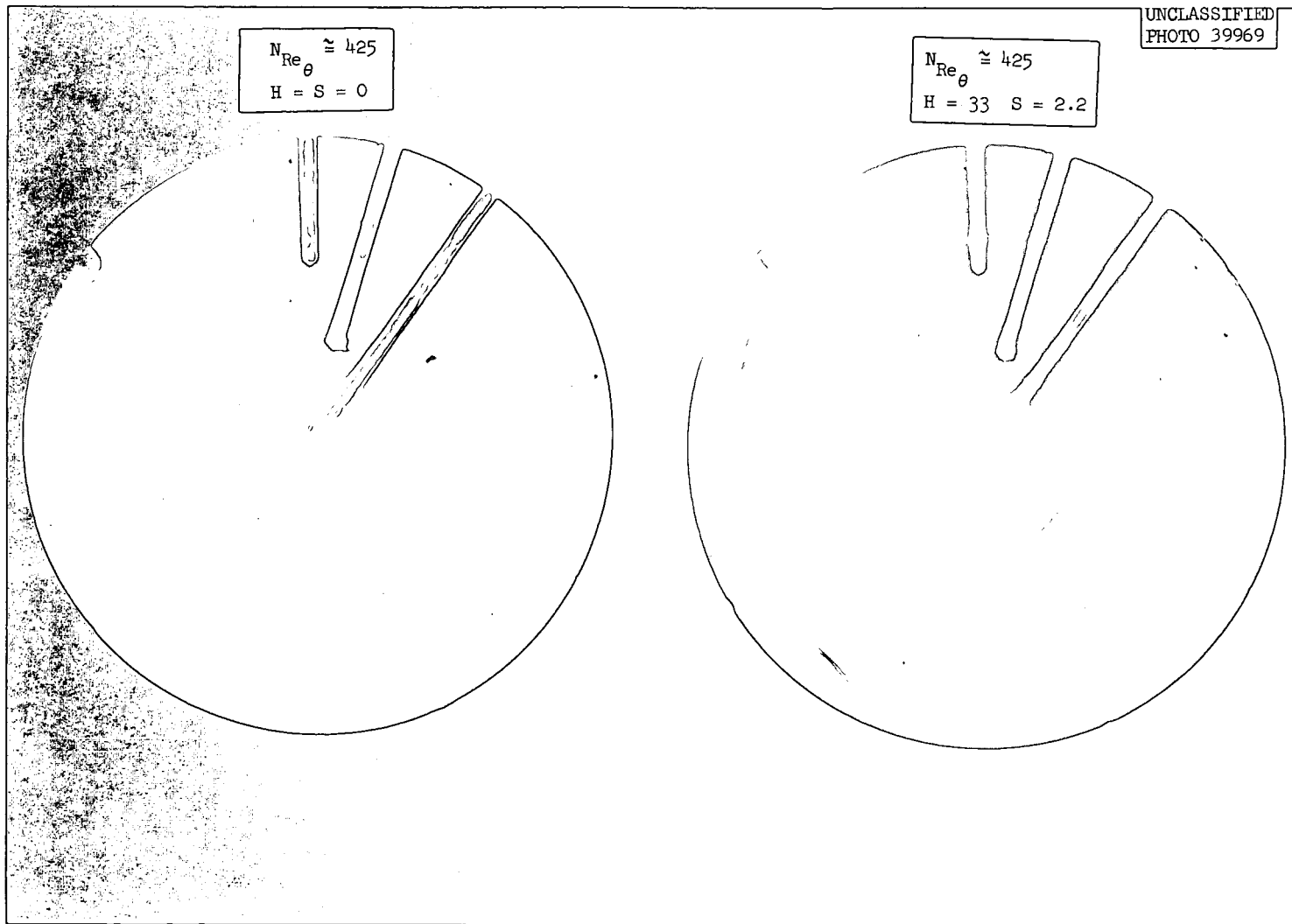


Fig. 3.16. Effect of an Axial Magnetic Field on the End Wall Boundary-Layer Flow. $N_{Re_r} = 6.5$.

The effect of the magnetic field on the strength of the vortex was investigated semiquantitatively by the dye pulse injection technique. A quantity indicative of the effectiveness of vortex generation is α , the jet velocity recovery ratio previously considered. For this case $\alpha \equiv Q_o/Q_j$, where Q_o is the tangential peripheral velocity (measured at a reference radius ratio $r' = r/r_o = 0.8$), and Q_j is the average velocity of the inlet jet. Figure 3.17[§] is a graph of the observed α values as a function of radial Reynolds modulus, $N_{Re_r} (= Q_r r \rho/\mu = m/2 \pi \mu)$, for the case of no magnetic field, $B_o = 0$ ($H = 0$), and for the case of an applied axial magnetic field, $B_o = 62$ kilogauss ($H = 39$ and 41). Note that $H (= B_o r_o \sqrt{\sigma/\mu})$ is the Hartmann modulus defined in terms of the tube radius, r_o .^{§§} Data for two runs (200°F and 210°F) are included. The spread between these runs is not believed to be a consequence of the small difference in temperature, but rather an indication of the large experimental uncertainties. The dashed curves are calculated from the theory of Rosenweig³⁷ assuming laminar flow for two assumed values of the parameter, $\lambda (= r_j/r_o$, where r_j is the effective radius of jet entry). With $H = 0$, onset of the instability described on page 66 was observed to occur at $N_{Re_\theta} \cong 370$ at 210°F, corresponding to $N_{Re_r} \cong 7.0$. Note that the measured curve for 200°F, ($H = 0$) is nearly parallel to the theoretical laminar curve for $\lambda = 0.9$ up to $N_{Re_r} \cong 8$, and that transition to a much flatter curve of α versus N_{Re_r} appears to occur in the range $8 < N_{Re_r} < 13$. This transition nearly coincides with visual observations of the onset of instability. When the 62-kilogauss field is applied, the measured curves of α versus N_{Re_r} are nearly parallel to the theoretical laminar curve up to $N_{Re_r} \cong 13$ (200°F) and to $N_{Re_r} \cong 17$ (210°F). The tangential Reynolds modulus at which transition was visually observed at 210°F is 1580, $N_{Re_r} \cong 17$, which is just below the transition region in the α curve. A magnetic field strength sufficient to give $H = 41$ has therefore increased the transition Reynolds modulus at 210°F by a factor of about 4.3.

Figure 3.18 summarizes the observed increase in jet velocity recovery ratio at constant N_{Re_r} as a function of the magnetic interaction parameter,

[§]The curves in Figs. 3.17 and 3.18 were faired through the data by eye.

^{§§} H^2 is proportional to the ratio of magnetic to viscous forces.

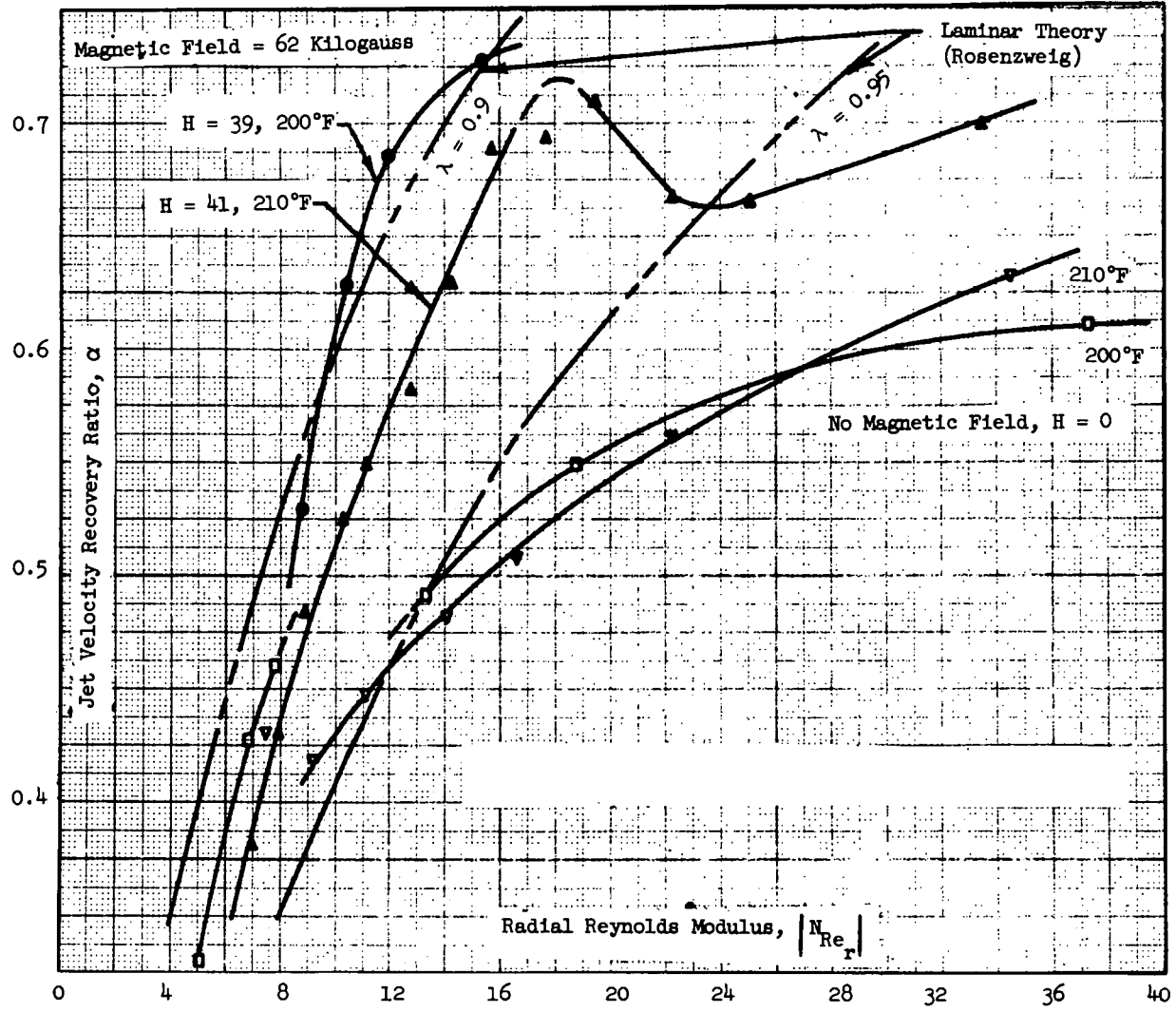


Fig. 3.17. Effect of a 62-Kilogauss Magnetic Field on Jet Velocity Recovery Ratio for Vortex-Type Flow.

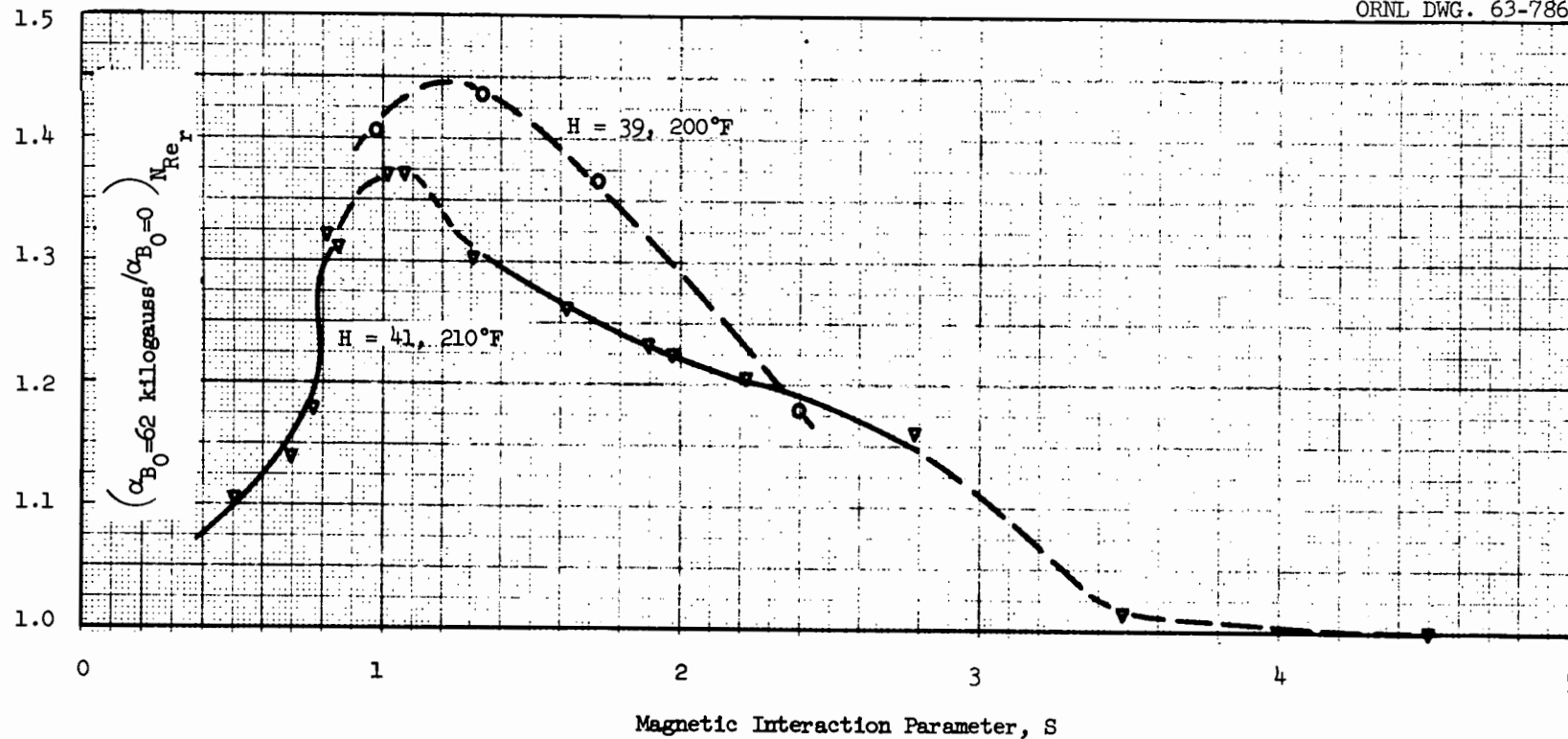


Fig. 3.18. Increase in Jet Velocity Recovery Ratio at Constant Radial Reynolds Modulus Correlated with Magnetic Interaction Parameter.

$S (= \sigma B_0^2 r_0 / \rho Q_0)$.[§] For large S , there is little effect of the field on α , since Q_0 , and hence N_{Re_θ} , is small; and the flow is stable without an applied field. As Q_0 is increased and S correspondingly decreased, the flow becomes unstable; and the magnetic field is effective in producing stability for S greater than about 1. Note that when S is less than 1 the flow is unstable, but α is still increased by the magnetic field. For $1 < S < 1.25$ (stabilized flow), α is increased by a factor of about 1.4. Using the torque balance analysis described earlier,³² estimates of skin-friction coefficients were made from the observed α values. This analysis indicates that, for $N_{Re_\theta} \approx 1800$, the wall shear stress is decreased by a factor of 2 to 2.5 by the application of a magnetic field to give $H \approx 40$, $S \approx 1$.

Figure 3.19 graphs the observed variation in the tangential Reynolds modulus at transition to instability, $N_{Re_\theta}^*$, with the square of the Hartmann modulus, H^2 .^{§§} Note that the variation in H^2 was obtained experimentally by varying B_0 while maintaining σ/μ constant. The data suggest a more or less linear increase of $N_{Re_\theta}^*$ with H^2 for $H^2 > 200$.

As a further test of the validity of H^2 as a characteristic magnetic parameter influencing the transition phenomenon, experiments were performed at 77°F where σ/μ is about 20% of the corresponding value at 210°F, giving $H^2 = 350$ for $B_0 = 62$ kilogauss. The transition Reynolds modulus was observed to be 730 under these conditions. For $H^2 = 0$, $N_{Re_\theta}^*$ was found to be 425, in agreement with the corresponding value at 210°F as plotted in Fig. 3.19. It is significant that by decreasing B_0 at 210°F to give $H^2 = 350$, a value of $N_{Re_\theta}^*$ of about 680 is read from Fig. 3.19, as compared with the value 730 observed at 77°F for $H^2 = 350$.

It is concluded from these initial experiments that the application of an axial magnetic field to jet-driven vortex flow of an electrically conducting liquid is effective in suppression of the boundary-layer instability on the concave wall which appears to initiate general turbulence throughout the flow field. A significant increase in the recovery of

[§] S is proportional to the ratio of magnetic to inertial forces.

^{§§}The curve through all the data points for the two runs was obtained by a third-degree polynomial least-squares analysis.

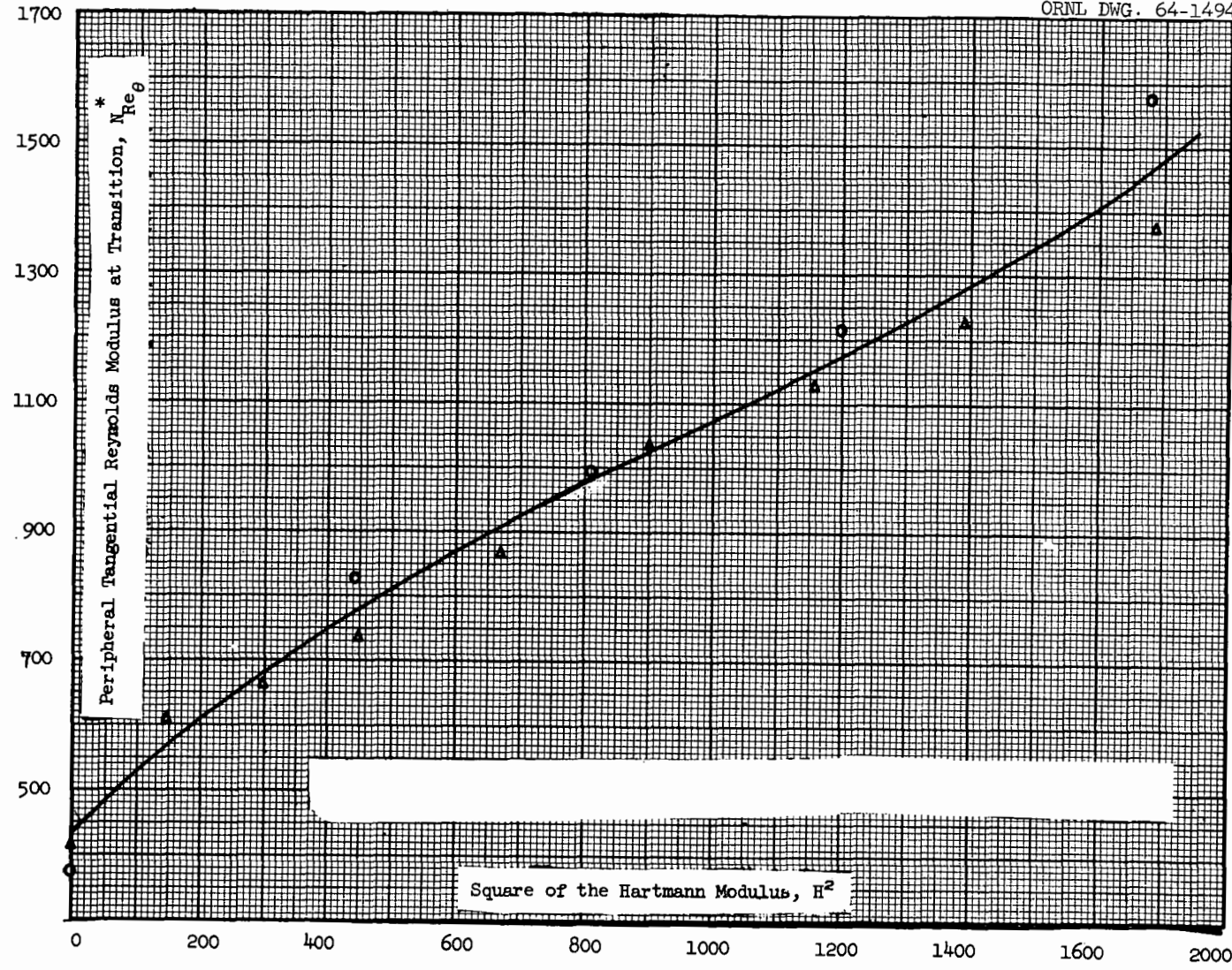


Fig. 3.19. Variation in Transition Reynolds Modulus with Hartmann Modulus Squared, Obtained by Variation in Magnetic Field Strength. 210°F data.

injection velocity as tangential velocity is thereby effected. The axial magnetic field is also effective in suppression of boundary-layer instability on the end wall, thus increasing the ratio of tangential to radial velocity. These results are sufficiently encouraging to justify continued effort in this area. For example, it is proposed to extend the range of Hartmann modulus by higher temperature operation, by the use of higher magnetic field strength,[§] and by increasing the size of the vortex chamber.

3.2. Turbulent Transport Studies

R. P. Wichner

The equations governing the mean velocity field in turbulent, incompressible flow are the Reynolds equations which may be written:

$$\frac{\partial v_i}{\partial t} + v_j \frac{\partial v_i}{\partial x_j} = - \frac{1}{\rho} \frac{\partial P}{\partial x_i} + \frac{\partial}{\partial x_i} \left[\nu \left(\frac{\partial v_i}{\partial x_j} + \frac{\partial v_j}{\partial x_i} \right) - \overline{v_i v_j} \right]. \quad (3.8)$$

The capital letters represent averaged values. The terms $\overline{v_i v_j}$ (the mean values of the products of the fluctuating i and j components of the velocity) are the Reynolds stresses. These represent the eddy contribution to the momentum conductivity of the fluid over and above the molecular conductivity,

$$\nu \left(\frac{\partial v_i}{\partial x_j} + \frac{\partial v_j}{\partial x_i} \right)$$

Since the molecular conductivity is known in terms of velocity gradients — this is simply the Navier-Stokes stress tensor — the above equation may be solved for the mean velocity when the eddy conductivity is absent; i.e., in laminar flow. No equivalent expression for the turbulent conductivity is known, hence it is impossible to solve for the turbulent velocity field.

[§]An 80-kilogauss solenoid is available in the ORNL Magnet Laboratory.

Although there have been a few notable attempts at theoretical analysis of the Reynolds stress problem, none has succeeded. It appears that if success is to be achieved in this approach to the turbulence problem, it will result from the examination and analysis of a body of Reynolds stress data from a variety of flow geometries.

Until the development of the hot-wire anemometer in the 1930's, it was not possible to measure these eddy stresses. Since then, some limited measurements on a few important geometries have been made; however, there has been no systematic study in this field, and the available experimental data on Reynolds stresses is inadequate to form a guide for a general theory. Therefore, a Reynolds stress measurement effort is being made which has thus far progressed through the following steps:

1. An improved theory relating the signal of a hot-wire anemometer to the Reynolds stresses has been formulated.⁴² The new method requires a linearized response anemometer and divulges the complete state of turbulent stress at a point from a single experiment. Older methods required that a separate attack be made on each of the six components of the stress. In addition, the proposed method has the capability of eliminating the need for the usual low-turbulence intensity approximation, so that flows which possess mean-square turbulent velocity fluctuations at least as great as 10% of the square of the mean velocity can be studied.

2. It was decided to perform the measurements using water in order to more directly relate the experiment to projects of interest at ORNL. A water loop has been fabricated in which test sections having various flow geometries may be placed (Fig. 3.20). The stringent fluid cleanliness, deaeration, and temperature stability requirements of water hot-wire anemometry have, after some difficulty, been met. In addition, extraneous flow fluctuations have been eliminated.

3. Selection of an appropriate hot-wire anemometer presented some difficulty. Most commercial anemometers are designed for use in air and

⁴²R. P. Wichner and F. N. Peebles, "Determination of the Six Reynolds Stresses by the Linearized-Response Hot-Wire Anemometer," p. 361 in Developments in Theoretical and Applied Mechanics, Vol. 1, Plenum Press, New York, 1963.

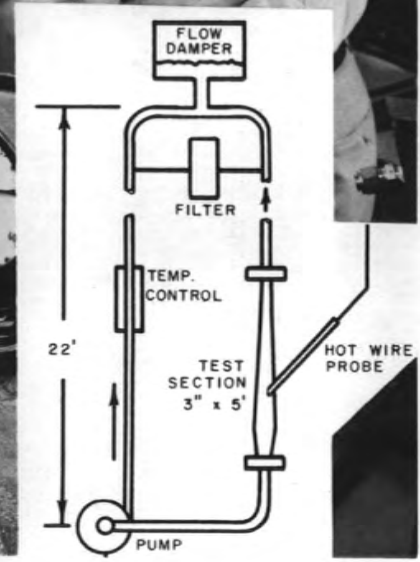
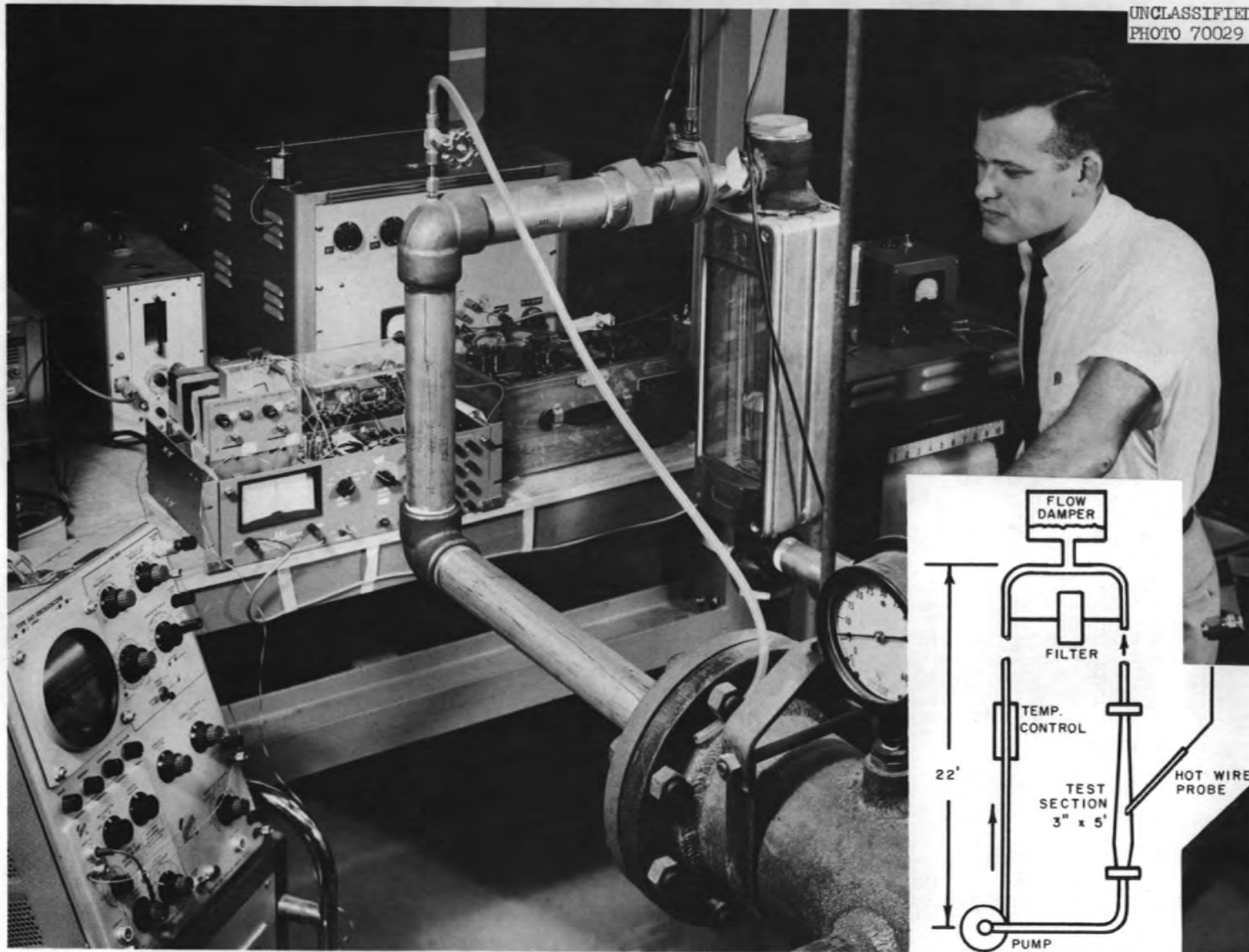


Fig. 3.20. Apparatus for Study of Reynolds Stresses in a Water Flow.

do not have adequate wire heating rates for water use. In addition, it was required that the anemometer output signal be linearized with respect to fluid velocity. It was, therefore, necessary to design and fabricate an instrument to meet the requirements of this experiment; this system is shown in the photograph and schematic of Fig. 3.20. The anemometer is built around an Electronics Associates TR-5 analog computer (Fig. 3.21). The linearization is accomplished by summing and squaring components of the computer. It can be shown that for the condition of the experiment, electrical compensation for the thermal inertia of the wire is not necessary.

4. After testing some commercially available hot-wire probes, most of which were designed for use in air or with a particular instrument, it was decided to fabricate these key items. Some of the handiwork is shown in Fig. 3.22; the support pins are sewing needles, and the wire is 0.0002-in.-diameter nickel. The probes yield an adequately stable reading and can withstand a velocity of 15 ft/sec.

5. Some typical calibration curves - plots of anemometer output voltage versus velocity - are shown in Fig. 3.23. These indicate that linearization of the anemometer response has been satisfactory. The high sensitivity to velocity is partially due to the high heating rate (a current of 0.175 amperes) which creates in the wire a power density of 10^7 kw/liter.

6. Some preliminary results for a test at a Reynolds modulus of 158,000 are shown in Fig. 3.24. It is seen that the level of turbulence in water flows is possibly less than anticipated based on measurements in air.⁴³

⁴³John Laufer, "The Structure of Turbulence in Fully Developed Pipe Flow," NACA-1174, 1954.

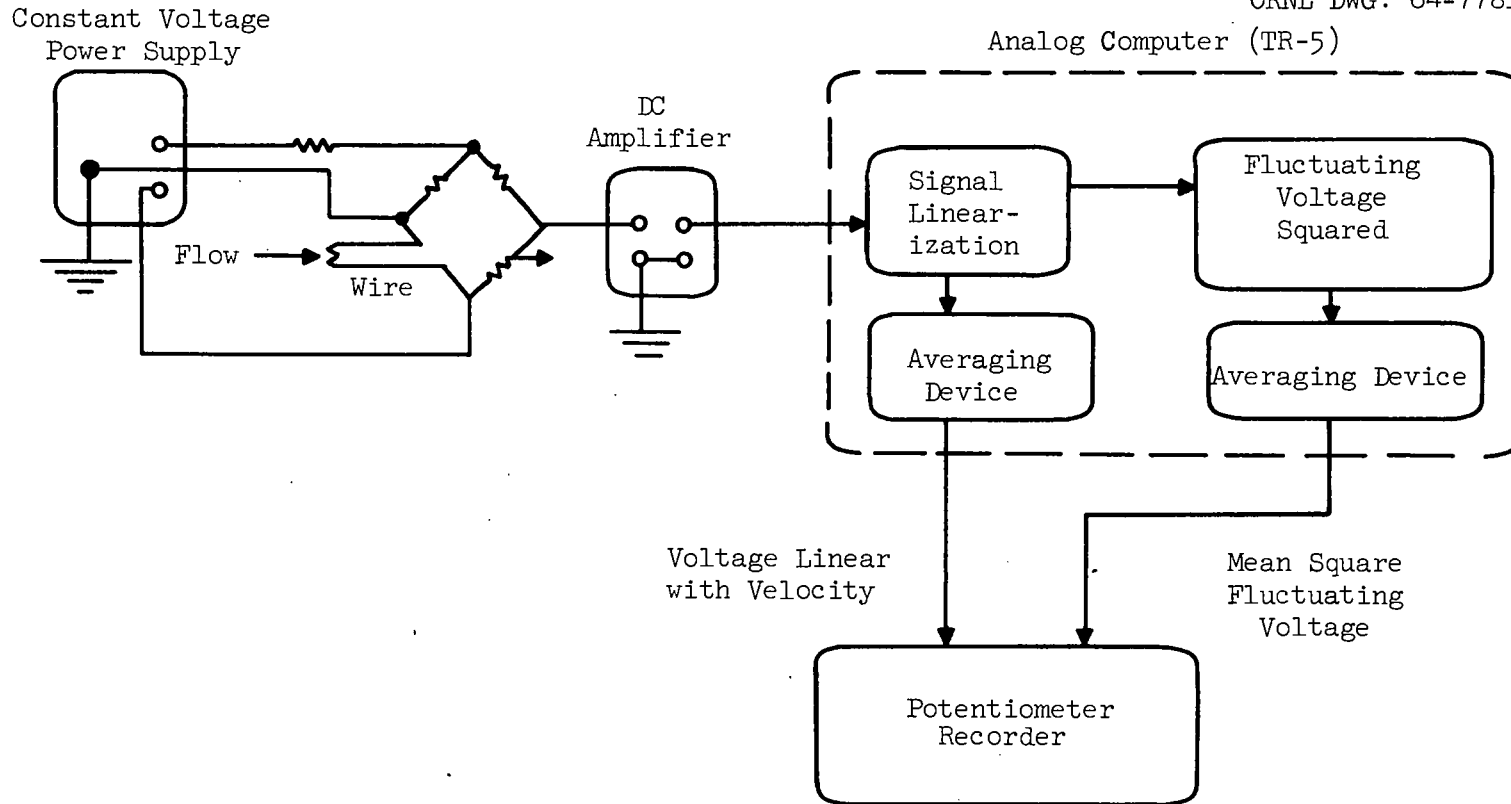


Fig. 3.21. Linearized Response, Constant Current Hot-Wire Anemometer System Schematic.

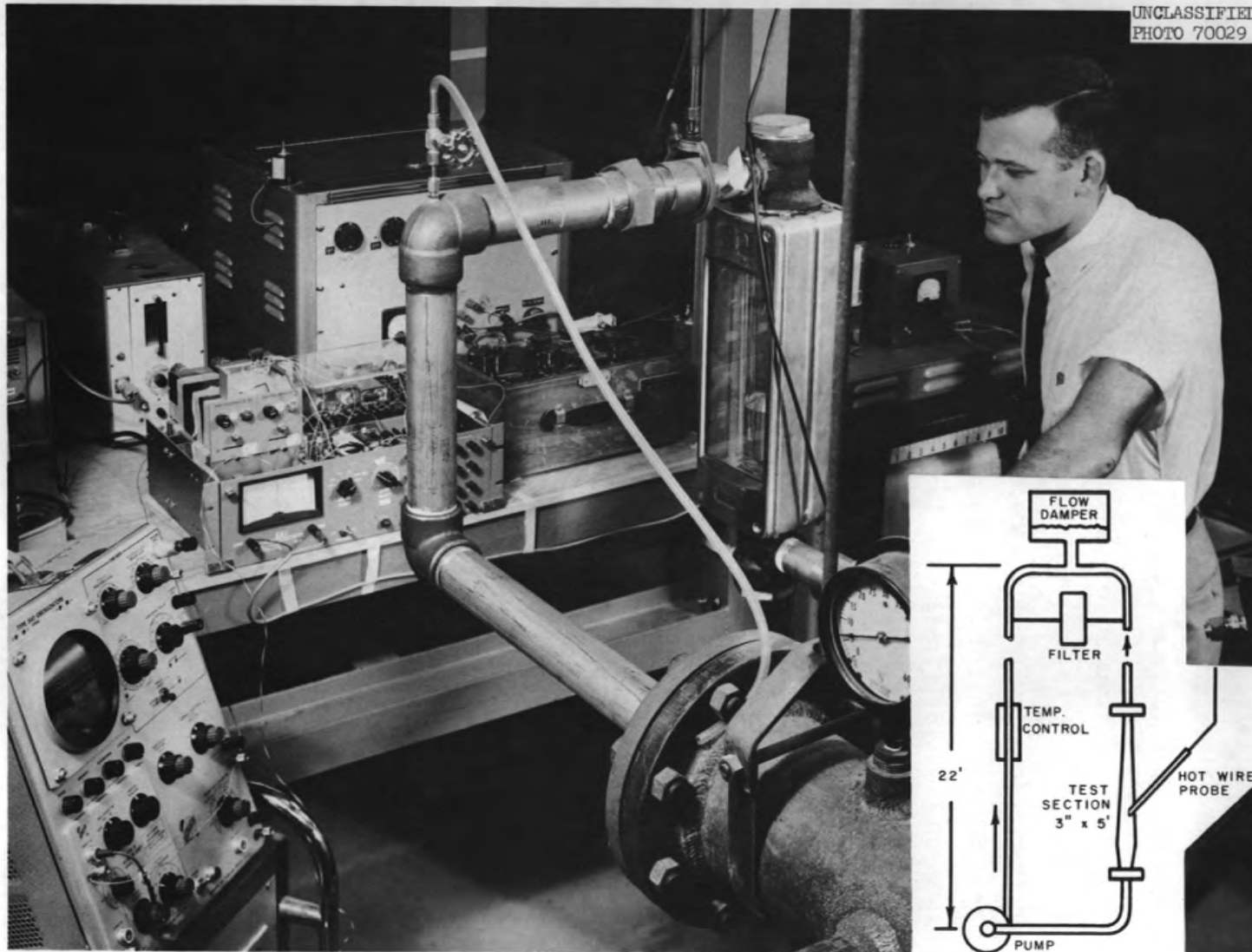


Fig. 3.20. Apparatus for Study of Reynolds Stresses in a Water Flow.

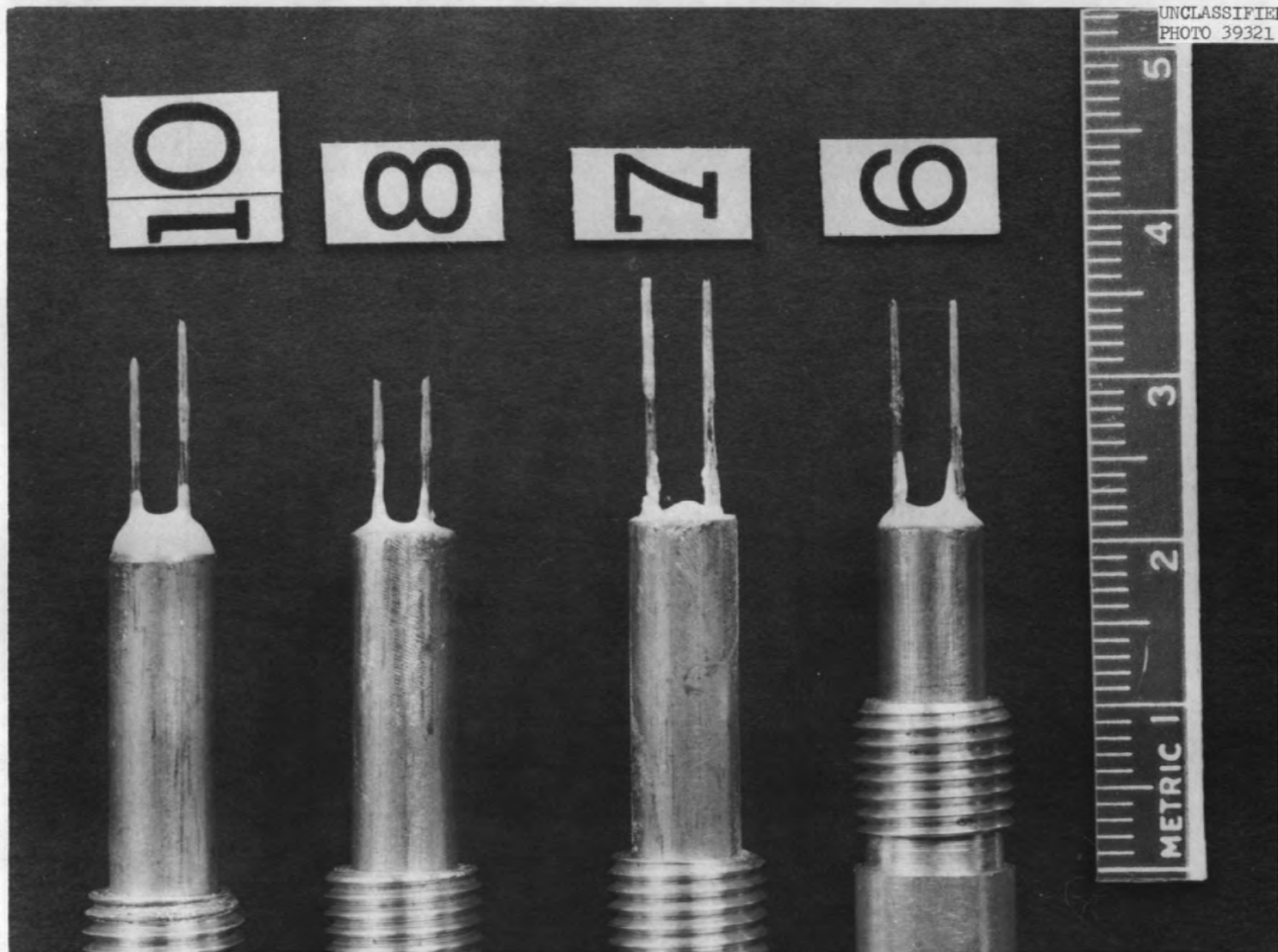


Fig. 3.22. Typical Hot-Wire Probes Constructed for Reynolds Stress Studies.

UNCLASSIFIED
ORNL DWG. 64-7782

Flow - 130 gal/min
 N_{Re} - 158,000

Position No.	Fractional Distance from Wall to Centerline
A	1.0
B	0.82
C	0.63
D	0.44
E	0.25
F	0.096

Ordinate Corresponds to Position Number

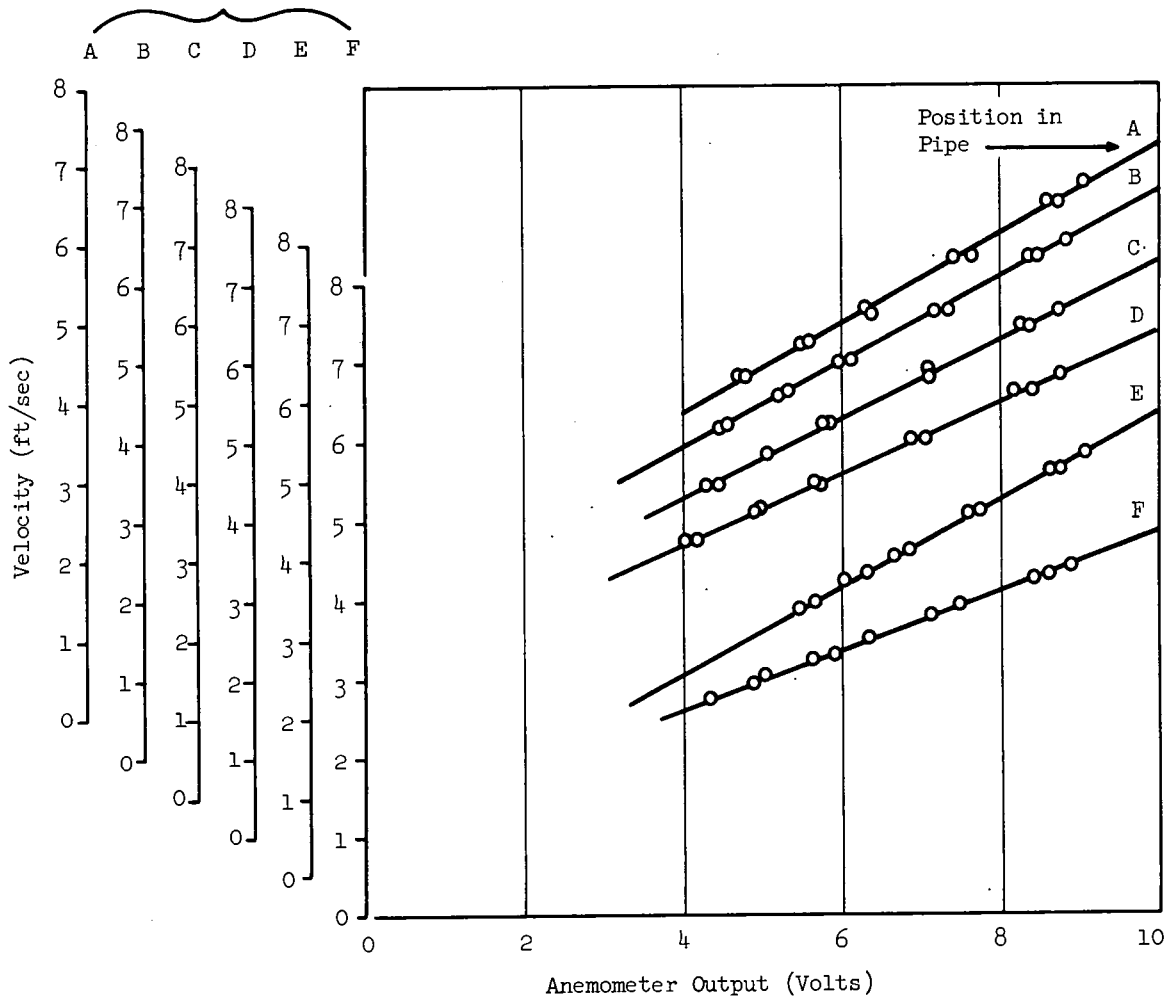


Fig. 3.23. Linearized Response Calibration Curves, Run LT6.

UNCLASSIFIED
ORNL DWG. 64-7783

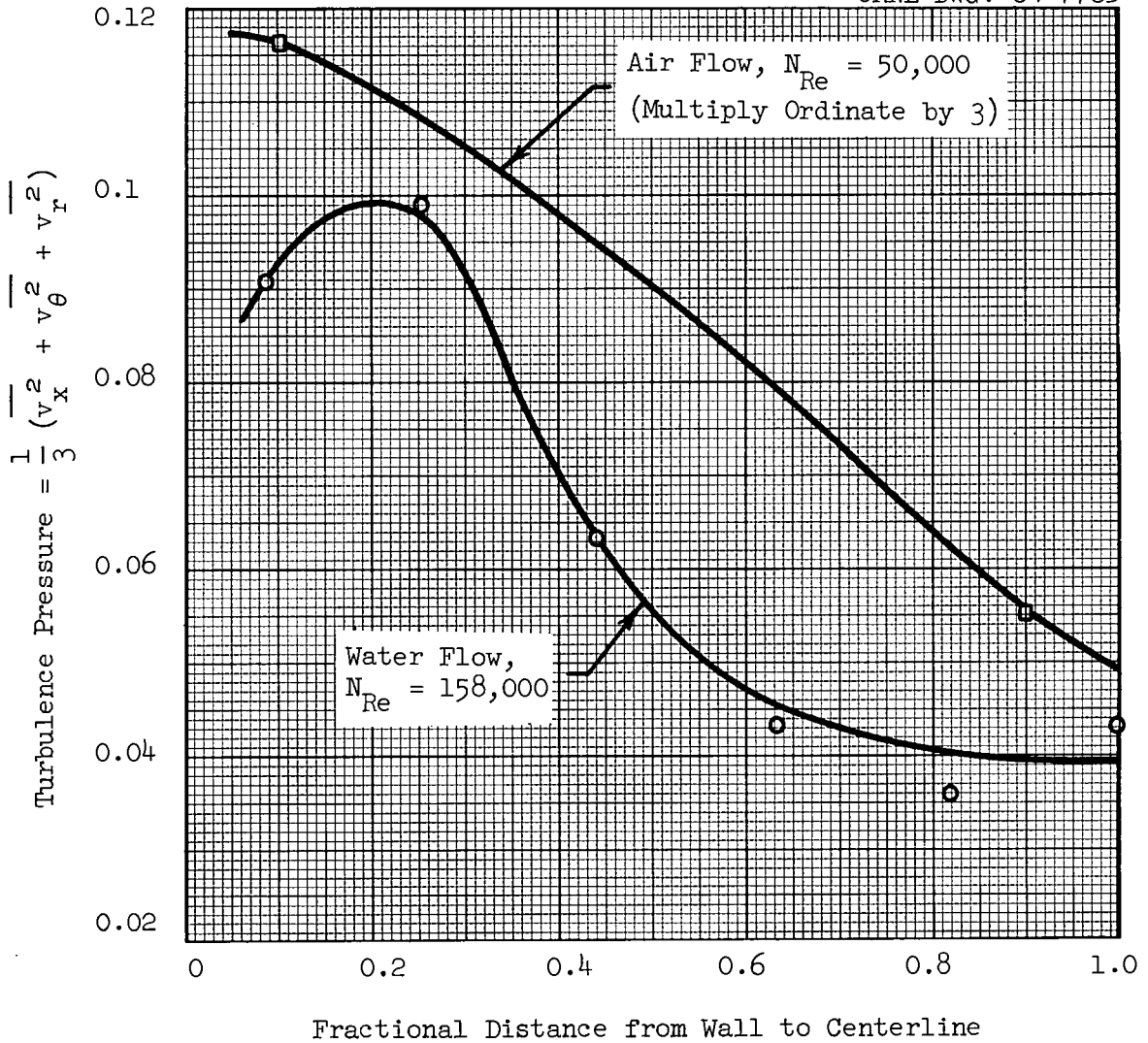


Fig. 3.24. Turbulence Pressure vs Position in Pipe.

3.3. Boundary-Layer Transient Phenomena

G. J. Kidd, Jr.

Previous studies^{44,47} at ORNL have indicated that cyclic stresses induced in a solid by thermal fluctuations in a fluid flowing past the solid surface can cause fatigue-type failures and/or accelerated corrosion in the solid. The extent of this damage was found to be a function of such factors as the amplitude of the temperature fluctuations, their frequency spectrum, the length of exposure, and the relative physical and thermal properties of the fluid and solid. Since moderately high-frequency fluctuations (0.1 to 10 cycles/sec) are normally generated continuously during the operating lifetime of a reactor, a sufficient number of cycles can be accumulated to produce fatigue-type failures even at low amplitudes.

These thermal transients are a result of the random motion of the fluid particles; thus, even in a geometry as simple as a tubular fuel element, internally cooled, turbulent eddies penetrate the viscous sub-layer adjacent to the bounding surface and cause rapid fluctuations in the local rate of heat removal. In entrance regions, diverging channels or downstream of obstructions, transients of large amplitude can be expected. For circulating-fuel reactors, the problem is further intensified by the possibility of adverse temperature profiles in the fluid streams. In addition, the combination of a good thermally conducting fluid in contact with a low-conductivity wall is especially likely to result in

⁴⁴J. J. Keyes, Jr. and A. I. Krakoviak, "High-Frequency Surface Thermal Fatigue Cycling of Inconel at 1405°F," Nuclear Sci. Eng., 9(4): (April 1961).

⁴⁵R. A. Suehrstedt et al., "Applications of Concepts of Penetration Theory to Heat Transfer," USAEC Report KT-378, MIT Practice School, December 1958.

⁴⁶A. E. Higinbotham et al., "Study of Unsteady Heat Transfer Between a Surface and a Flowing Fluid," USAEC Report KT-397, MIT Practice School, May 1959.

⁴⁷H. W. Hoffman et al., "Fundamental Studies in Heat Transfer and Fluid Mechanics - Status Report July 1, 1959 - February 29, 1960," USAEC Report ORNL-CF-60-10-6, Oak Ridge National Laboratory, October 4, 1960.

large surface temperature oscillations. These thermal oscillations will, in many instances, persist beyond the confines of the reactor core and can cause damage in connecting lines and external heat exchangers.

In that the mechanism of thermal transient generation arises from the effects of turbulence near a wall, an understanding of the nature of turbulent instabilities in boundary layers is needed. At present, the theoretical and experimental knowledge of such characteristics of the flow as eddy size and velocity distribution near a wall is meager. Several recent investigations⁴⁷⁻⁵¹ concerned primarily with mass transfer have suggested that the viscous sublayer is, in fact, intermittent, breaking up periodically into turbulent eddies or at least being thinned sufficiently to permit eddies from the bulk of the flow to approach the wall. This investigation will attempt to answer, through the quantitative study of turbulent velocity and temperature profiles at a solid surface, some of the questions concerning thermal instabilities related to conditions and geometries of interest in reactor design.

The experimental system to be used in this study is shown pictorially in Fig. 3.25 and diagrammatically in Fig. 3.26. A constant head, once through, deaerated water supply system is utilized to provide a steady flow, free from fluctuations from pumps, valves, etc. The constant head tanks are approximately 2 ft in diameter and 15 ft tall; flow is adjusted by changing the elevation of either or both of the overflow lines. A 200-gpm cold water (vacuum) deaerator has been installed and is in operation. The deaerator supplies water to the test section with a dissolved gas concentration of less than 0.05 cc/liter. The necessity for using deaerated water arises from the fact that the signal created by a gas bubble flowing past one of the sensing elements is indistinguishable from that produced by an eddy of cool fluid.

⁴⁸P. V. Dankwerts, Ind. Eng. Chem., 43: 1460 (1951).

⁴⁹P. Harriott, "A Random Eddy Modification of the Penetration Theory," Chem. Eng. Sci., 17: 149-154 (1962).

⁵⁰L. P. Reiss and T. J. Hauratty, "Measurements of Instantaneous Rates of Mass Transfer to a Small Sink on a Wall," A.I.Ch.E. Journal, 8(2): 245-247 (May 1962).

⁵¹J. Sternberg, "A Theory for the Viscous Sublayer of a Turbulent Flow," Fluid Mech., 13: 241-271 (1961).

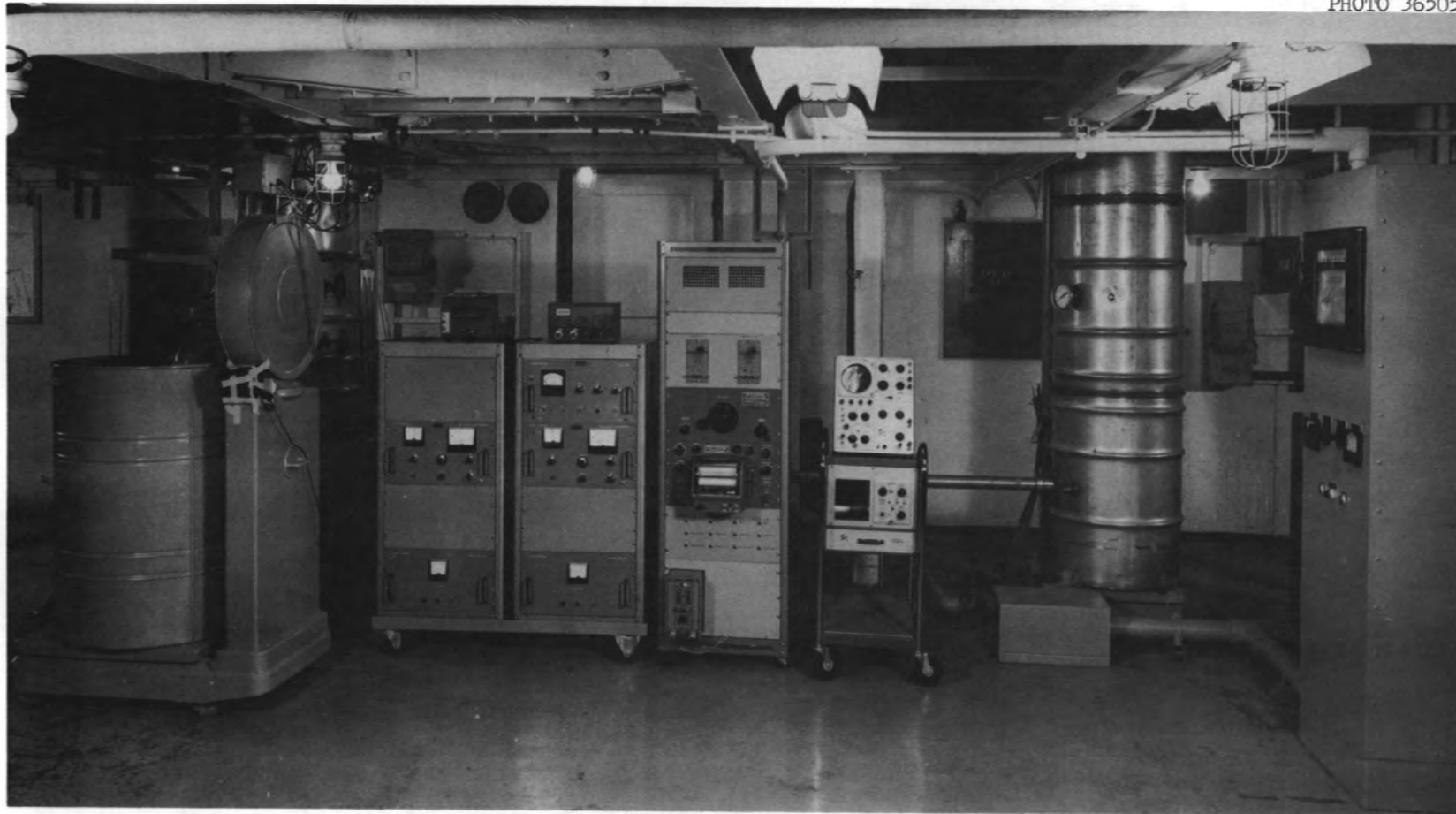


Fig. 3.25. Experimental System for Study of Boundary-Layer Transient Phenomena.

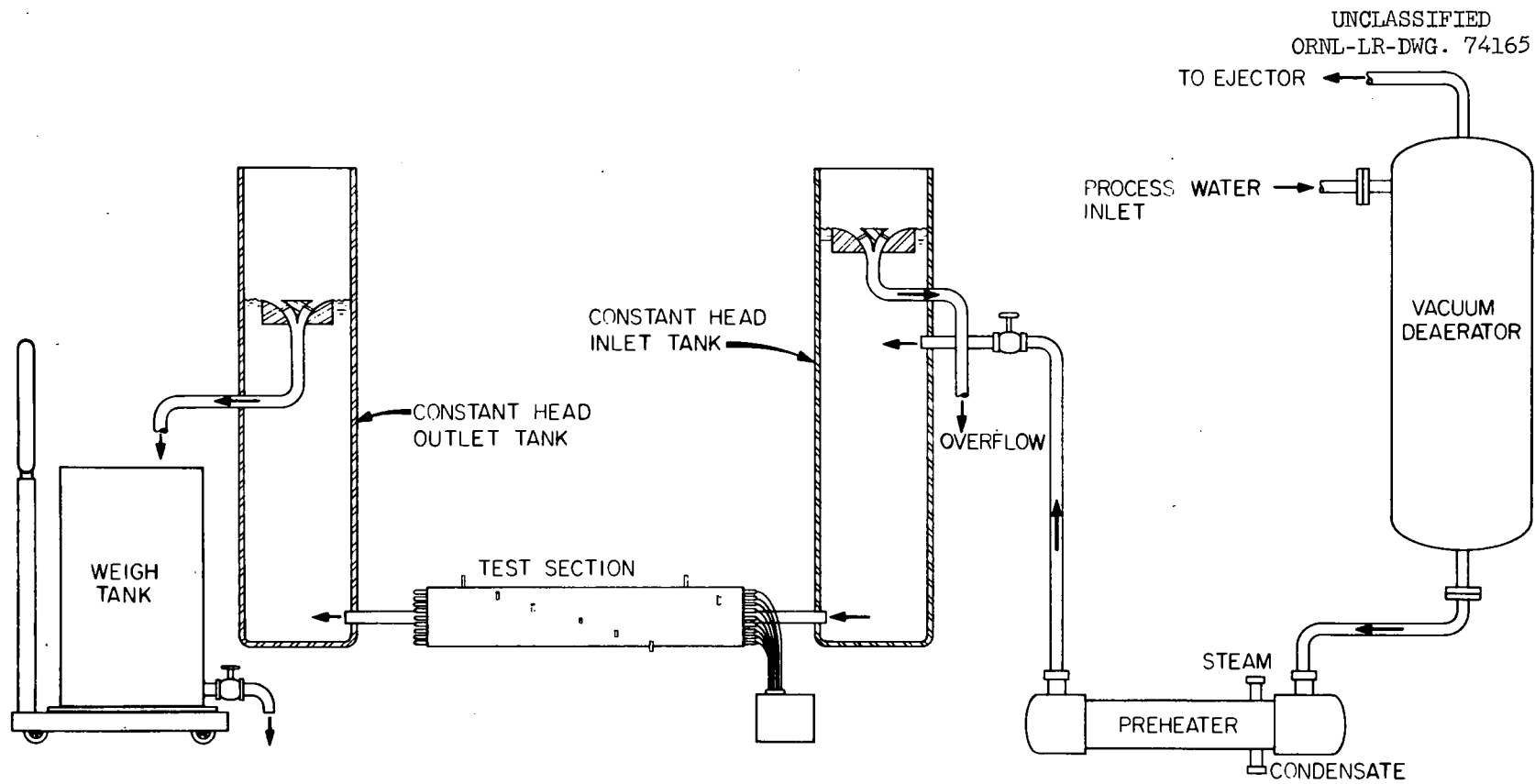


Fig. 3.26. Schematic Representation of System for Study of Boundary-Layer Transient Phenomena.

The test section illustrated in Fig. 3.27 has been used to investigate several design concepts and to check out the instrumentation. A number of qualitative experiments have also been performed. There are 20 "Calrod" 5-kw heaters embedded in an aluminum casting, surrounding a section of 2-in. schedule 40, type 347 stainless steel pipe. The pipe is 10-ft long with the heater encompassing the last 6 ft. Four gunbarrel-type thermocouples are located 1 ft from the outlet. Operating experience gained from this test section has demonstrated that this type of thermocouple can be fabricated and installed to very close tolerances so that meaningful data can be obtained. For example, analysis of the thermal emfs by means of an analogue filtering device using the techniques of frequency domain analysis was used to compute the preliminary power spectral density (PSD) of the surface temperature fluctuations which is plotted in Fig. 3.30. Here the PSD is a statistical quantity defined as the mean-square fluctuation per unit bandwidth. Note that most of the transient thermal power per unit bandwidth is in the range of frequencies below one cps; these low-frequency thermal oscillations are believed to be significant from the standpoint of thermal fatigue.

A second, more sophisticated, test section now under construction is shown in Fig. 3.28. It is made from a solid piece of type 321 stainless steel, 8-ft long with an inside diameter of 2 in. and an outside diameter of 5 in. and will contain 16 gunbarrel thermocouples placed along the entire length of the channel. There are three access ports in the section through which hot-film anemometer probes and/or stream temperature probes can be inserted. The heaters are specially shaped Chromalox rods designed to provide greater heating area per unit length; they are brazed into matching grooves along the final 6 ft of the test section. The electrical power supply for the heaters is a 472/550 v, 400/467 kw Westinghouse dc generator. Direct current is necessary to keep the background ac noise level as low as possible since the signals produced by the thermocouples are very small (of the order of 10 to 100 microvolts).

A simple mathematical model of the temperature distribution and heat transfer across the boundary layer has been developed⁵² which takes

⁵²J. J. Keyes, Jr., "Penetration Theory of Transient Heat Transfer Between a Surface and a Fluid in Turbulent Flow," to be published.

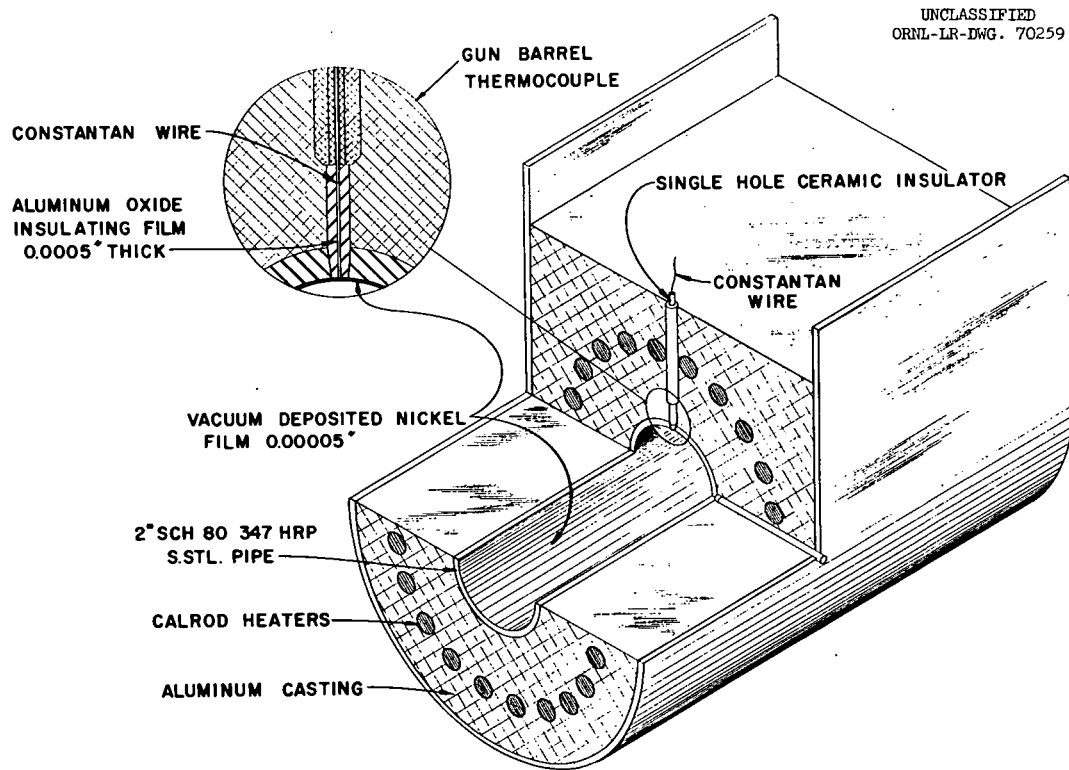


Fig. 3.27. Test Section for Study of Temperature Fluctuations at a Heat-Transfer Surface.

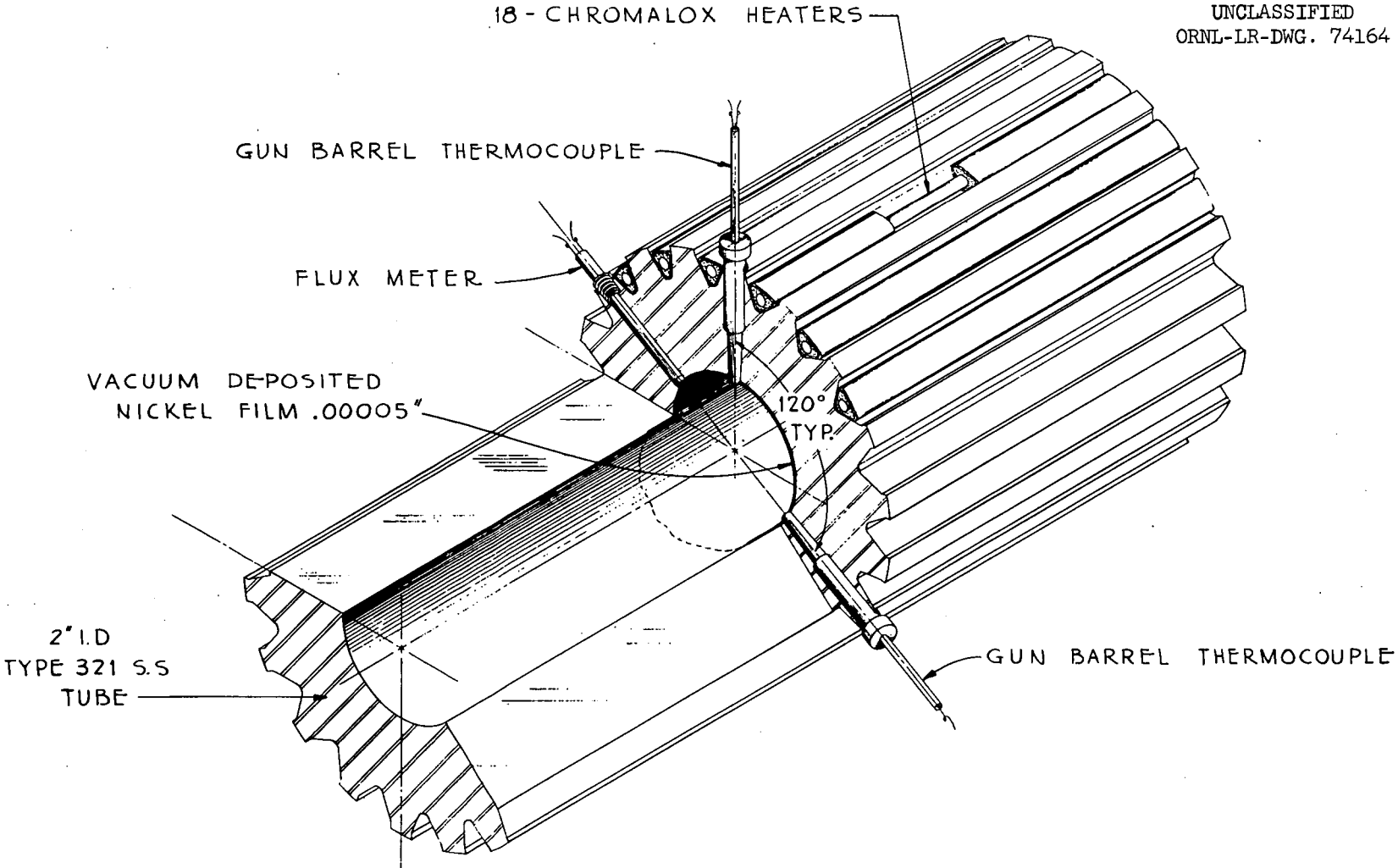


Fig. 3.28. Transient Heat-Transfer Test Section No. 2.

into account the breaking up of the viscous sublayer and eddy penetration. This model has been analyzed using an analog computer, and it was found that the preliminary results obtained from experiments on the first test section were qualitatively consistent with the simple theory. It is anticipated that more accurate data will be obtained with the new test section and improved instrumentation; this will provide a better basis for refinements in the analytical model.

Assembly and calibration of an integrated instrumentation system (Fig. 3.29) for recording and analyzing the complex transient signals generated by the temperature and velocity (hot-film anemometer) probes is essentially completed. This system will enable direct multichannel recording of signals as low as 10 microvolts peak-peak in the frequency range from 0 to 2000 cps. The read-out system consists of a low-frequency spectrum analyzer with provision for direct amplitude-frequency, true rms amplitude-frequency, or power spectral density-frequency scanning, a typical spectral-density profile is shown in Fig. 3.30. This instrument will analyze signals in the frequency range from about 0.5 to 2000 cps directly with resolution of as low as 0.3 cps. Using an FM carrier-type tape record-reproduce system for frequency multiplication, the system will analyze signals with frequencies as low as 0.05 cps.

A hot-film surface probe has been developed which has enabled direct determination of the instantaneous rate of heat transfer and of the instantaneous coefficient of heat transfer at the surface of the test section. It consists of a very thin strip of gold 0.005-in. wide by 0.250-in. long vacuum deposited across a pair of platinum electrodes cast in epoxy resin. The surface of the probe is accurately contoured to fit flush with the inside wall of the test section. By utilizing one of the circuits of the constant temperature hot-film anemometer to power the probe and by analyzing the voltage required to maintain the constant film temperature by means of the power spectral density analyzer, the spectrum of instantaneous surface heat flux can be recorded. This is also the spectrum of the instantaneous heat-transfer coefficient defined by the relation,

$$h(\theta) \equiv \frac{q(\theta)/A}{\Delta t} , \quad (3.9)$$

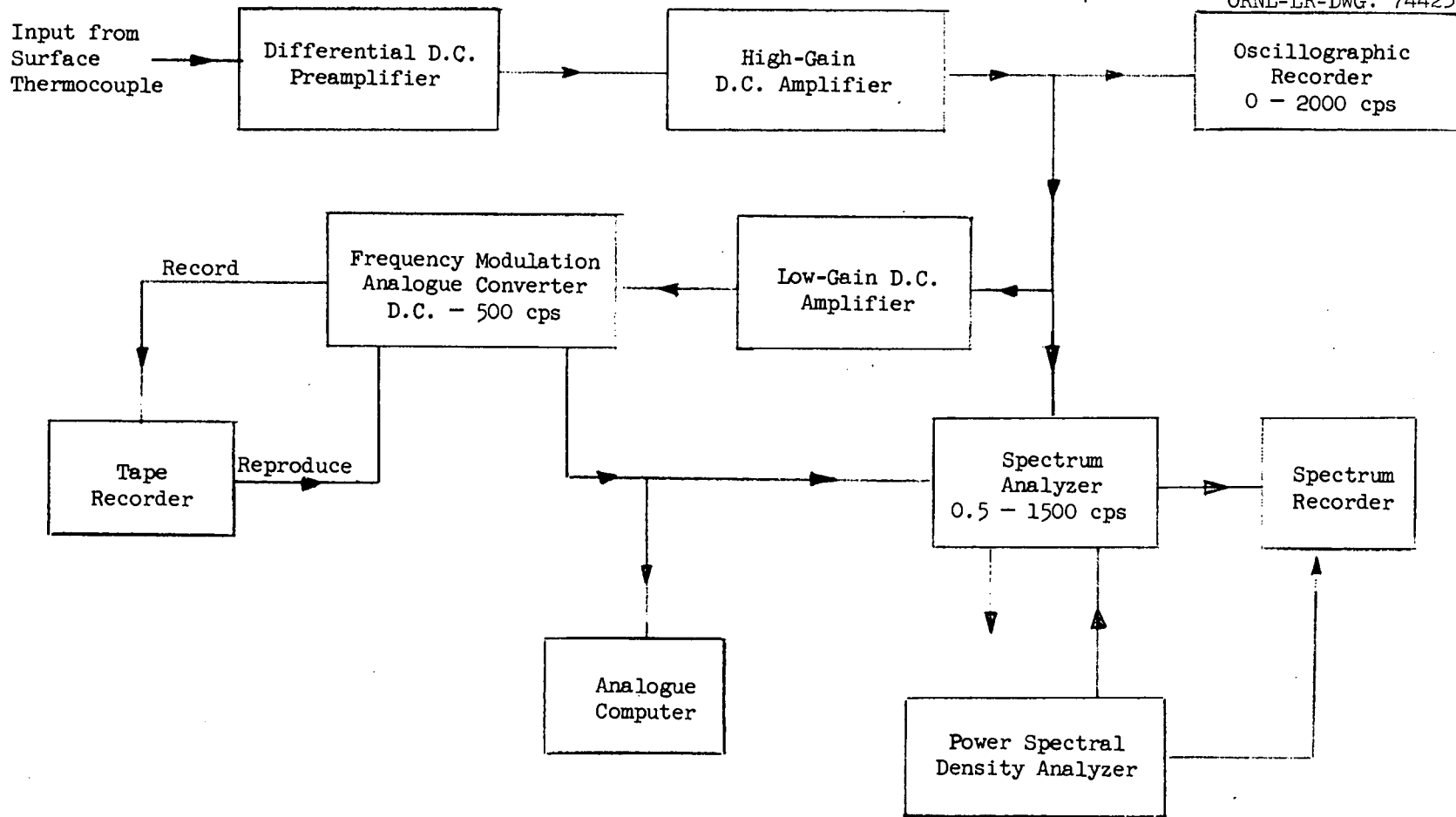


Fig. 3.29. Instrumentation Diagram for Analysis of Transient Thermal EMFS.

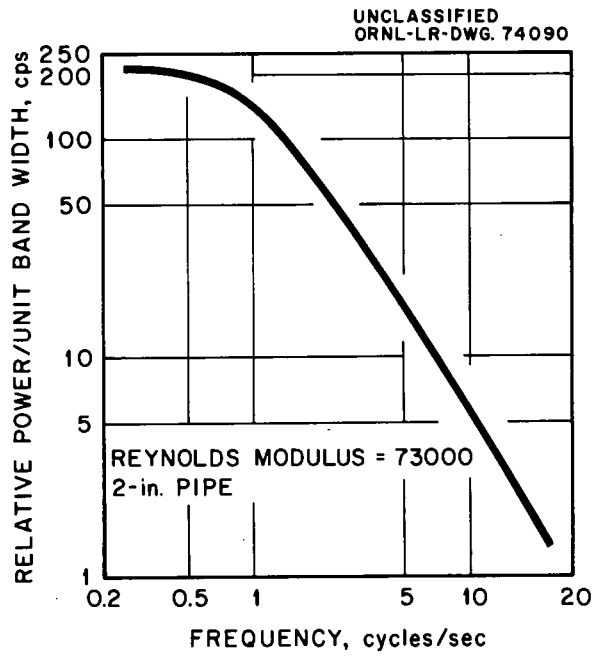


Fig. 3.30. Preliminary Power Spectral-Density Analysis of Surface Thermal Instabilities for Turbulent Flow of Water.

since Δt is maintained constant by the electronic circuitry. It is intended to compare the $h(\theta)$ spectrum with the $t(\theta)$ spectrum [where $t(\theta)$ is the instantaneous surface temperature at an adjacent point in a heated test-section wall as obtained by a surface thermocouple] in an effort to delineate more clearly the nature of the boundary-layer fluctuations giving rise to these transient surface phenomena.

4. THERMOPHYSICAL PROPERTIES

4.1. Alkali Liquid Metals

J. W. Cooke

4.1.1. Thermal Conductivity of Lithium

The measurement of the thermal conductivity of molten lithium (99.82 wt % Li) at temperatures to 1550°F has been completed; details of the apparatus and of the measuring procedure are to be found in Refs. 53 and 54. Final results (Fig. 4.1) can be expressed by the equation

$$k = 19.76 (1 + 5.01 \times 10^{-4} t) \quad , \quad (4.1)$$

between 600° and 1500°F, where k is in Btu/hr·ft·°F for t in °F. A detailed error analysis indicated the accuracy of the data to vary from ±7% at the lower temperature to ±12% at the upper end of the range.

The present results are compared in Fig. 4.2 with predicted and experimental values by other investigators. The unpublished measurements of Miller and Ewing (Naval Research Laboratory) in the temperature range between 540° and 770°F fall roughly parallel to, but 4% below the current data. Nikol'skii and co-workers⁵⁵ (1959) found a lesser dependence of the thermal conductivity on the temperature. At the higher temperatures, a mean line through their data lies 16% below the ORNL results; however, the total scatter in the Nikol'skii data is such

⁵³J. W. Cooke, "The Experimental Determination of the Thermal Conductivity of Molten Lithium from 600 to 1550 Degrees Fahrenheit," USAEC Report ORNL-3390, Oak Ridge National Laboratory, January 1964.

⁵⁴J. W. Cooke, "Experimental Determination of the Thermal Conductivity of Molten Lithium from 320° to 830°C," J. Chem. Phys., 40(7): 1902-1909 (April 1, 1964).

⁵⁵N. A. Nikol'skii et al., "Thermal and Physical Properties of Molten Metals and Alloys," p. 10-11 in Problems in Heat Transfer, ed. by M. A. Mikheev, Publishing House of the Academy of Sciences USSR, Moscow, 1959.

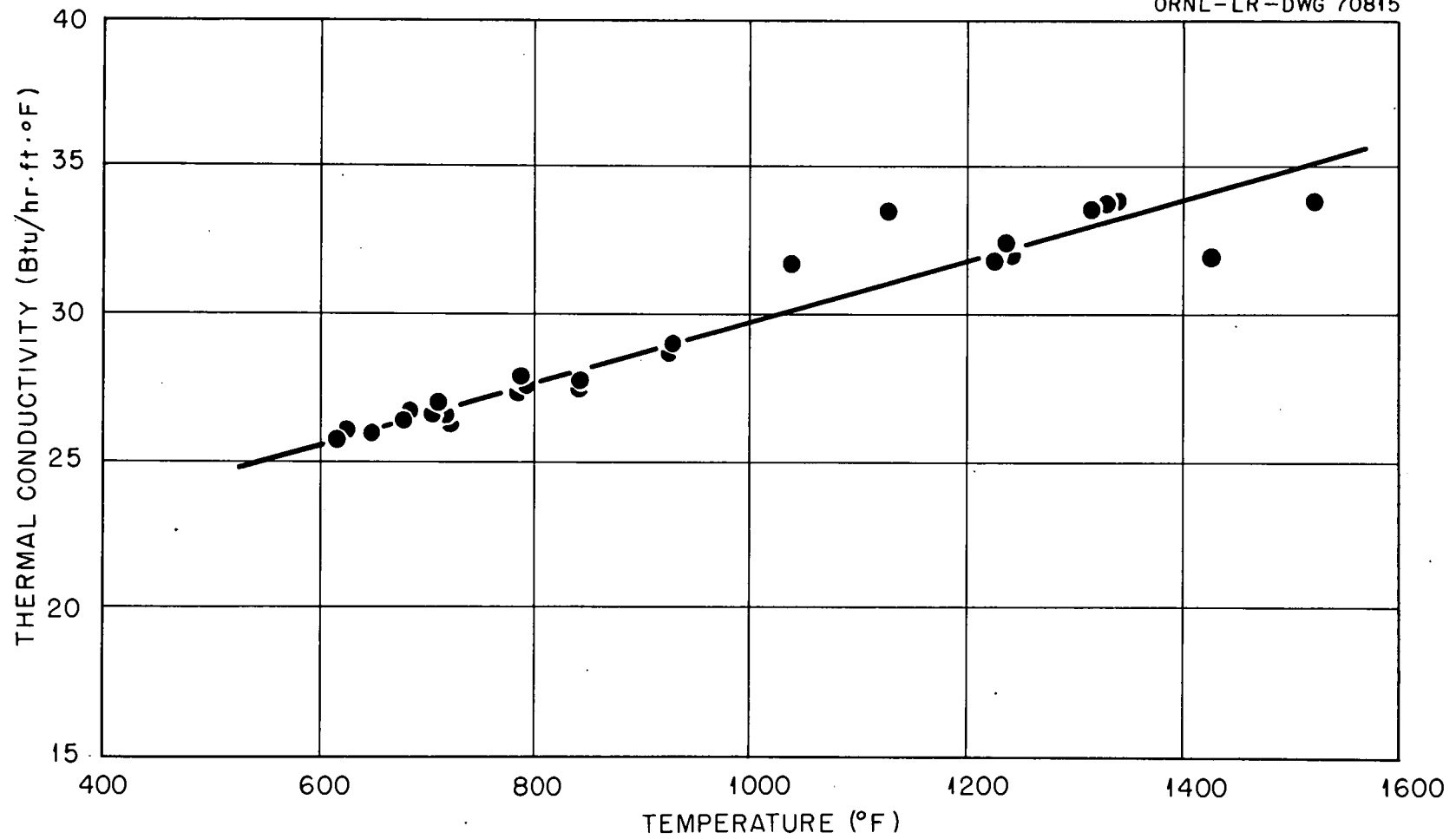


Fig. 4.1. Thermal Conductivity of Molten Lithium as a Function of Temperature.

UNCLASSIFIED
ORNL-LR-DWG 70817

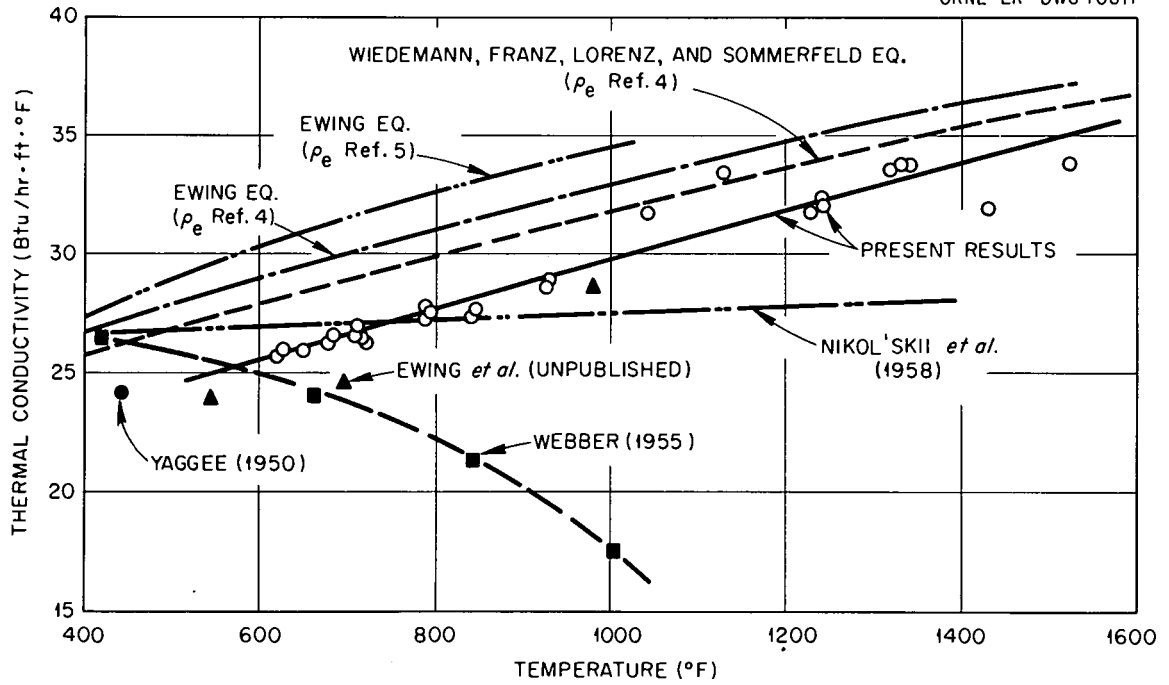


Fig. 4.2. Comparison of Measurements on the Thermal Conductivity of Molten Lithium.

as to embrace the present data. Most recently, Rudnev et al.⁵⁶ (1961) completed measurements on the thermal diffusivity of lithium from 653° to 1845°F. Thermal conductivities derived from this data fall a maximum of 4% above the current results. Finally, it is seen in Fig. 4.2 that the early data of Webber et al.⁵⁷ (1955) are in substantial disagreement in regard to both magnitude (except at the low liquid temperatures) and dependency on temperature with all later results.

In Fig. 4.2 the present data are also compared with predictions based on the correlation of Ewing et al.⁵⁸ and the theoretical expression of Wiedemann and Franz⁵⁹ as modified by Lorenz⁶⁰ and later by Sommerfeld⁶¹ (using recent electrical resistivity values determined by Kapelner⁶²). The agreement is good in respect to the slopes of the curves, but the predicted values fall 10% and 6%, respectively, above the ORNL data. Further, using the results of Bidwell⁶³ for the thermal conductivity of the solid lithium, agreement is found with the theoretical expressions of Mott⁶⁴ and Rao⁶⁵ that the ratio of the thermal conductivities of a

⁵⁶I. I. Rudnev, V. S. Lyshenko, and M. D. Abramovich, "Diffusivity of Sodium and Lithium," Atomnaya Energiya, 11: 230-232 (September 1961); see Atomic Energy, 3: 877-880 (March 1962), translated by Consultants Bureau.

⁵⁷H. A. Webber et al., "Determination of the Thermal Conductivity of Molten Lithium," Trans. Am. Soc. Mech. Engrs., 77: 97 (1955).

⁵⁸C. T. Ewing et al., "Thermal Conductivities of Metals," Chem Eng. Prog. Symposium Series, No. 20, 23: 19-24 (1957).

⁵⁹G. Wiedemann and R. Franz, "The Thermal Conductivities of Metals," Ann. Physik. u. Chem., 89: 497-531 (1853).

⁶⁰L. Lorenz, "The Conductivity of Metals for Heat and Electricity," Ann. Physik, 13: 422-447 (1881).

⁶¹A. Sommerfeld, "The Electron Theory of Metals Based on Fermi Statistics," Z. Physik, 47: 1-32 (1928).

⁶²S. N. Kapelner, "The Electrical Resistivity of Lithium and Sodium-Potassium Alloy," Pratt and Whitney Aircraft Report PWAC-349, June 30, 1961.

⁶³C. C. Bidwell, "Thermal Conductivity of Li and Na by a Modification of the Forbes Bar Method," Phys. Rev., 28, 584-597 (1926).

⁶⁴N. F. Mott, "The Resistance of Liquid Metals," Proc. Roy. Soc. (London), Series A, 146: 465-472 (1954).

⁶⁵M. R. Rao, "Thermal Conductivity of Liquid Metals," Indian J. Phys., 16: 155-159 (1942).

liquid metal before and after melting should be equal to the square of the ratio of the corresponding atomic frequencies. In contrast to results with sodium and potassium, the thermal conductivity of molten lithium exhibits a positive trend with temperature (both experimentally and theoretically in the temperature range of Fig. 4.2) This is believed to be related to differences in the structural change which occurs at melting; and it has been noted that at the melting point the ratio of solid-to-liquid conductivities is greater for lithium than for sodium or potassium ($k_S/k_L = 1.8, 1.3, \text{ and } 1.6$ for lithium, sodium, and potassium, respectively).

4.1.2. Surface Tension of Potassium

Preliminary results for the surface tension, relative to helium, of 99.96 wt % potassium have been obtained in the temperature range 70 to 308°C using the maximum-bubble pressure apparatus illustrated schematically in Fig. 4.3. High-purity helium was supplied at very low flow to a capillary tube whose end was immersed to various depths in the liquid. The maximum pressure attained within the slowly growing bubble before disengagement from the capillary tip was measured with a micromanometer (sensitivity, ± 0.01 mm) using Octol S fluid. The immersion depth was established by a dial indicator (sensitivity, ± 0.025 mm) which was zeroed at the point of electrical contact of the capillary with the liquid surface. The surface tension can then be calculated, following the iterative technique of Sugden⁶⁶ which accounts for the nonspherical shape of the bubble, using the inside radius of the capillary tip, the maximum bubble pressure, and the immersion depth. For these experiments, it has been established that the simpler calculation using Schroedinger's equation,⁶⁷

$$\sigma = \frac{pr}{2} \left[1 - \frac{2}{3} \left(\frac{r}{h} \right) - \frac{1}{6} \left(\frac{r}{h} \right)^2 \right], \quad (4.2)$$

⁶⁶S. Sugden, "The Determination of Surface Tension from Maximum Pressure in Bubbles," J. Chem. Soc., 1: 858 (1922).

⁶⁷G. Schroedinger, "Note on the Capillary Pressure in Gas Bubbles," Ann. Physik, 46: 413 (1915).

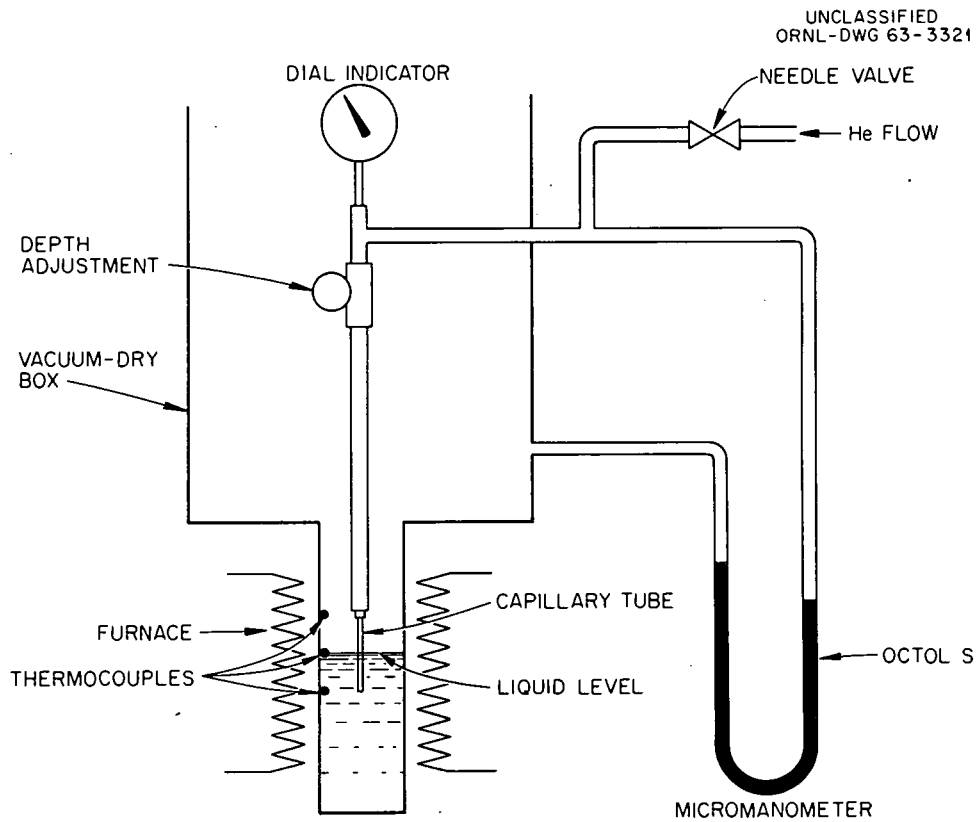


Fig. 4.3. Maximum-Bubble-Pressure Apparatus for Surface-Tension Determinations with Liquid Metals.

gives values agreeing to within a fraction of a per cent with those obtained by the Sugden procedure. In Eq. 4.2, σ is the surface tension (dyne/cm), r , the tip radius (cm), and h , the hydrostatic head of fluid above the capillary tip (cm).

For the current measurements, the apparatus differed from that described above in that water, rather than Octol S, was used in the manometer. The water and potassium were separated by liquid-nitrogen-cooled molecular-sieve traps. Some loss in sensitivity in the pressure measurements resulted from the effect of the compressible gas volume in these traps. Further, it was found that the capillary tip could be immersed to only 1/4 of its design depth; this introduced an additional loss in precision. Finally, since the helium purification system had not yet been completed, some contamination of the potassium possibly occurred; the helium purity was of the order of 99.9+% rather than the 99.99+% desired.

The data of this preliminary measurement, plotted in Fig. 4.4, can be represented, using a least-squares fitting technique, by the equation,

$$\sigma = 118.5 - 0.0998 t + 7.65 \times 10^{-5} t^2 \quad , \quad (4.3)$$

for t in °C over the temperature range 70 to 308°C. The rms deviation was 0.54 dyne/cm. As noted in Fig. 4.4, the data obtained while the potassium temperature was decreasing are consistent with those for the initial temperature-increasing period. Also shown in Fig. 4.4 are the results of Quarterman and Primak⁶⁸ obtained by a capillary rise technique. These investigators state that their data may be low by as much as 15% due to errors introduced into the measurement of the magnitude of the liquid rise by uncertainties in the liquid meniscus.

Refinement of the apparatus is not expected to change the results described by Eq. 4.3. This is indicated by the results of a determination of the surface tension of triply distilled, doubly deionized water using the same apparatus arrangement as for the potassium measurements.

⁶⁸L. A. Quarterman and W. L. Primak, "The Capillary Rise, Contact Angle, and Surface Tension of Potassium," J. Am. Chem. Soc., 72: 3035 (1950).

It was found that σ for water against helium at 28°C was 2% below the value reported by Dorsey⁶⁹ for water relative to air. Gambill⁷⁰ pointed out that the major part of this 2% discrepancy can be attributed to the effects of using different gases for the measurements.

These studies will be continued at higher temperatures after incorporation of the changes necessary to bring the apparatus to design specification.

4.1.3. Contact-Angle Determinations

The extent to which a liquid "wets" a surface can be characterized by the angle of contact between a liquid droplet and the surface on which the droplet rests; the angle of contact, θ , is defined in Fig. 4.5. From thermodynamic considerations,^{71,72} it can be shown that

$$\sigma_{sl} = \sigma_{sv} - \sigma_{lv} \cos \theta, \quad (4.4)$$

where the subscripts s , l , v indicate solid, liquid, and vapor, respectively, and in combination designate the phase interfaces. When σ_{sl} exceeds σ_{sv} , θ will be greater than 90 deg; this is a nonwetting condition. Conversely, if the liquid spreads on the surface, $\sigma_{sv} > \sigma_{sl}$ and $\theta < 90$ deg.

Since the wetting characteristics of a liquid against a surface are of importance to a complete understanding (and prediction) of boiling and condensing phenomena, a program to measure the contact angle for the alkali liquid metals in contact with various surfaces has been instituted

⁶⁹N. E. Dorsey, Properties of Ordinary Water Substance, Reinhold Publishing Corp., New York, 1940.

⁷⁰W. R. Gambill, "Surface Tension of Pure Liquids," Chem. Eng., 56: 146 (April 1958).

⁷¹W. D. Harkins, The Physical Chemistry of Surface Films, Reinhold Publishing Corp., New York, 1952.

⁷²A. Bondi, "Spreading of Liquid Metals on Solid Surfaces; Surface Chemistry of High-Energy Substances," Chem. Revs., 42(2): 417-458 (1953).

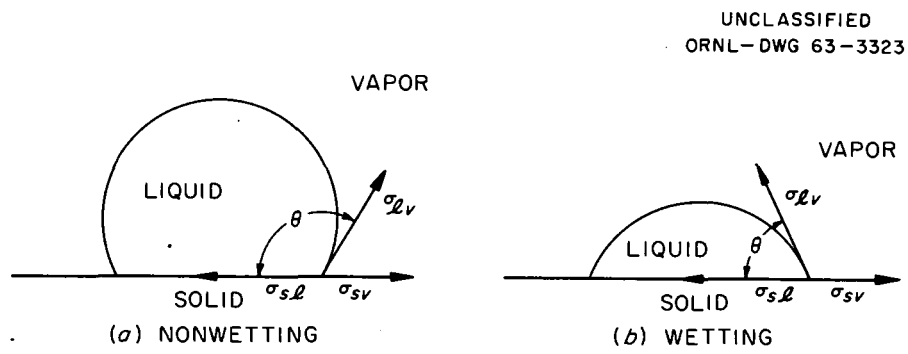


Fig. 4.5. Shape of Sessile Drops for Wetting and Nonwetting Conditions.

using the sessile-drop method. This technique, and a calculational procedure for extracting the surface tension from the measurements, have been discussed in detail by Gilliland.⁷³ Preliminary experiments to establish feasibility in the current application have been completed with potassium on a polished flat, horizontal, type 316 stainless steel plate. Periodic photographs of the droplet were obtained while the surface temperature was increased steadily to 600°C; typical results are shown in Fig. 4.6. It was observed that the angle of contact varied from an initial value of approximately 120-deg at 70°C to 0-deg at 500°C some 95 minutes later. A second droplet placed on the surface at 180°C produced an initial contact angle of 50 deg. Above 600°C, experimental difficulties resulting from evaporation of the droplet (loss of material, obscuring of the view by the generated vapor, etc.) were encountered.

Following completion of a more refined optical system, these experiments will be continued so as to differentiate the influence of the variables time, temperature, and surface condition.

4.2. Miscellaneous Materials

4.2.1. Electrical Resistivity of Brass

W. R. Gambill

The temperature dependence of the electrical resistivity of seamless 70-30 brass tubing was determined over the temperature range of 70 to 500°C. The results obtained with two test specimens of different lengths were in good agreement. The mean values of resistivity are given in Table 4.1.

Table 4.1. Electrical Resistivity of Seamless 70-30 Brass

t (°C)	100	200	300	400	500
ρ_e (μ ohm-cm)	7.39	8.29	9.37	10.58	11.75

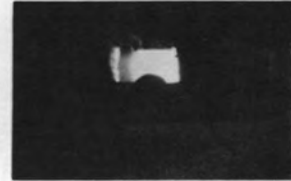
⁷³R. G. Gilliland, "Investigation of the Wettability of Various Pure Metals and Alloys on Beryllium," USAEC Report ORNL-3438, Oak Ridge National Laboratory, May 1963.

UNCLASSIFIED
PHOTO 62327

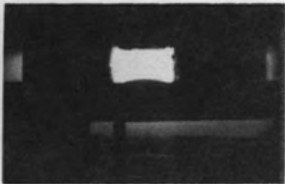
(a) TIME = 0 min
TEMPERATURE = 147° F



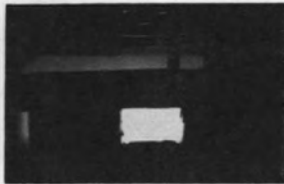
(b) TIME = 26 min
TEMPERATURE = 329° F



(c) TIME = 47 min
TEMPERATURE = 445° F



(d) TIME = 72 min
TEMPERATURE = 772° F



(e) TIME = 95 min
TEMPERATURE = 904° F

Fig. 4.6. Sessile-Drop Shapes with Molten Potassium on a Stainless Steel Surface as a Function of Temperature and Time.

5. BIBLIOGRAPHY

The information presented in this current report derives, in general, from studies initiated prior to this report period. It seems desirable, therefore, to list ORNL reports and open-literature publications issued since the inception of these programs so that the reader is able to acquaint himself conveniently with the full scope of these studies.

Boiling Potassium Heat Transfer

1. W. R. Gambill and H. W. Hoffman, "Boiling Liquid-Metal Heat Transfer," American Rocket Society Paper No. 1737-61, May 1961.
2. H. W. Hoffman and A. I. Krakoviak, Forced Convection Saturation Boiling of Potassium at Near-Atmospheric Pressure, pp. 182-203, "Proceedings of 1962 High-Temperature Liquid-Metal Heat Transfer Technology Meeting," USAEC Report BNL-756, Brookhaven National Laboratory.
3. H. W. Hoffman, Studies in Two-Phase Flow and Boiling Heat Transfer at the Oak Ridge National Laboratory, pp. 18-23, "Two-Phase Flow Problems," EURATOM Report, EUR 352.e, 1963.
4. A. I. Krakoviak, "Notes on the Liquid-Metal Boiling Process," USAEC Report ORNL-TM-618, Oak Ridge National Laboratory, July 10, 1963.
5. A. I. Krakoviak, Superheat Requirements with Boiling Liquid Metals, "Proceedings of 1963 High-Temperature Liquid-Metal Heat Transfer Technology Conference," USAEC Report ORNL-3603, Oak Ridge National Laboratory (in publication).
6. H. W. Hoffman, Recent Experimental Results in ORNL Studies with Boiling Potassium, "Proceedings of 1963 High-Temperature Liquid-Metal Heat Transfer Technology Conference," USAEC Report ORNL-3603, Oak Ridge National Laboratory (in publication).

General Boiling Studies

1. W. R. Gambill and R. D. Bundy, "Burnout Heat Fluxes for Low-Pressure Water in Natural Circulation," USAEC Report ORNL-3026, Oak Ridge National Laboratory, December 20, 1960.
2. W. R. Gambill and R. D. Bundy, "HFIR Heat-Transfer Studies of Turbulent Water Flow in Thin Rectangular Channels," USAEC Report ORNL-3079, Oak Ridge National Laboratory, June 5, 1961.
3. W. R. Gambill, "A Survey of Boiling Burnout," British Chem. Eng., 93-98 (February 1963).

4. W. R. Gambill, "Generalized Prediction of Burnout Heat Flux for Flowing, Subcooled, Wetting Liquids," Chem. Eng. Progr. Symposium Series, 59(41): 71-87 (March 1963); also see W. R. Gambill, "Burnout Heat Flux Prediction for Flowing, Subcooled, Wetting Liquids," pp. 112-137, Proceedings of Research Reactor Fuel Element Conference, Gatlinburg, Tennessee, September 1962, USAEC Report TID-7643 (Book I), 1963.

Swirl-Flow Heat Transfer

1. W. R. Gambill and N. D. Greene, "A Study of Burnout Heat Fluxes Associated with Forced-Convection, Subcooled, and Bulk Nucleate Boiling of Water in Source-Vortex Flow," USAEC Report ORNL CF-57-10-118, Oak Ridge National Laboratory, October 29, 1957.
2. W. R. Gambill and N. D. Greene, "A Preliminary Study of Vortex-Boiling Burnout Heat Fluxes," Jet Propulsion, 28(3): 192-194 (March 1958).
3. W. R. Gambill and N. D. Greene, "A Preliminary Study of Boiling Burnout Heat Fluxes for Water in Vortex Flow," USAEC Report ORNL CF-58-4-56, Oak Ridge National Laboratory, April 12, 1958; also see A.I.Ch.E. Preprint 29, Second National Heat Transfer Conference, August 18-21, 1958.
4. N. D. Greene and W. R. Gambill, "A Preliminary Investigation of Air Film Heat-Transfer Coefficients for Free- and Forced-Vortex Flow Within Tubes," USAEC Report ORNL CF-58-5-67, May 23, 1958.
5. W. R. Gambill and N. D. Greene, "Boiling Burnout with Water in Vortex Flow," Chem. Eng. Progr., 54: 68-76 (October 1958).
6. W. R. Gambill, R. D. Bundy, and R. W. Wansbrough, "Heat, Burnout, and Pressure Drop for Water in Swirl Flow Through Tubes with Internal Twisted Tapes," USAEC Report ORNL-2911, Oak Ridge National Laboratory, March 28, 1960; see also Chem. Eng. Progr. Symposium Series, 57(32): 127-137 (1961).
7. W. R. Gambill and R. D. Bundy, "An Evaluation of the Present Status of Swirl-Flow Heat Transfer," ASME Paper No. 62-HT-42, Houston, Texas, August 1962; see also USAEC Report ORNL CF-61-4-61, Oak Ridge National Laboratory, April 24, 1961.
8. W. R. Gambill and R. D. Bundy, "High-Flux Heat Transfer Characteristics of Pure Ethylene Glycol in Axial and Swirl Flow," A.I.Ch.E. Journal, 9(1): 55-59 (January 1963).

Vortex Gas Dynamics

1. J. L. Kerrebrock and R. V. Meghreblian, "An Analysis of Vortex Tubes for Combined Gas-Phase Fission Heating and Separation of the Fissionable Material," USAEC Report ORNL CF-57-11-3 (Revision 1), Oak Ridge National Laboratory, April 11, 1958.

2. J. L. Kerrebrock and P. G. Lafyatis, "Analytical Study of Some Aspects of Vortex Tubes for Gas-Phase Fission Heating," USAEC Report ORNL CF-58-7-4, Oak Ridge National Laboratory, July 1958.
3. J. L. Kerrebrock and J. J. Keyes, Jr., "A Preliminary Experimental Study of Vortex Tubes for Gas-Phase Fission Heating," USAEC Report ORNL-2660, Oak Ridge National Laboratory, February 1959.
4. J. J. Keyes, Jr., and R. E. Dial, "An Experimental Study of Vortex Flow for Application to Gas-Phase Fission Heating," USAEC Report ORNL-2837, Oak Ridge National Laboratory, April 1960.
5. J. J. Keyes, Jr., "An Experimental Study of Gas Dynamics in High Velocity Vortex Flows," Proceedings of the 1960 Heat Transfer and Fluid Mechanics Institute, pp. 31-36, Stanford University Press, Stanford, California.
6. J. L. Kerrebrock and R. V. Meghreblian, "Vortex Containment for the Gaseous Fission Rocket," J. Aerospace Science, 28: 710-724 (1961).
7. J. J. Keyes, Jr., "An Experimental Study of Flow and Separation in Vortex Tubes with Application to Gaseous Fission Heating," Am. Rocket Soc. Journal, 1204-1210 (September 1961).

Vortex Magnetohydrodynamics

1. T. S. Chang, "Magnetohydrodynamic Stability of Vortex Flow - A Non-dissipative, Incompressible Analysis," USAEC Report ORNL TM-402, Oak Ridge National Laboratory, October 23, 1962.
2. J. J. Keyes, Jr., "Some Applications of Magnetohydrodynamics in Confined Vortex Flows," USAEC Report ORNL TM-479, Oak Ridge National Laboratory, February 28, 1963.

Turbulent Transport Studies

1. R. P. Wichner and F. N. Peebles, "Determination of the Six Reynolds Stresses by the Linearized-Response Hot-Wire Anemometer," pp. 361-370 in Developments in Theoretical and Applied Mechanics, Vol. 1, Plenum Press, New York, 1963.

Boundary-Layer Transient Phenomena

1. J. J. Keyes, Jr., and J. E. Mott, "An Investigation of Thermal-Transient Decay at a Fluid-Solid Interface and in Turbulent Flow Through Circular Ducts," USAEC Report ORNL-2603, Oak Ridge National Laboratory, December 2, 1958.
2. R. A. Suehrstedt et al., "Applications of Concepts of Penetration Theory to Heat Transfer," USAEC Report KT-378, MIT Practice School, Oak Ridge Gaseous Diffusion Plant, December 1958.

3. A. E. Higinbotham et al., "Study of Unsteady Heat Transfer Between a Surface and a Flowing Fluid," USAEC Report KT-397, MIT Practice School, Oak Ridge Gaseous Diffusion Plant, May 1959.
4. J. J. Keyes, Jr., and A. I. Krakoviak, "High-Frequency Surface Thermal Fatigue Cycling of Inconel at 1405°F," Nucl. Sci. Eng., 9: 462-474 (1961).

Progress Reports

1. H. W. Hoffman et al., "Fundamental Studies in Heat Transfer and Fluid Mechanics, Status Report July 1, 1959 - February 29, 1960," USAEC Report ORNL CF-60-10-6, Oak Ridge National Laboratory, October 1960.

INTERNAL DISTRIBUTION

- | | | | |
|--------|----------------------|--------|---|
| 1. | L. G. Alexander | 55. | J. A. Lane |
| 2. | R. A. Armistead, Jr. | 56. | G. E. Larson |
| 3. | S. E. Beall | 57. | M. E. LaVerne |
| 4. | M. Bender | 58. | C. G. Lawson |
| 5. | E. S. Bettis | 59. | J. Lones |
| 6. | E. P. Blizard | 60. | M. I. Lundin |
| 7. | A. L. Boch | 61. | R. N. Lyon |
| 8. | E. G. Bohlmann | 62. | H. G. MacPherson |
| 9. | G. E. Boyd | 63. | R. E. MacPherson |
| 10. | C. A. Brandon | 64. | H. C. McCurdy |
| 11. | R. B. Briggs | 65. | W. B. McDonald |
| 12. | R. D. Bundy | 66. | A. J. Miller |
| 13. | S. J. Claiborne, Jr. | 67. | R. L. Miller |
| 14. | T. S. Chang | 68. | T. C. Min |
| 15. | T. E. Cole | 69. | F. N. Peebles |
| 16. | J. W. Cooke | 70. | A. M. Perry |
| 17. | W. B. Cottrell | 71. | M. W. Rosenthal |
| 18. | F. L. Culler | 72. | A. F. Rupp |
| 19. | R. E. Dial | 73. | G. Samuels |
| 20. | J. A. Edwards | 74. | H. W. Savage |
| 21. | D. M. Eissenberg | 75. | A. W. Savolainen |
| 22. | W. K. Ergen | 76. | M. J. Skinner |
| 23. | A. P. Fraas | 77. | A. H. Snell |
| 24. | J. H. Frye, Jr. | 78. | I. Spiewak |
| 25. | U. C. Fulmer, Jr. | 79. | R. M. Summers |
| 26. | W. R. Gambill | 80. | B. J. Sutton |
| 27. | W. F. Gauster | 81. | J. A. Swartout |
| 28. | B. L. Greenstreet | 82. | W. C. Thurber |
| 29. | W. R. Grimes | 83. | D. B. Trauger |
| 30. | A. G. Grindell | 84. | D. H. Wallace |
| 31. | R. P. Hammond | 85. | J. S. Watson |
| 32. | P. N. Haubenreich | 86. | A. M. Weinberg |
| 33. | P. H. Hayes | 87. | G. D. Whitman |
| 34. | J. W. Hill | 88. | Gale Young |
| 35-44. | H. W. Hoffman | 89-91. | Central Research Library (CRL) |
| 45. | W. H. Jordan | 92-93. | Y-12 Document Reference
Section (DRS) |
| 46-50. | J. J. Keyes, Jr. | 94-96. | Laboratory Records Department (LRD) |
| 51. | G. J. Kidd, Jr. | 97. | Laboratory Records Department -
Record Copy (LRD-RC) |
| 52. | R. B. Kormeyer | 98. | Reactor Division Library,
Bldg. 9204-1 |
| 53. | A. I. Krakoviak | | |
| 54. | K. A. Kraus | | |

EXTERNAL DISTRIBUTION

- 99-113. Division of Technical Information Extension (DTIE)
 114. Research and Development Division, ORO
 115-116. Reactor Division, ORO

- 117. A.E.G., AEG Hochhaus, Frankfurt, Germany (M. Schuller)
- 118. Aerojet-General Nucleonics (K. Johnson)
- 119. Allis-Chalmers Manufacturing Co. (K. F. Neusen)
- 120. Alsthom, Paris, France (M. P. Domenjoud)
- 121. Argonne National Laboratory (Dr. Paul Lottes)
- 122. Argonne National Laboratory (Dr. M. Petrick)
- 123. Atlantic Research Nuclear Corp. (Dr. M. Markels, Jr.)
- 124. Atomics International (Dr. L. Bernath)
- 125. Babcock & Wilcox Co. (D. F. Judd)
- 126. Brookhaven National Laboratory (Dr. O. E. Dwyer)
- 127. Centre d'Etudes Nucléaires, Grenoble, France (M. Mondin)
- 128. Centre d'Etudes Nucléaires de Saclay, Gif sur Yvette, France
(M. J. Horowitz)
- 129. CHEN, Roma, Italy (Prof. F. Ippolito)
- 130. CISE, Milano, Italy (Prof. M. Silvestri)
- 131. Compagnie Francaise, Gagneux, France (M. Lefranc)
- 132. Dartmouth College, Thayer School of Engineering (Dr. G. B. Wallis)
- 133. Dynatech Corporation (Dr. M. Suo)
- 134-135. EURATOM, Bruxelles, Belgium (Dr. P. Kruys)
- 136. EURATOM, Ispra, Italy (M. R. Morin)
- 137. FIAT, Torino, Italy (M. G. Cesoni)
- 138-139. General Electric Co., Atomic Power Equipment Dept. (Dr. S. Levy)
- 140-141. General Electric Co., Advanced Technology Laboratory
(Dr. Novak Zuber)
- 142. Geoscience Ltd. (Dr. H. F. Poppendiek)
- 143. Hanford Atomic Products Operation (Dr. John Batch)
- 144. MAN, Nürnberg, Germany (Dr. Mayinger)
- 145. Massachusetts Institute of Technology (Dr. P. Griffith)
- 146. Massachusetts Institute of Technology (Dr. W. M. Rohsenow)
- 147-149. National Aeronautics & Space Administration, Lewis Research
Center (Library)
- 150-151. National Aeronautics & Space Administration, Lewis Research
Center [R. Weltmann (SEPO)]
- 152. North Carolina State University, Department of Chemical
Engineering (Dr. J. K. Ferrell)
- 153. Reactor Centrum Nederland, 's Gravenhage, Netherlands (M. Pelser)
- 154. SNECMA, Division Atomique, Suresnes, France (M. Fouré)
- 155. Technische Hogeschool, Eindhoven, Netherlands (Prof. Bogaardt)
- 156. University of Minnesota, Department of Chemical Engineering
(Dr. H. S. Isbin)
- 157-158. U. S. Atomic Energy Commission, Division of Reactor Development
(R. M. Scroggins)
- 159. U. S. Atomic Energy Commission, Division of Reactor Development
(Office of Civilian Power, Water Reactors Branch)
- 160. U. S. Atomic Energy Commission, Division of Reactor Development
(Office of Army Reactors, Technical Evaluation Branch)
- 161. U. S. Atomic Energy Commission, Division of Reactor Development
(Office of Nuclear Safety, Research and Development Branch)
- 162. U. S. Atomic Energy Commission, Division of Safety Standards
(R. Impara)
- 163. Westinghouse Electric Corporation, Atomic Power Division
(Dr. L. S. Tong)